MODEL PREDICTIVE-BASED VOLTAGE CONTROL OF ACTIVE DISTRIBUTION NETWORKS

Arunima Dutta

MODEL PREDICTIVE-BASED VOLTAGE CONTROL OF ACTIVE DISTRIBUTION NETWORKS

A

Thesis Submitted

in Partial Fulfilment of the Requirements

for the Degree of

DOCTOR OF PHILOSOPHY

By

Arunima Dutta

under the supervision of

Dr. Sanjib Ganguly and **Dr. Chandan Kumar**

Department of Electronics and Electrical Engineering

Indian Institute of Technology Guwahati

Guwahati - 781 039, India

May 2022

Certificate

This is to certify that the thesis entitled **"MODEL PREDICTIVE-BASED VOLTAGE CONTROL OF ACTIVE DISTRIBUTION NETWORKS"** submitted by **ARUNIMA DUTTA** to the Indian Institute of Technology Guwahati, Guwahati, India for the award of the degree of Doctor of Philosophy is a bonafide record of the research work done by her under our supervision. The contents of this thesis, in full or in parts, have not been submitted to any other Institute or University for the award of any degree or diploma.

Place: Guwahati
Date:

Dr. Sanjib Ganguly
Research Guide
Associate Professor
Department of Electronics and Electrical Engineering
IIT-Guwahati, 781 039

Place: Guwahati
Date:

Dr. Chandan Kumar
Research Guide
Associate Professor
Department of Electronics and Electrical Engineering
IIT-Guwahati, 781 039

Declaration

I certify that:

1. The work contained in this thesis is original and has been done by me under the guidance of my supervisors.
2. The work has not been submitted to any other Institute for any degree or diploma.
3. I have followed the guidelines provided by the Institute in preparing the thesis.
4. I have conformed to the norms and guidelines given in the Ethical Code of Conduct of the Institute.
5. Whenever I have used materials (data, theoretical analysis, figures, and text) from other sources, I have given due credit to them by citing them in the text of the thesis and giving their details in the references.

Place: Guwahati
Date:

Arunima Dutta

This Thesis is dedicated to the

Loving Memory of My **mother**

Bhabani Dutta Baruah

(28/01/1957)-(10/03/2021)

Acknowledgement

I take this opportunity to acknowledge my heartfelt gratitude to all those people who directly or indirectly helped me to carry out this research work successfully.

Foremost, I am heartily thankful to my supervisors, Dr. Sanjib Ganguly and Dr. Chandan Kumar, for their encouragement, guidance and support during my research work. I express my gratitude for their willingness to help and timely advices on the issues I faced during the doctoral studies.

I would like to acknowledge the financial, academic and technical support of the Indian Institute of Technology Guwahati for this research. I am grateful to the Head of the Department of Electronics and Electrical Engineering for providing me all the facilities to carry out my research work. I am sincerely grateful to Dr. Praveen Tripathy, Dr. Indrani Kar, and Dr. Ravindranath Adda, for assessing the work and giving invaluable suggestions as members of Doctoral Committee.

I would like to express gratitude to the services being offered by Mr. Paban Bujor Barua, staff of Power and Control Laboratory II and Mr. Mukut Baruah, office staff of Electronics and Electrical Engineering department.

The Smart Energy Conversion group members have contributed immensely to my personal and professional time during my stay in the institute. I especially thank Manokumar R, Hrishikeshan VM and Dwijasish Das for their valuable help during my research. I am extremely thankful for the support extended by friends from Power and Control Laboratory II.

I am thankful to my friends Atanu, Juna, Jinti, Birjit, Samarjit, Sumita and all other friends for sharing beautiful moments during my life in IIT Guwahati.

My earnest thanks are to my mother (in loving memory) and father who have always supported this endeavor through their deeds and prayer. Their unconditional love and affection are always the sources of inspiration for my future life. Many thanks to my father-in-law and my mother-in-law for giving me the freedom of what I wanted to be. I thank my sisters Geetima and Jyotsna, and my

brother-in-law for their loving care and support all these years.

Last but not the least, I would like to thank my husband, Dr. Sanjoy Debbarma who has always stayed at my side with unceasing guidance, motivation, love and care.

Place: Guwahati
Date:

Arunima Dutta

Abstract

KEYWORDS: Model Predictive Control (MPC); volt/var control (VVC); active distribution network (ADN); local control.

Electricity generation and transportation sectors are significant contributors to the increasing carbon foot print of the society. The utilization of greener generation technologies in both these sectors is the solution to the increasing carbon emissions. Microgrid is considered as the key technology for integrating distributed energy resources (DER) in distribution networks. However, increased penetration of DERs in distribution networks brings new challenges in the operation and management of power system, among which voltage fluctuation is the most severe. Moreover, the stochastic nature and concentrated power profile of photovoltaics (PVs) and electric vehicles (EVs) further aggravate the situation by interfering with the voltage control devices. This necessitates development of a proper control structure that optimally coordinates all the entities such as distributed generation (DG) units, energy storage system (ESS), EVs and other voltage regulating devices present in a network.

In this thesis, a model predictive control (MPC)-based centralized control approach has been developed that optimally coordinates the different entities, such as, actions of on-load tap changer (OLTC), distribution static synchronous compensator (DSTATCOM), and active and reactive power set-points of PV and EV inverters to manage the node voltage variations and fulfill other objectives. Further, the proposed controller follows a set of $if - then - else$ rules to effectively utilize the MPC in controlling node voltages as well as minimizing energy losses in active distribution network integrated with microgrids. To investigate different volt/var control devices based on different temporal characteristics, the proposed control strategy has been further converted to a two-stage control structure. The two functionalities of active distribution management system (ADMS), i.e., demand response (DR) and conservation voltage reduction (CVR) strategies are included in this two-stage voltage control

methodology to enhance energy efficiency of the distribution networks.

Due to the availability of on-board chargers, opportunities emerge for EV to provide services to the distribution network operators through vehicle-to-grid (V2G) technology. EV chargers can provide reactive power at different state of charge (SoC) without degrading the battery life cycle. Although EV infrastructure benefits the distribution system through V2G services, the increasing number of EVs creates congestion in the feeders, resulting in network overloading. Thus, a dual-stage centralized control strategy has been developed to mitigate voltage variations and line congestion. Moreover, the effects of locations of EV charging stations in an industrial or a residential lateral of distribution networks are further studied.

A three-stage MPC-based centralized coordinated approach has been further developed to schedule charging of EV and volt/var devices. The approach aims at maintaining bus voltage magnitudes and SoC of EV battery within desired limits with minimal usage of control resources and cost of electricity consumption. The additional third stage schedules charging of EV half-hourly with respect to the real-time electricity price. The control approach ensures that EVs attain the desired SoC at the time of their departure from the charging station without violating the voltage limits. The economic aspects of EV aggregators in charge scheduling and reserve scheduling have been further evaluated to add value to the third stage. Moreover, DR has been used in the third stage of operation. The effects of slow and fast charging on the voltage profile, and cost of electricity consumption have been further explored in this study. Furthermore, the reactive power set-points achieved from the centralized control scheme follow the integrated local Q(V) characteristics according to DER integration standards so as to establish the control problem as multi-level control structure.

The 33-bus and 38-bus radial distribution networks are used to validate all the proposed control approaches. The CONOPT/CPLEX solver of General Algebraic Modelling System (GAMS)/IBM ILOG community edition software is used as the solution tool. The simulation results show that the proposed MPC-based coordinated control approach could effectively bring the voltage magnitudes within the desired limits and limit line congestion. Integrated CVR and DR in the proposed approach further helps in reducing voltage error, energy loss, and energy consumptions. Moreover, it ensures that EVs attain the desired SoC at the time of their departure from the charging station.

Contents

List of Figures

List of Tables

List of Acronyms

ADN	Active Distribution Network.
RES	Renewable Energy Sources.
MPC	Model Predictive Control.
PV	Photovoltaics
DR	Demand Response.
CVR	Conservation Voltage Reduction.
PSAT	Power System Analysis Toolbox
RTP	Real-Time Price
VVC	Volt/Var Control
DNO	Distribution Network Operator.
OLTC	On-load tap changer.
APC	Active Power Curtailment
DSTATCOM	Distribution Static Synchronous Compensator.
DER	Distributed Energy Resource
DG	Distributed Generation
AMI	Automated Metering Infrastructure
DSTATCOM	Distribution Static Compensator
RHC	Receding Horizon Control.
EV	Electric Vehicle
ADMS	Active Distribution Management System
SCADA	Supervisory Control and Data Acquisition
IEEE	Institute of Electrical and Electronics Engineers
IRENA	International Renewable Energy Agency
EVA	Electric Vehicle Aggregator.

EVCS	Electric Vehicle Charging Station.
RTU	Remote Terminal Unit.
PCC	Point of Common Coupling
QP	Quadratic Programming
WT	Wind Turbine
FC	Fuel Cell
DS	Distributed Storage
MILP	Mixed Integer Linear Programming
SQP	Sequential Quadratic Programming
APC	Active Power Curtailment
IPP	Independent Power Producer
NLP	Non Linear Programming
MINLP	Mixed Integer Non Linear Programming
KF	Kalman Filter
FAHPSO	Fuzzy Adaptive Hybrid Particle Swarm Optimization
MAS	Multi Agent System MPC: Model Predictive Control
SA	Sensitivity Analysis
GA	Genetic Algorithm
MOGA	Multi-Objective Genetic Algorithm
LMI	Linear Matrix Inequalities
PDIPM	Primal Dual Interior Point Method
ADMM	Alternating Direction Method of Multipliers
QSL	Quasi Stationary Line
AANN	Adaptive Artificial Neural Network
MPSO	Modified Particle Swarm Optimization
CAO	Cluster Autonomous Optimization
DICCO	Distributed Inter-Cluster Coordination Optimization
WCA	Water cycle Algorithm
QCMIQP	Quadratic Constrained Mixed Integer Quadratic Programming
SM	Smart Meter

PMU	Phasor Measurement Unit
SG	Smart Grid
MG	Microgrid
VVO	Volt/VAR Optimization
GAMS	General Algebraic Modeling System
V2GQ	Vehicle to Grid Reactive Power Support
PEV	Plug in Electric Vehicle
EPSO	Evolutionary Particle Swarm Optimization
SVC	Static Var Compensator

List of Symbols

K_{st}, T_{st}	Gain and time constant of DSTATCOM controller.
i_{st}, Q_{st}	Current and reactive power of DSTATCOM.
N_P	Prediction horizon.
N_C	Control horizon.
P_{PV}, Q_{PV}	Active and reactive power generation of PV units.
$\frac{\delta V}{\delta u}$	Sensitivities of voltages with respect to control variables
$\frac{\delta I}{\delta u}$	Sensitivities of currents with respect to control variables
P_{EV}, Q_{EV}	Active and reactive power of EV.
P_L, Q_L	Active and reactive power absorption by loads.
S_{PV}, S_{EV}	Rating of PV and EV.
y_P	Output Prediction Matrix.
P_{loss}	Ohmic loss of the distribution network.
u_{min}	control input vector with minimum values of control variables.
u_{max}	control input vector with maximum values of control variables.
Δu_{min}	change in control input vector with minimum values of control variables.
Δu_{max}	change in control input vector with maximum values of control variables.
$\Delta u_{min\,slow}$	change in control input vector with minimum values of control variables.
$\Delta u_{max\,fast}$	change in control input vector with maximum values of control variables.
E_{min}	Minimum value of energy demand
E_{max}	Maximum value of energy demand
t_s, k	Sampling time, instant.
σ	Slack variable for voltages.
ν	Slack variable for state-of-charge.
μ	Slack variable for energy demand.

Ω_{PV}	Set of buses with PV generators.
Ω_{VDL}	Set of buses with voltage dependent loads.
Ω_{FL}	Set of buses with flexible loads.
Ω_{L}	Set of buses with power varying loads.
Ω_{D}	Set of buses with DSTATCOM.
m	index of buses.
$P^{L}_{m,nom}$	Active power demand of bus m measured at the nominal voltage.
$Q^{L}_{m,nom}$	Reactive power demand of bus m measured at the nominal voltage.
$CVR_{g(kW)}$	Active CVR factor.
$CVR_{g(kVAr)}$	Reactive CVR factor.
$V_m(t)$	Voltage magnitude of bus m at time instant t
λ	Demand flexibility factor.
η	Efficiency of battery charger.
t_a, t_d	Arrival and departure times of EV to EVCS.
t_{park}	Parking time of EV in EVCS.
SoC_{ini}, SoC_{fin}	Initial and final SoC of EV.
y_{min}	minimum value of controlled output.
y_{max}	maximum value of controlled output.
A, B, C	System, input and output matrices of the prediction model.
V_{tap}	Reference voltage of OLTC.
V_{stat}	Reference voltage of DSTATCOM.
P_{FL}	Active power demand of flexible loads.
S_{PV}	Rating of PV.
S_{EV}	Rating of EV
$V(k+i\|k)$	Predicted value of bus voltage with current measurement of voltages taken at instant k
$E(k+i\|k)$	Predicted value of energy demand with current measurement of energy demand taken at instant k
$I(k+i\|k)$	Predicted value of branch current with current measurement of branch current taken at time instant k

B_{cap}	Capacity of EV battery
$Profit_{EVA}$	Profit earned by EVA
Rev_{EVA}	Revenue generated for EVA
$Cost_{EVA}$	Cost of expenses incurred by EVA
M	Mark-up price
d_t	Regulation-down price
u_t	Regulation-up price
SP	Selling price of electricity
τ_{ch}	Binary variable that represents charging process.
τ_{dis}	Binary variable that represents discharging process.

1

Introduction

Contents

1.1 Introduction

Distributed energy resources (DERs), such as, micro turbine, fuel cells, photovoltaic (PV) and wind energy systems play a crucial role in the alley towards future energy landscape [1–5]. These renewable energy based distributed generation (DG) units have gained popularity with the promotion of policies by government, including feed-in-tariffs, renewable portfolio standards, tradable green certificates, investment tax credits, and capital subsidies [1]. With the technological growth, there is a massive transformation of passive distribution networks into active distribution networks (ADN) accompanied by the role of more energy collection and storage [1, 2, 4].

Although the DG units play an important role in reducing pollution and enhance the economics by minimizing transmission loss, the intermittent nature of DG units brings several crucial challenges to the operation of power systems [6–8]. Some of the key challenges faced by the operator are inverse/reverse power flow, temporary over/under voltage, line congestion, frequency stability issues, protection equipment design to meet the reliability standards, voltage fluctuations and its regulation, etc. Voltage regulation problem is identified as one of the main challenges in ADN that restrict the incorporation of DG units [6, 8–10]. Basically, DG units due to their bidirectional energy flow uplift the voltage across feeders. Besides, DG units due to their intermittent power fluctuations and penetration to LV/MV network cause severe voltage excursions. Traditionally, DG units are asked by distribution network operator (DNO) to operate at zero reactive power, which limits the application of DG units as voltage control devices. However, with the advancements in technology, the level of complexity of ADN has increased manifold with a wide variety of DG units, energy storage system (ESS), controllable loads, and voltage regulators. Moreover, typical conventional techniques, such as, on-load tap changer (OLTC) and capacitors switching may not be sufficient enough to regulate voltages under inverter dominated grid. Consequently, the usage of DG units as voltage regulators requires urgent investigation.

The different control elements that are used as voltage regulators can be classified into

(i) legacy voltage control devices and

(ii) power electronics interfaced devices.

The OLTC, set-voltage regulators, shunt capacitors fall under legacy voltage regulation devices.

The manipulation of active and reactive power of power electronics interfaced devices, such as, PV, EV, ESS, distribution static synchronous compensator (DSTATCOM) and other custom power devices, controllable loads act as voltage violation mitigation techniques.

An illustration of the voltage control problem in a small distribution network with wide-variety of distributed energy resources is depicted in Fig. 1.1. Initially, the DNO defines a target voltage for each bus in the network. The security or economical purpose, e.g., network losses minimization might be the basis of choosing the target voltages. However, reaching the actual target values is impractical and likely infeasible. Thereby, the network voltages are kept within some limits around the target values. These limits are referred to as normal operation limits. Maintaining the voltages within the prescribed limits is one of the main objectives of the controller. While the voltages of some buses fall in the undesirable region, the controller uses the minimum control actions to bring these voltages within the acceptable limits. As the voltages cross the emergency limits, the controller uses all its efforts to maintain voltages in the specified band of operation.

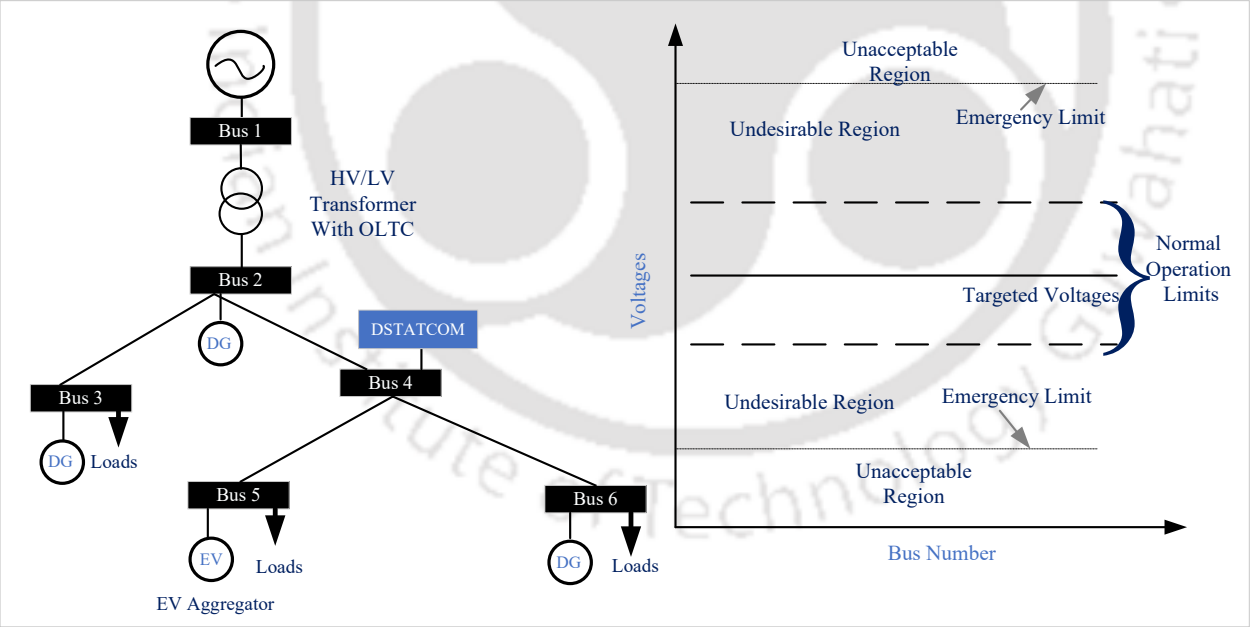

Figure 1.1: An illustration of voltage control problem of active distribution network.

Over the past decades, focus has been made on the control schemes to maintain the voltages within an acceptable level rather than investing in reconfiguration of the whole network to accommodate DG units. There has been a growing emphasis on centralized, decentralized, and distributed control schemes in the distribution network housed with large number of DER units [6–11]. As shown in Fig. 1.2, a dedicated central controller in the centralized control scheme collects the data and

calculates the control actions for all the single units at a single point. This scheme requires an extensive communication infrastructure. Decentralized and distributed control structures do not require a central controller. Fully decentralized control scheme relies on the local controller based on local information. While the decentralized controller is unaware of the information of the system and other units, the distributed controller performs control calculations by gathering information and measurements from the neighboring controllers. An illustrative example of different control schemes used in a small distribution network is shown in Fig. 1.2.

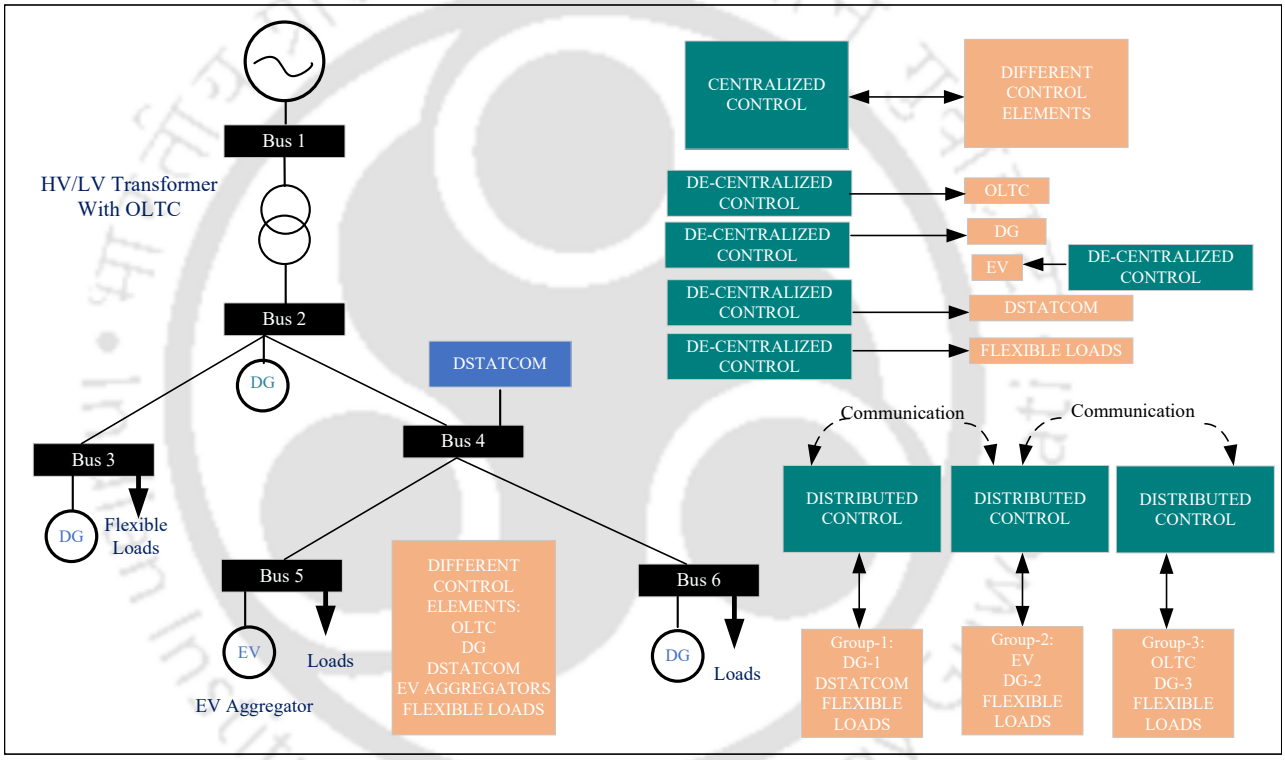

Figure 1.2: Different control schemes used in active distribution networks: (i) centralized, (ii) decentralized (iii) distributed.

Although each control scheme has its own set of advantages and disadvantages, the usage of multi-layer/hierarchical [12–14] control structure is seen frequently in recent literature as the standardized solution to the efficient ADN energy management. The hierarchical control structure distributes the control functions into local controllers and upper level controllers, so that the complete system operates in a more efficient way [1–4]. Further, the multi-layer control structure is restructured to a multi-level hierarchy where decentralized and distributed control schemes occupy the local level control [7, 13] and centralized control scheme occupies the upper level control.

The primary, secondary and tertiary control levels constitute the multi-level control structure. The

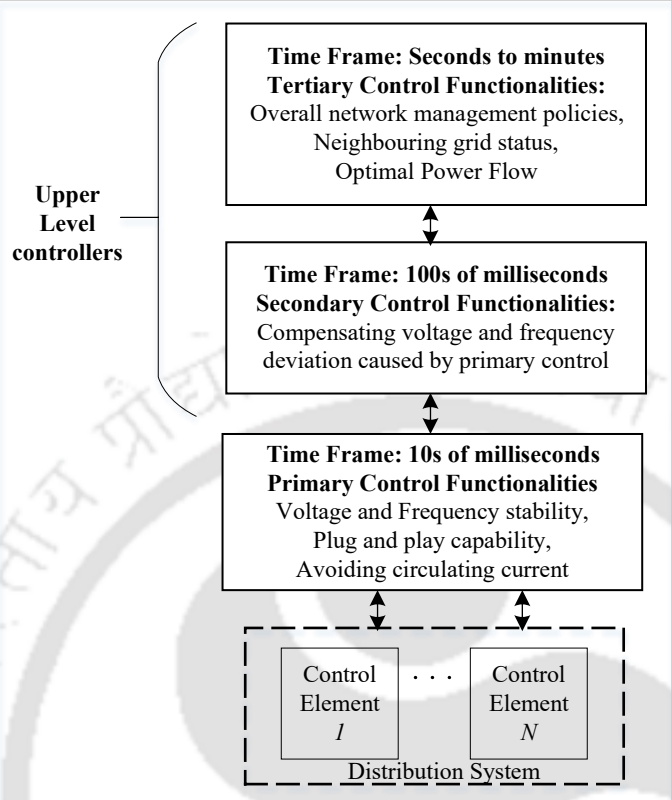

Figure 1.3: Multi-level control structure implementation in active distribution network.

primary control is basically a decentralized local control method which features the fastest response. Master-slave and peer-to-peer control are the two main methods for primary control [1, 2]. Secondary control is used to compensate the frequency and voltage deviations induced by primary control and to realize a prescribed power sharing scheme among DG units. Tertiary control enables an optimal operation of the system on a longer time scale. Both secondary and tertiary control structures work in coordination to form the energy management system (EMS) [1]. However, the definitions of these control schemes vary in different literature. For example, in some papers, tertiary control is established as an entity responsible for coordinating the operation of multiple microgrids interacting with one another in the system [1]. In that scenario, the secondary control structure is entrusted with added functionality apart from regulating voltage and frequency. The choice of the control structure varies according to the type of microgrids (residential, commercial, or military), and the legal and physical features (location, ownership, size, and topology) [2]. A schematic of hierarchical control structure with specific objectives and operation times is depicted in Fig. 1.3 [4].

Recently, several cutting-edge algorithms are being developed and utilized as optimal voltage

regulation schemes that persuade different network elements to work in a coordinated and cooperative manner. These optimal voltage regulation algorithms use either single-step or multi-step optimization techniques to optimally change the control variables, which is predefined in the system. The active and reactive power of DG units and the voltage set point of OLTC are controlled externally by many researchers to achieve the targeted voltages. With a view to minimize the voltage deviation in a distribution system, the objective functions are formulated as linear, non-linear or mixed integer problems. The complexity in terms of data handling and computation time in real-time scenario needs considerable amount of attention in the designing of these voltage regulation algorithms. The power systems researchers around the globe have significantly contributed on real-time optimal voltage control of ADN during the last decade.

In this chapter, the works on voltage control are systematically presented. A classification tree is developed for voltage control, as shown in Fig. 1.4. It consists of three levels based on different attributes. The Level #1 classification is based on the functionality of the control approach. The way the different control schemes are implemented is the basis of Level #2 classification. The Level #3 classification is based on the different voltage control methodologies reported in literature. The special emphasis is given in the literature review to identify the optimal voltage control approaches. A wide variety of literature on optimal control of voltage is presented in the next section.

1.2 Literature review

This section describes literature review on voltage control in ADN. A level-wise classification tree is shown in Fig. 1.4. The studies on voltage control in ADN are divided into two broad categories in Level #1 classification:

(i) local control approach and

(ii) coordinated control approach.

Local control approach typically describes the control actions taken at DER level [7, 10, 11] that include the actions applied to the inverter such as, proportional active/reactive power sharing, inner voltage and current control loops, maximum power point tracking (MPPT) strategy in PVs/wind generation, etc., without any communication. The local control layer also performs several rudimentary functions like control of generation/consumption and management of ESS locally. This approach can

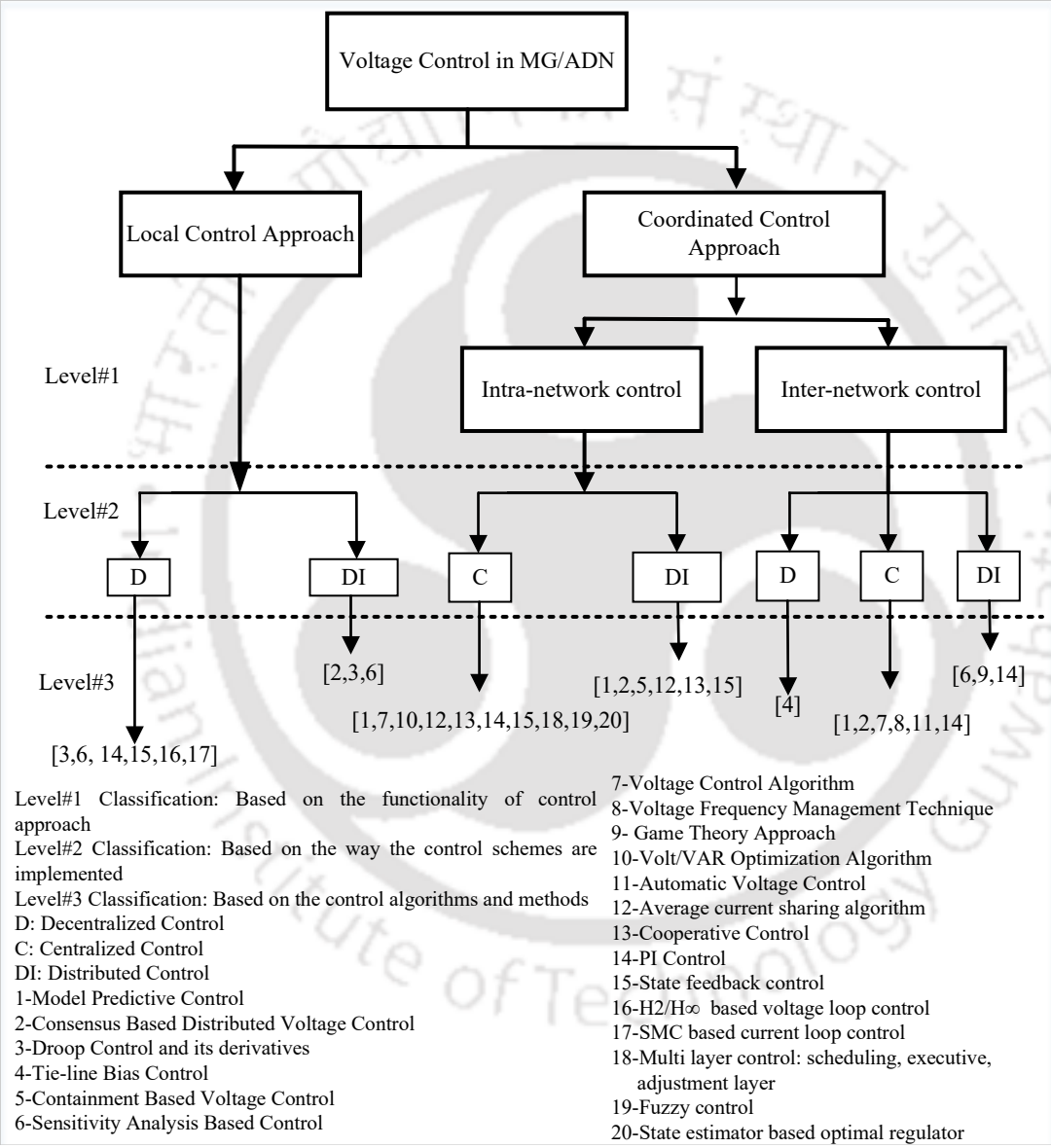

Figure 1.4: Level-wise classification tree of voltage regulation/control approaches in active distribution network.

be considered as the first level of hierarchical control structure. With the increasing complexity of network, the local control is not enough to maintain the voltage within prescribed limits, thereby, the need of a coordinated control approach is felt by many researchers [6, 7, 9–15]. That is why, in some papers [10–13, 16, 17], both the approaches are investigated in hierarchy manner.

The coordinated control approach is further divided into

(i) intra-network control and

(ii) inter-network control.

Intra network control approach refers to the presence of a robust controller at upper level [6,7,9–15] to coordinate the actions of the control elements present in an ADN or microgrid (MG). Authors in [10] have utilized both local and coordinated voltage control schemes as real time control. The recent trend is towards interconnecting multiple MGs to enhance reliability of the system. For a multi-microgrid system, a higher level control (inter-network control) [16–19] is required to integrate all the MGs present in a system such that they work in a coordinated fashion. The DNO is at the highest level to monitor power transfer between all MGs and command the microgrid controller accordingly. Moreover, DNO can optimize the MG operation in a more economical way and can provide the platform for competitive market among the MGs. Paper [18] proposes a voltage frequency management technique for multi-MGs system that gets activated when the lower level controller fails to maintain voltage and frequency within acceptable limits. It is to be noted that the coordinated control approach can be referred to as the secondary and tertiary levels of control in multi-level control structure.

The Level #2 further classifies the Level #1 classification based on the way of implementation of the control approach. The control schemes are implemented basically in three ways: (i) centralized, (ii) decentralized and (iii) distributed. An illustration of these schemes are presented in Fig. 1.2. While the local control approaches are usually implemented either in decentralized or distributed manner, the coordinated control approaches are implemented in centralized, decentralized or distributed manner. Decentralized and distributed structures do not require a central controller. Decentralized control, as defined in [8], performs regulation based on local measurements, while, distributed control is based on both local measurements and neighboring communication [7, 11]. Reference [8] discusses a method of maximum available active power extraction by utilizing a sensitivity analysis based decentralized control. Reference [11] presents an agent based scheme wherein locally measured data is

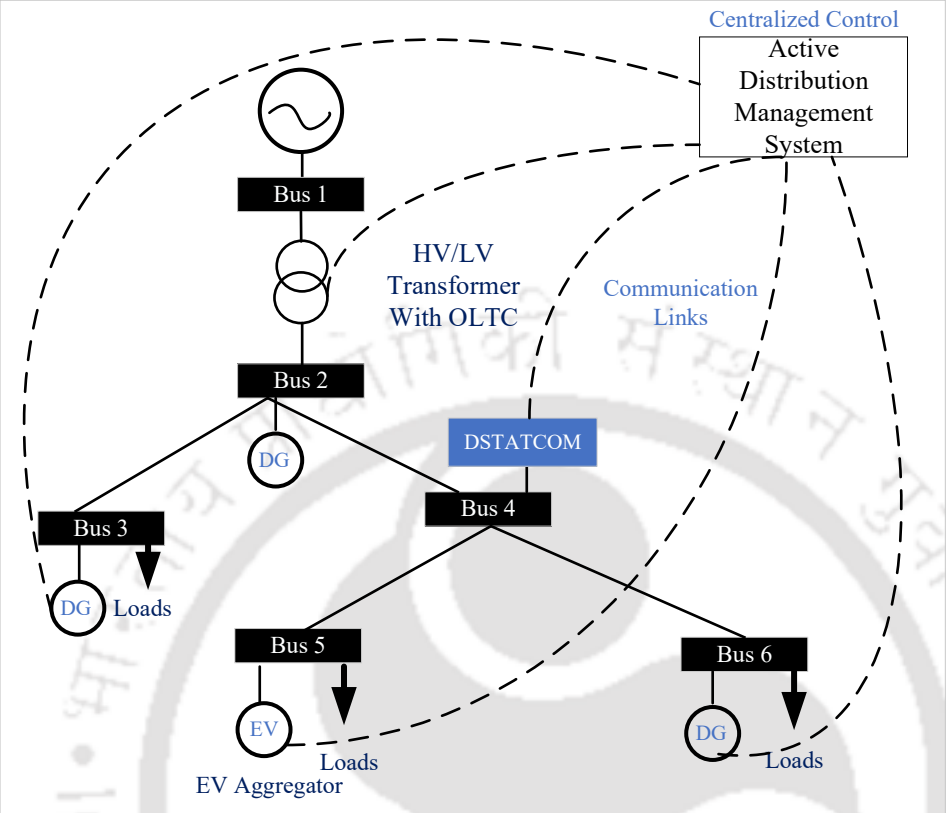

Figure 1.5: Centralized coordinated control structure.

used by distributed controllers to alleviate voltage deviations. Here, a switching control framework is proposed wherein the DERs are managed with a constant power factor keeping bus voltages within specifications. There exists a central controller in centralized structure, which collects and transmits information to local control elements [6, 14]. Reference [6] employs model predictive controller (MPC) centrally for voltage control in distribution networks and, they have found acceptable result following extreme abnormal conditions. Here, the controller acts together on the power outputs of DG units and the voltage set-point of the OLTC to maintain the voltages within acceptable values. A fast and reliable communication infrastructure is essential for the centralized control. The optical fibre or Wifi communication technologies have been developed to achieve fast and reliable data transfer [14]. The IEC 61850 standard that has been designed by the international electrotechnical commission (IEC) technical committee 57 can be used to meet the communication requirements of a centralized control scheme by using the existing infrastructure or in some cases with some specific hardware [1]. An illustration of centralized coordinated control structure has been shown in Fig. 1.5.

Although, the distributed approach reduces the communication burden compared to the centralized

approach, it suffers from certain drawbacks. Because of its case-specific approach and inability to provide an optimal solution, this approach is still in its developing stage. However, each control scheme has its own advantages and disadvantages. A comparative analysis between these control schemes is tabulated in Table 1.1. The comparison among these three schemes are based on the attributes: computational cost, communication facilities cost, flexibility/expandability, reliability, and difficulty in implementation. In recent past, several authors establish the voltage regulation problem as a multi-level control [7, 11–13, 16, 17]. There are different levels of control in this scheme with predefined objectives as presented in Fig 1.3 [2]. Each level in the control hierarchy may be centralized, decentralized or distributed according to the control objectives.

Table 1.1: Comparison between different control schemes.

Control Scheme	Centralized	Distributed	Decentralized
Computational Cost (complexity, time and space)	High	Medium	Low
Communication facilities cost	High	Medium	Low
Flexibility/Expandability	Low	Medium	High
Reliability(concerning single point of failure)	Low	High	High
Difficulty in implementation	Low	High	High

The Level #3 classifies Level #2 further based on the control algorithms and methods reported by various researchers. The voltage control methodologies can be either

(i) optimization based or

(ii) non-optimization based.

Optimization based approaches find an optimal way to control the voltages by minimizing or maximizing objective functions. Depending on the optimization problems formulated, the solution strategies might be quadratic program (QP) [6], non-linear programming (NLP) [20], mixed integer quadratic programming (MIQP) [21], mixed integer linear program (MILP) [22], etc. Reference [20] proposes a consecutive three-stage optimization algorithm to reduce OLTC operations and active power curtailment (APC) to satisfy the charging demand of plug-in electric vehicles (PEV) and meet the voltage requirements. A robust optimization framework is developed in [22] to address the model uncertainties such as admittance matrices of a distribution network with DGU. The optimizer embedded

in MPC [6, 7, 12, 14, 15] calculates the optimal control actions in certain discrete steps. Reference [15] utilizes a two-stage MPC to allow PEVs to participate as a reactive power compensator in distribution network. The different attributes of optimal voltage control are summarized in Table 1.2. The different attributes considered are: objective function, solution strategy, type of DG units, type of network, and the control scheme used in the paper.

Despite several advantages imposed by optimization based voltage control approaches, several authors opt for non-optimization based approaches [11, 23–25]. Reference [23] have developed a consensus based distributed algorithm to coordinate the charging/discharging of PEVs with minimum use of APC for voltage control problems. Authors in [24] have described a coordinated control strategy based on some rules. The OLTC act on the voltages of the buses where the wind turbines are not present. Droop control [7, 12, 13], proportional integral control (PI) [10], multi agent system (MAS) based control [16], etc. are a few popularly used non-optimization approaches in the literature.

1.3 Motivations behind the thesis

The main challenge in ADN is identified as voltage regulation that restricts the incorporation of DG units [6, 8, 10, 14, 16, 20, 21, 26–28]. Over the past decades, focus has been made on the control schemes to maintain the voltages within an acceptable level rather than investing in reconfiguration of the whole network to accommodate DG units. Several strategies (OLTC, shunt capacitors, DG units, etc.) are discussed in the literature for mitigation of voltage violations in the distribution networks. Nevertheless, without proper coordination among these strategies, oscillations would be induced in networks due to unnecessary competition among the control devices to perform voltage regulation. Thereby, coordinated control strategy has become the subject of interest to the researchers. The coordinated control approaches can be either rule-based or optimization-based. The optimization-based coordinated voltage control methods could avoid the drawbacks of non-optimization-based control to achieve optimal operation of systems.

With the introduction of high amount of uncertainty due to renewable energy resources, real-time optimal voltage control has gained attention among the DNO. Model predictive controller is one of the popularly used real-time optimal voltage control strategies [6, 10, 14, 21].

MPC is a closed-loop control framework that possesses the following features:

(i) It relies on measurements and estimation of system states.

(ii) It predicts the future states based on the explicit model and anticipated disturbances.

(iii) It makes optimal decisions over the control horizon by considering all the constraints.

The MPC is formulated as convex quadratic, mixed integer linear as well as non-linear programming. The three variants of MPC that are commonly used in literature are: (i) deterministic, (ii) stochastic and (iii) robust [28]. On the basis of timescale decomposition of voltage control devices, MPC can operate either in (i) single-timescale or (ii) multi-timescale.

From the literature survey carried out so far, the following research gaps are identified:

- Although numerous works have been reported on voltage regulation using MPC, none of them has formulated the coordinated control approach utilizing OLTC and reactive power compensation capability of PV inverters, that can minimize energy losses and can maintain the node voltages, as well. In this context, this study proposes a rule-based MPC (RBMPC) approach to optimally coordinate different control actions to maintain voltages within the prescribed limits as well as minimize energy losses in the presence of PV units. These rules are designed with the aim to utilize the MPC effectively along the day.

- Despite several works on demand response (DR) and conservation voltage reduction (CVR) [29], they have not been integrated together in coordination with the volt/var control (VVC) in an MPC-based coordinated framework. Moreover, coordination of different voltage regulation devices with different temporal characteristics requires multi-timescale coordinated voltage control framework to minimize the switching operations of discrete devices, such as, OLTC. In this context, this study considers timescale decomposition of VVC devices to regulate voltages incorporating CVR and DR.

- The effects of locations of electric vehicle charging stations (EVCS) on VVC are not explored much in the literature. Moreover, with the increasing number of EVCSs and PV units, congestion becomes prevalent in the network lines [10]. However, management of line congestion in presence of DERs (PV and EV) in the coordinated voltage control framework has not been considered in recent works. This study presents a centralized algorithm to coordinate the several control actions which include reactive power compensation capability of PV inverters, DSTATCOM and EV inverters, and tap movement of OLTC.

- The MPC-based EV charge scheduling has been discussed in many literature [30, 31]. However, the optimal coordination between EVs' charging and other voltage regulation devices has not been explored yet. Moreover, the studies of economic aspects by including EV aggregator's profit from the ancillary and charging/discharging services in MPC-based framework have not been explored yet. Moreover, recent DER integration standards (IEEE 1547 standard) propose the implementation of local characteristics in the DERs to absorb/supply the reactive power. In this context, the local level controller is incorporated along with the upper level control structure that adjusts the reactive power set-points of PV and EV inverters obtained from upper level controller.

Thus, these research gaps are the motivations behind the present work.

1.4 Organization of the thesis

This thesis is organized as follows:

- In Chapter 2, an MPC-based centralized control approach is presented for maintaining the voltages of the buses within permissible limits in the presence of high photovoltaic (PV) penetration. The proposed control scheme optimally coordinates the actions of OLTC and PV inverters to fulfill the desired objectives. The objectives are minimization of change in control variables, slack variables, energy loss, and voltage error. These objectives are weighted to form the overall objective function. Three rules are formulated based on the severity of voltage magnitudes. The weights of the objectives are adjusted according to these pre-defined rules.

- In Chapter 3, a dual-stage model predictive based voltage control is proposed that optimally coordinates the reference voltage of DSTATCOM and OLTC, and PV inverters' active and reactive powers set points to maintain network voltages within the operating limits. The two functionalities of active distribution management system (ADMS), i.e., demand response and conservation voltage reduction are further explored in the voltage control methodology to enhance energy efficiency of the distribution networks.

- Chapter 4 presents a dual-stage coordinated control approach for voltage regulation and congestion management of ADN in the presence of PV generators and EVCS. The proposed scheme operates on RBMPC to optimally manage the settings of the regulating devices, i.e., OLTC,

DSTATCOM, PV generators, and EV inverters that have different temporal characteristics. Here, the voltage and branch current magnitudes are the outputs as well as the states of MPC.

- The Chapter 5 proposes a three-stage MPC-based centralized coordinated approach to schedule charging of EV and volt/var devices. The approach aims at maintaining bus voltage magnitudes and state-of-charge of EV battery within desired limits with minimal usage of control resources and cost of electricity consumption. The first stage determines the optimal operating points of traditional discrete control devices on an hourly basis. The second stage dispatches the optimal set-points of power electronics interfaced fast devices [PV and EV inverters] every one minute. The third stage schedules charging of EV half-hourly with respect to the real-time electricity price. The control approach ensures that EVs attain the desired state-of-charge (SoC) at the time of their departure from the charging station without violating the voltage limits.
- EV aggregators (EVA), being the interface between DNO and EV users, is an independent entity that also seeks its own sustainable benefits from the coordinated optimal scheduling and regulation services. In Chapter 6, the scheduling of EV charging is done half-hourly, considering EVA's profit, and benefits for EV users. Moreover, the voltage regulation objective in all the stages benefits DNO technically. The optimization function for the third stage is formulated considering the benefits of the three parties: EVA, EV users and the DNO. The first and the second stages of the proposed approach optimally dispatch the active and reactive power set-points of PV and EV inverters, and reference voltage of OLTC.
- In Chapter 7, the conclusion of the whole work is presented along with some future directions of the research in this area.

The Appendix of this thesis provides the simulation data for the 33-bus and 38-bus radial distribution networks, and time varying load demand and PV generation.

1.5 Contributions of the thesis

The contributions of the thesis are summarized as follows:

- A rule-based MPC approach has been formulated for coordinating OLTC and PV inverters which can minimize energy losses and can maintain the bus voltages, as well. The proposed approach acts as a corrective controller that brings the voltage magnitudes within their desired limits in ADN integrated with and without microgrids.

- An MPC scheme based on dual-time scale coordinated algorithm has been developed, that coordinates different voltage regulation devices, such as, OLTC, PV inverters and DSTATCOM with different temporal characteristics. Moreover, energy efficiency is enhanced through CVR and DR techniques in MPC framework.
- An MPC-based dual-stage voltage control algorithm has been developed to manage line congestion in addition to voltage violations of ADN due to increased penetration of EVs and PVs, with minimal actions of the OLTC tap positions and dispatch of active power from PV, reactive power from DSTATCOM, EVCS, and PV units.
- A third stage is further added to the previously developed two-stage MPC framework to perform EV charge scheduling by taking into consideration the balance between the operating cost and customer satisfaction. The optimal EV scheduling fulfills the objectives of reaching the desired state-of-charge at desired time, in addition to reducing voltage fluctuations and charging of EVs at less price.
- Furthermore, the EV aggregators' profits from charging/discharging and ancillary services have been considered in the economic MPC-based charge scheduling of EVs. Moreover, DR is enabled in the third stage of the MPC-based framework through price-based and incentive-based mechanisms.

In this thesis, the following performance indices are considered to analyze the performance of active distribution networks.

- Energy/power loss: The minimization of network energy loss over the day is considered as one of the objectives throughout the thesis.
- Minimum and maximum voltage magnitude: The minimum and maximum voltage magnitudes among all the buses are evaluated before and after the control actions are applied.
- Line congestion ratio: It is defined as the ratio of branch current to the thermal limit of the distribution line.
- Controllable resources utilization: The different controllable resources that have been used in this thesis are active/reactive power set-points of PV and EV inverters, tap operations of OLTC, and reactive power of DSTATCOM.

- Peak energy demand: The demand at the peak hour is evaluated to measure the benefits of DR operation in the volt/var control.
- Cost of electricity consumption: The cost of electricity consumption at peak time or throughout the day is evaluated in some of the chapters.

Legends: QP: Quadratic Programming, EPSO: Evolutionary Particle Swarm Optimization, MOGA: Multi-Objective Genetic Algorithm, NLP: Non Linear Programming, MINLP: Mixed Integer Non Linear Programming, KF: Kalman Filter, FAHPSO: Fuzzy Adaptive Hybrid Particle Swarm Optimization, MAS: Multi Agent System , MPC: Model Predictive Control, SA: Sensitivity Analysis, GA: Genetic Algorithm, LMI: Linear Matrix Inequalities, PDIPM: Primal Dual Interior Point Method, ADMM: Alternating Direction Method of Multipliers, QSL: Quasi Stationary Line, AANN: Adaptive Artificial Neural Network, MPSO: Modified Particle Swarm Optimization, CAO: Cluster Autonomous Optimization, DICCO: Distributed Inter-Cluster Coordination Optimization, HT: Hydro Turbine, WT: Wind Turbine, DGU: Distributed Generation Units, PV: Photovoltaics, CB: Circuit Breakers, SVR: Static Voltage Regulators, OLTC: On-load Tap Changers, EV: Electric Vehicle, ADN: Active Distribution Network, MG: Microgrids, APC: Active Power Curtailment, QCMIQP: Quadratic Constrained Mixed Integer Quadratic Programming, IPP: Independent Power Producer, WCA: Water Cycle Algorithm, VVO: Volt/Var Optimization, PCC: Point of Common Coupling, DER: Distributed Energy Resources, DPSO: Discrete Particle Swarm Optimization.

Table 1.2: Literature review on optimal voltage control

Ref.	Objective Function	Solution Strategy	Type of DG	Type of Network	Control scheme
[6]	Change of controlled variables	QP	HT, WT	ADN	Centralized
[7]	State disagreements, control energy, deviations between individual states	QP	Not mentioned	AC MG	Hierarchical, Distributed
[8]	Reactive power flow through distribution network and power loss	MOGA	PV, WT	ADN	Distributed
[9]	the total line losses number of switching in OLTCs and SVCs	MINLP	PV	unbalanced DN	Centralized

Ref.	Objective Function	Solution Strategy	Type of DG	Type of Network	Control scheme
[10]	The deviations of the DG active and reactive corrections	QP	HT, WT	ADN	Decentralized, Centralized
[12]	The difference between the state variables; their nominal values	QP	PV, WT, Natural gas cogenerator	AC MG	Hierarchical, Centralized
[13]	Voltage errors and reactive power deviation	PDIPM	Not mentioned	AC MG	Hierarchical
[14]	Voltage deviations; curtailed energy	QP	Not mentioned	ADN	Centralized
[15]	The voltage deviation, and other inputs from their reference values	QP	EV	DN	Centralized
[16]	The profit of a MG agent	MAS, SA	PV, Biomass	AC MG	Decentralized Distributed
[17]	The total amount of reactive power received collectively from all MGs	GA	FC, PV WT	DC MG	Hierarchical (Tertiary)
[18]	Total energy trading, operational cost and minimum environmental impact	MPSO, MINLP	PV, WT	AC MG	Hierarchical
[20]	The energy delivered to PEV and DG extracted power, system V deviation	NLP	PV, EV	ADN	Centralized
[21]	Active/reactive power of DG, OLTC, CB and SVR settings	MIQP	OLTC, SVR, DGU, CB	ADN	Centralized
[22]	Schedule the active and reactive injections of DERs in coordination with OLTC	MILP sensitivity coefficients	Not mentioned	ADN	Centralized
[32]	The effect of load changes on the voltages at PCCs and obtaining state feedback controller	LMI, convex	Not mentioned	AC MG	Decentralized
[33]	voltage errors and reactive power sharing error	KF, SA	Not mentioned	AC MG	Distributed
[34]	Total cost of generation	Lagrange multiplier	Not mentioned	AC MG	Hierarchical; Distributed
[35]	Adjustment cost and accelerate regulating speed	QP	PV, DS	ADN with multi MG	Distributed
[36]	Voltage control actions	EPSO	PV, batteries, controllable loads	Smart AC MG	Hierarchical
[37]	APC, tap and capacitor bank deviation	MIQP	PV	ADN	Centralized
[38]	reducing the comprehensive cost	MINLP, FAHPSO	Not mentioned	ADN	Centralized

Ref.	Objective Function	Solution Strategy	Type of DG	Type of Network	Control scheme
[39]	The sum of the DG reactive power owned by internal power producers	sequential QP	WT, PV	ADN	Decentralized Centralized
[40]	Network losses and MG′s power quadratic deviation from reference.	Global solver	Not mentioned	AC MG	Centralized
[41]	The cost and CO_2 emissions	QP	FC, micro turbines	AC MG	Centralized
[42]	The APC of PV and active power loss	ADMM	PV	ADN	Centralized, Distributed
[29]	the expected cost of purchasing electricity by reducing the load consumption	MINLP	PV, BESS	ADN	Centralized
[30]	voltage deviations overall system cost	MIP	shapeable loads, battery	DN	Centralized
[31]	Total charging cost voltage deviations	WCA	EV	DN	Centralized
[26]	The voltage deviation, power loss	ADMM	PV, WT	ADN	Distributed
[28]	The change in control inputs, cost of power curtailment, sum of maximum cost of voltage violations	QCMIQP	PV	ADN	Centralized Robust
[43]	CVR cost, network loss cost, VVO devices operating cost	DPSO, Droop control	EV, PV	ADN	Centralized Local
[44]	voltage deviations from referential set-points, control cost	SLP	PV, WT storage unit	ADN	Centralized stochastic

2

Model Predictive Control-Based Optimal Voltage Regulation of Active Distribution Networks with OLTC and Reactive Power Capability of PV Inverters

Contents

In Chapter 1, the challenges associated with integrating renewables based distributed generation and various solutions are explained. It also gives an introduction to voltage control methodologies.

This chapter presents a model predictive control-based centralized control approach for maintaining the voltages of the buses within permissible limits in the presence of high photovoltaic (PV) penetration. The proposed control scheme coordinates the actions of on-load tap changers and PV inverters optimally to fulfill the desired objectives. The objectives are minimization of change in control variables, slack variables, energy loss, and voltage error. These objectives are weighted to form the overall objective function. Three rules are formulated based on the severity of voltage magnitudes. The weights of the objectives are adjusted according to these pre-defined rules. Simulations are performed in an active distribution network (ADN) integrated with and without microgrids, where both demands and generations vary hourly over the day. As power is injected by the microgrids during most of the time of the day, the excursions of bus voltages are slightly higher in the microgrids integrated ADN. Moreover, the incorporation of the proposed rule-based MPC drastically reduces the energy loss due to active power loss in distribution networks, as evident from the simulation results obtained by comparing the proposed approach with an existing MPC-based approach.

2.1 Introduction

Electric distribution networks are experiencing a fundamental transfiguration due to increase in penetration of DER. With relatively easy installation procedures, zero green energy emissions, and abundant input energy, PV generators have evolved as the complete game-changer in the DG technology [45]. According to international renewable energy agency (IRENA), installed capacity of solar PV globally would rise six-fold by 2030 (2,840 GW) compared to installations in 2018 (480 GW) [46]. However, incorporation of dispersed PV units in large scale in distribution networks would cause over-voltage, under-voltage, line congestions and fluctuation of feeder power [8, 47]. Moreover, PV units possess dynamic characteristics concerning various scenarios, namely, installation location in the feeder, nature of the feeder, loading conditions, etc. [48].

The system voltage fluctuation is one of the most severe problems that arises due to reverse power flow caused by DER [8,11,16,25,37], [48]. Several strategies have been adopted in the distribution networks to address short-term over/under voltage issues [8,16,37]. Some of the conventional methods to mitigate voltage variations are automatic OLTC, static VAr compensators, set-voltage regulators, and

shunt capacitors [25, 37], [48]. However, non-coordination among these methods would cause competition among the control actions or among the newly installed PV units, thereby inducing oscillations in the network [37]. In [37], a multi-stage optimal operation of cascaded regulators and PV inverter has been proposed for the optimal voltage regulation while ensuring minimal activation of regulating devices. Ref. [25] introduces a strategy to coordinate several regulating devices. However, distribution network operator (DNO) cannot control the voltage profile using only conventional regulators as they are restricted by their slow response and discrete voltage regulation [6, 11]. Moreover, reinforcement of the network to deal with these challenges is not economically acceptable for the DNO. Therefore, advanced control strategies are required to effectively regulate the voltage profile. The utilization of reactive power capability of smart inverter interfaced PV units has been explored in [45, 47, 49]. Moreover, curtailment of PV power during the peak generation hours is one of the less encouraging options to mitigate voltage rise [6, 48]. Following this, energy storage is introduced in [14] to overcome the shortcomings of the curtailment process. However, additional energy storage upraises the overall investment and operational cost.

The coordinated centralized approaches are preferred over the local decentralized approaches as the latter cannot handle the negative interactions and high DG penetration [6, 14]. In [16], a distributed approach to regulate network voltage using bi-level game bidding process is reported. However, such method is case specific due to its dependency on accuracy of the coordinated algorithm which needs to be updated when system condition changes [20]. Some works have been reported on multi-stage control structure to regulate the voltages [20, 50]. Three-stage optimization algorithm is proposed in presence of DG units, OLTC, and plug-in electric vehicles in [20]. In [50], a two-stage real-time control scheme based on zoning of distribution networks for voltage regulation is devised. Although considerable works have been reported in literature, it would be interesting to develop an advanced control strategy that coordinates the conventional regulating devices and PV inverters, while minimizing the energy losses in distribution networks.

Recently model predictive control has gained world-wide interest due to its capability to adapt to model inaccuracies and DG fluctuations [6, 7, 10, 14, 15, 21, 26, 44]. Owing to its prediction capabilities, MPC has been modeled for voltage regulation in active distribution networks in presence of OLTC and DG units [6]. Here, the controller coordinately modulates the DG units' output and the voltage set-point of the OLTC to maintain the voltages within acceptable values. An MPC-based voltage

regulation scheme is provided in [6] to coordinate the actions of different DG units and energy storage systems (ESS). In [14], basically two operational modes are proposed within MPC; namely, preventive control and corrective control to classify the control actions depending upon the severity of the problem. Although the reactive power capability of the inverter interfaced DG units is explored, power variations in DG units and the loads throughout the day are not considered in [14]. Moreover, ESS technology is still expensive to implement in distribution level. An advanced technology to control PV inverters can be found in [49]. Ref. [51] presents an autonomous smart PV inverter technology that can be controlled as dynamic reactive power compensator to modulate voltage variations. It is suggested that a PV inverter with very less response time can perform similar functions as DSTATCOM in distribution networks [51]. Although the approach in [51] is focused on the reactive power exchange capability of PV inverters through different operating modes, it lacks an optimal coordination scheme. A double-time scale voltage control approach, coordinating the actions of DG units and OLTC considering temporal characteristics of OLTC is presented in [21]. Ref. [10] provides an MPC-based approach to refine the reactive power set-point corrections of DG units centrally, obtained from the local control. In [26], MPC is used as local voltage control strategy to frequently tune the local curve of DG units to adjust with the DG uncertainties. A distributed MPC is proposed as a secondary control scheme for autonomous microgrids in [7]. Although the aforesaid works have investigated to devise approaches for voltage regulation using MPC, none of them has formulated the coordinated control approach of OLTC and PV inverters which can minimize energy losses and can maintain the bus voltages, as well.

In this context, the present work proposes a rule-based MPC approach to optimally coordinate different control actions to maintain voltages within the prescribed limits as well as minimize energy losses in the presence of PV units. With constant rise of PV units in the distribution network, over voltage has become a common issue and mostly observed around mid-day. The proposed MPC approach effectively operates to regulate the bus voltages following the load and generation variations. However, during other times of the day, when bus voltages are within the desired limits, the proposed MPC approach is aimed at minimizing energy loss of the network. The proposed controller follows a set of *if-then-else* rules to effectively utilize the MPC in controlling bus voltages as well as minimizing energy losses. The main contributions of this work are:

- To develop an MPC-based approach that follows a set of *if-then-else* rules for voltage regulation and energy losses minimization.

- To modulate PV inverters' output for reactive power compensation in voltage regulation and energy loss minimization.
- To effectively utilize MPC as a real-time control.

This work is organized as follows: Section 2.2 describes the modeling of active distribution networks. The MPC-based approach is illustrated in Section 2.3. Case studies are presented in Section 2.4, while Section 2.5 summarizes this work.

2.2 Active distribution network modelling

A radial distribution network is considered here with N number of buses. Let $\Omega = 1, 2, ..., N$ be the set of buses. It is assumed that the bus-1 is the secondary side of step down transformer equipped with OLTC. The distribution lines of the network are denoted as set of edges $\epsilon = (i, j) \subset \Omega \times \Omega$. Any distribution line is modeled as series admittance $Y_{ij} = 1/(R_{ij} + j\omega \mathrm{X}_{ij})^{-1}$, where R_{ij}, X_{ij}, are the line resistance and reactance and ω is the system frequency. It is assumed that all the operations described here are for three-phase balanced network. The Newton Raphson method is adopted to model the power flow equations of the network. The power flow equations of the ADN are modelled as:

$$P_i = \sum_{i=1}^{N} |V_i||V_j|Y_{ij}cos(\theta_{ij} + \delta_j - \delta_i) \tag{2.1}$$

$$Q_i = \sum_{i=1}^{N} |V_i||V_j|Y_{ij}sin(\theta_{ij} + \delta_j - \delta_i) \tag{2.2}$$

where δ_i and δ_j are the voltage phase angles at bus i and j, respectively. P_i and Q_i represent the active and reactive power at bus i, respectively.

The loads are modelled as PQ loads varying hourly over the day. The active and reactive power (P_L and Q_L) consumed by loads are specified according to the types of load, namely, residential, commercial or industrial. The load profiles are depicted in Fig. 2.1(a). The PV units are represented as power injectors; both active and reactive power varying over the day. As the PV generations are functions of solar irradiance, the active power injection at each bus varies hourly over the day. The active power generation of PV, P_{PV} is shown in Fig. 2.1(b). Reactive power generation, Q_{PV} is computed as,

$$Q_{PV} = \sqrt{{S_{PV}}^2 - {P_{PV}}^2}$$

where, S_{PV} is the rating of the PV inverter. The power injection by generators are represented as negative of power absorption by loads.

Microgrids represent distributed generators, loads, and distributed storages. Here, microgrids are represented as point of common coupling (PCC) power as shown in Fig. 2.1 (c). The microgrids are modelled as active power injectors (absorbers) according to injection (absorption) of real power to (from) the distribution networks. Negative PCC power implies power injection by microgrids to distribution networks. Here, the reactive power injection (absorption) of the microgrids to (from) the ADN is not considered. The control of these microgrids is not within the scope of this work.

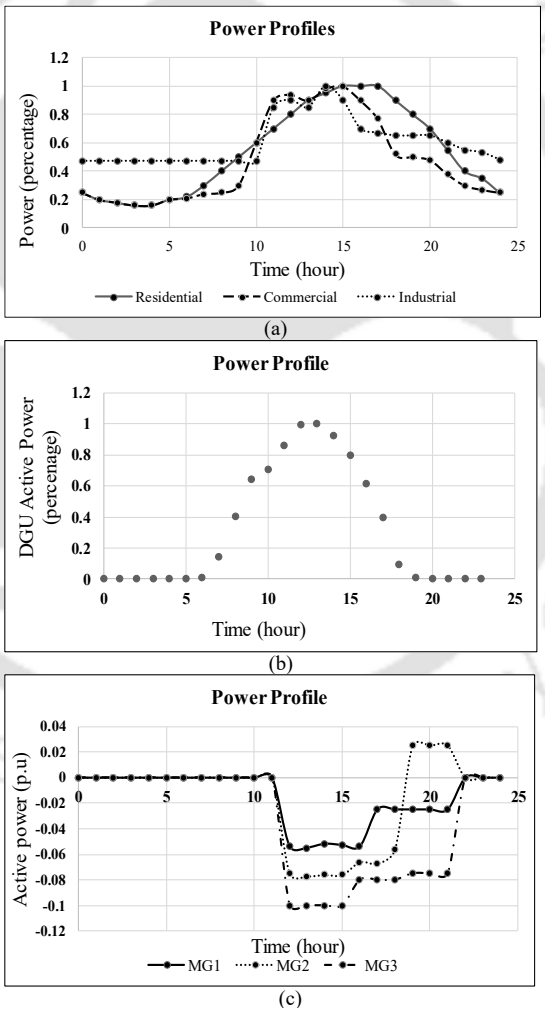

Figure 2.1: Power profiles of (a) loads: residential, commercial and industrial, (b) PV generation and (c) PCC power.

2.3 Coordinated control of OLTC and PV inverters utilizing MPC to regulate voltages

The reference voltage of OLTC ($V_{tap'}$), active power and reactive powers of PV inverters (P_{PV} and Q_{PV}) are considered as the potential candidates for control actions. The proposed approach aims to coordinate the actions of these control variables in such a manner that the cheapest control actions (PV reactive power and OLTC) are utilized more often to regulate voltage than PV active power curtailment. The desired limit of voltage is considered to be [0.95 1.05] p.u. The operating principles of MPC and the voltage control problem formulations are described in Sections 2.3.1 and 2.3.2, respectively.

2.3.1 Operating principles of MPC

As illustrated in Fig. 2.2, the data acquisition system of DNO collects the essential measurements from the remote terminal units (RTU), such as, nodal voltages, active and reactive power of DG units, voltage set-point of OLTC. MPC, being deployed at the heart of DNO for real-time optimal control of voltages in ADN, extracts this information and calculates a sequence of optimal control actions in steps, defined as control horizon (N_C) and predicts the responses of these actions in steps, known as prediction horizon (N_P) as illustrated in Fig 2.3(a). A sequence of control inputs $u(k)$, actual outputs $y(k)$, and predicted outputs $y_P(k+1)$ are shown in Fig. 2.3(b). Here, k refers to the sampling instants.

If sampling time, t_s, is 10 seconds and the control and prediction horizon are both equal to 3, then at each sampling instant, a sequence of control actions, $[\Delta u(k),\ \Delta u(k+1),\ \Delta u(k+2)]$ is computed in such a manner that the predicted outputs, $[y_P(k+1),\ y_P(k+2),\ y_P(k+3)]$ reach the set-point target as shown in Fig. 2.3(b). From the sequence of control actions, obtained by optimization of an objective function, the first control action $\Delta u(k)$ is taken into consideration, while the rest are discarded. The network elements due to latency take a while to bring the control actions into practice. The control sampling time is chosen accordingly to accommodate the latencies. This whole process is repeated at the next sampling instant with a new set of measurements that are reflected upon the elements after the implementation of the control actions. This interesting feature of MPC is described as a moving horizon or receding horizon control approach. If any new information is observed in the form of real-time measurements at some instant between the previous and the current instant, this distinguishing property of MPC helps to consider it immediately, rather than postponement of control actions to be

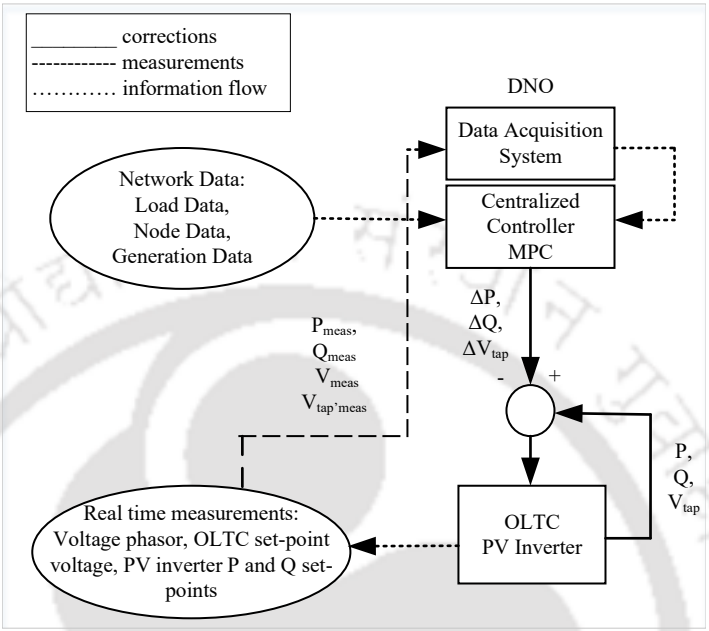

Figure 2.2: Block diagram of the MPC-based coordinated control strategy.

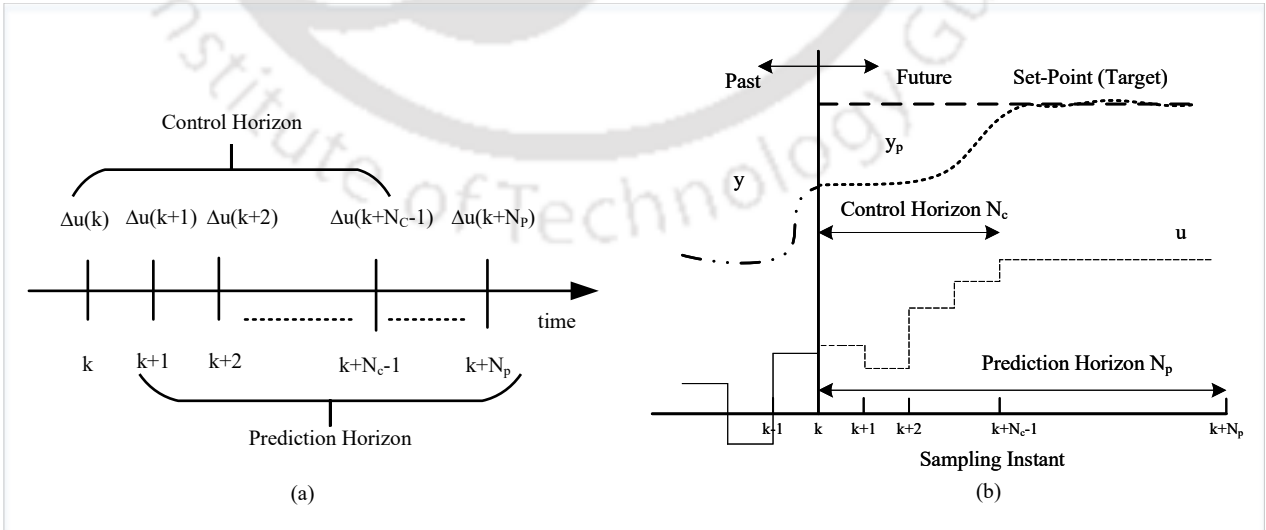

Figure 2.3: Operating Principles of MPC: (a) control and prediction horizon, (b) MPC illustration.

taken based on new measurements till the next control interval, $N_C.t_s$ seconds [52].

2.3.2 Problem formulation

The operation of MPC requires an empirical model of a plant, which is represented by a state-space model [6, 53]. Let the state-space model be represented by:

$$x(k+1) = \boldsymbol{A}x(k) + \boldsymbol{B}\Delta u(k) \tag{2.3}$$

$$y(k) = \boldsymbol{C}x(k). \tag{2.4}$$

It is to be noted that change in control inputs are the inputs of the system rather than the control inputs. The bus voltages are the states and the output variables of the system. Active as well as reactive powers of PV inverters and the reference voltage of OLTC are the controllable resources. The uncertainties of PV generation and loads are considered as disturbances. While the voltages of certain buses increase beyond the limits [0.95 1.05] during day time due to high solar irradiance, the PV inverter remains idle during the other times of the 24 hour span. The capability of the PV inverter to inject or absorb reactive power to compensate voltage deviations has been reported in the recent literature [49, 51], thereby adjustment of reactive power set-points of PV units by MPC is one of the control actions described in this study. Here, PV inverters would be capable of injecting a finite amount of reactive power (typically 44%) even at 100% of active power rating [51]. Further, the internal losses of PV inverters are assumed to be zero, since these are not comparable with the total line losses of distribution networks. However, if these are of significant number, the network owners, which are the beneficiaries of this loss reduction, need to pay this to the customers or the PV owners. Alternatively, the network owners need to appropriately devise incentives to the PV owners.

The MPC considered here, calculates an optimal set of control actions $\Delta u(k+i)$ for $i = 0, 1, 2, ..., N_C - 1$, where,

$$\Delta u(k) = [\Delta V_{tap}(k),\ \Delta Q_{PV}(k),\ \Delta P_{PV}(k)]^T$$

are the control variables. The length of the prediction horizon N_P should be at least equal to or greater than the control horizon length N_C [6, 53]. It is assumed that $\Delta u(k+i) = 0$ for $i \geq N_C$. Let, the set of input variables that is calculated at every sampling instant be represented by Δu:

$$\Delta u(k) = [\Delta u(k)^T \Delta u(k+1)^T .... \Delta u(k+N_C-1)^T]^T \tag{2.5}$$

and the set of predicted output variables be represented by $\boldsymbol{y_P}$:

$$\boldsymbol{y_P} = [y(k+1|k)^T y(k+2|k)^T .....y(k+N_P|k)^T]^T \tag{2.6}$$

The future state variables and the predicted output can be calculated sequentially with the help of control variables [53]. The future states variables are:

$$x(k+2) = \boldsymbol{A}x(k+1) + \boldsymbol{B}\Delta u(k+1) \tag{2.7}$$

Using eq. (2.3) in eq. (2.7)

$$x(k+2) = \boldsymbol{A}^2 x(k) + \boldsymbol{AB}\Delta u(k) + \boldsymbol{B}\Delta u(k+1) \tag{2.8}$$

Thus, the prediction matrices can be formulated as:

$$y(k+1) = \boldsymbol{C}x(k+1) = \boldsymbol{C}[\boldsymbol{A}x(k) + \boldsymbol{B}\Delta u(k)] \tag{2.9}$$

which implies,

$$y(k+1) = \boldsymbol{CA}x(k) + \boldsymbol{CB}\Delta u(k) \tag{2.10}$$

Similarly, $y(k+2)$ can be written as:

$$y(k+2) = \boldsymbol{C}x(k+2) = \boldsymbol{CA}^2 x(k) + \boldsymbol{CAB}\Delta u(k) + \boldsymbol{CB}\Delta u(k+1) \tag{2.11}$$

Thus, in concise form, the prediction matrices can be represented in the following form [53]:

$$\boldsymbol{y_p} = \boldsymbol{F}x(k) + \boldsymbol{\phi}\Delta u \tag{2.12}$$

where,

$$\boldsymbol{F} = [\boldsymbol{CA} \quad \boldsymbol{CA}^2 \quad \boldsymbol{CA}^3 .... \boldsymbol{CA}^{N_P}]^T \tag{2.13}$$

and

$$\phi = \begin{bmatrix} \boldsymbol{CB} & 0 & 0.... & 0 \\ \boldsymbol{CAB} & \boldsymbol{CB} & 0.... & 0 \\ \boldsymbol{CA^2B} & \boldsymbol{CAB} & \boldsymbol{CB}.... & 0 \\ \boldsymbol{CA}^{N_P-1}\boldsymbol{B} & \boldsymbol{CA}^{N_p-2}\boldsymbol{B} & \boldsymbol{CA}^{N_P-3}\boldsymbol{B}.... & \boldsymbol{CA}^{N_P-N_C}\boldsymbol{B}. \end{bmatrix} \tag{2.14}$$

The prediction matrices are formulated with the aid of the calculated set of optimal control actions. The optimal control actions are computed in such a manner that the predicted outputs reach within

Table 2.1: Description of the rules.

Rule No.	Voltage Range	Weights of objectives
1	$V > 1.1$ or $V < 0.9$	$R_P = 100, R_Q = 5,$ $R_{V_{tap}} = 1, Q = 0.001,$ $S = 1000, T = 0$
2	$0.9 \leq V < 0.95$ or $1.05 < V \leq 1.1$	$R_P = 500, R_Q = 10,$ $R_{V_{tap}} = 1, Q = 0.001,$ $S = 1000, T = 0$
3	$0.95 \leq V \leq 1.05$	$R_P = 1000, R_Q = 10,$ $R_{V_{tap}} = 1, Q = 0.001,$ $S = 0, T = 1$

the desired limits [53]. Here, the optimization problem is modeled as quadratic programming problem as described in (2.15).

$$f(x) = min \begin{cases} \sum_{i=0}^{N_C-1}[\|\Delta V_{tap}(k+i)\|^2_{R_{V_{tap}}} + \|\Delta P_{PV}(k+i)\|^2_{R_P} \\ +\|\Delta Q_{PV}(k+i)\|^2_{R_Q}] \\ \sum_{i=1}^{N_P}\|V_{ref}(k+i|k) - V_P(k+i|k)\|^2_Q \\ \|\sigma\|^2_S \\ \sum_{i=1}^{N_P}\|P_{loss}\|^2_T \end{cases} \tag{2.15}$$

In eq. 2.15, the reference voltage set-point, V_{ref} is set to 1.0 p.u. $\boldsymbol{R}$ ($\boldsymbol{R_P}$, $\boldsymbol{R_Q}$ and $\boldsymbol{R_{V_{tap}}}$), $\boldsymbol{Q}$, $\boldsymbol{S}$, and $\boldsymbol{T}$ represent the weights associated with the different objectives: minimization of change of control variables (PV active power, PV reactive power, and OLTC reference voltage), voltage error, slack variables, and energy loss, respectively. Based on the magnitude of voltages three conditions are defined through *if-then-else* rules to establish the MPC problem as a rule-based MPC (RBMPC). The weights of the objective function are altered according to the three rules. The rules are described in Table 2.1.

The weights in the proposed approach are determined empirically based on the dependence of control actions on the magnitude of voltages. The weighing matrices are further described as follows:

- Output weighing matrices: $\boldsymbol{Q}$ and $\boldsymbol{T}$ are the output (voltage) weighing matrices. $\boldsymbol{Q}$ is associated with voltage error and $\boldsymbol{T}$ is associated with energy loss. Both the voltage error and energy loss are functions of voltage magnitudes. In the proposed approach, $\boldsymbol{T}$ is set to 0 when the voltage magnitude of the buses is outside the limits [0.95, 1.05] p.u to signify absence of power loss

objective. $\boldsymbol{T}$ is set to 1 when voltages reach the desired limits. This implies that the power loss objective comes into picture only when the voltage magnitudes reach the defined limits. Minimization of voltage error is of less significance than maintaining the voltages within the desired limits. Keeping all other weights constant, $\boldsymbol{Q}$ is changed from 0 to 0.001, then 0.05, 0.5 and 1. There is not much change in the responses found due to variations in $\boldsymbol{Q}$ alone. After a series of trial, $\boldsymbol{Q}$ is set to 0.001 (low priority) for all the rules described in the proposed approach. Hence, $\boldsymbol{Q}$ and $\boldsymbol{T}$ vary from (0, 1).

- Input weighing matrices: $\boldsymbol{R}$ ($\boldsymbol{R_P}$, $\boldsymbol{R_Q}$ and $\boldsymbol{R_{V_{tap}}}$), referred as input diagonal weighing matrix, allows input control variables to be weighted according to their relative importance. The weight assigned to each control variable is directly related to the operational cost of the device to regulate voltages. Minimization of control variables implies to the minimal use of these control actions for maintaining voltages within the desired limits. The proposed approach intends to utilize active power curtailment (expensive control action) the least. For minimal usage, $\boldsymbol{R_P}$ is weighted more in comparison to $\boldsymbol{R_Q}$ and $\boldsymbol{R_{V_{tap}}}$ for all the rules in the proposed approach. $\boldsymbol{R_P}$ is assigned after performing certain trials. For example, when assigning $\boldsymbol{R_P}$ value lesser than 70, it is observed that MPC tries to control the voltage by utilizing the curtailment action more as compared to reactive power modulation. Thus, when the voltages deviate from the prescribed limits by a large amount, $\boldsymbol{R_P}$ is set to 100 for better results. Once the voltages reach near to the desired limits, the use of curtailment action needs to be further minimized. The greater value of $\boldsymbol{R_P}$ ensures less usage. However, there is no significant change in usage of these actions when $\boldsymbol{R_P}$ is varied between 200 and 700. That is why $\boldsymbol{R_P}$ is set to 500 in the intermediate range. Moreover, $\boldsymbol{R_P}$ is set to 1000 once the voltages reach the prescribed limits. This is done to penalize it more so as to reduce the possibility of using active power curtailment as control action. Nevertheless, no noticeable change is seen when $\boldsymbol{R_P}$ is set greater than 1000 in this case. Being cheaper than active power curtailment but expensive than OLTC reference voltage, $\boldsymbol{R_Q}$ is weighted five times (voltage deviations excessively large) and ten times (other instants) more than $\boldsymbol{R_{V_{tap}}}$. The weight $\boldsymbol{R_Q}$ is assigned keeping in mind the availability of reactive power capability after extraction of active power from PV inverters. It is noteworthy that if the cheaper control actions are unable to control the bus voltages, expensive control actions could be used to fulfill the desired objectives. For this reason, $\boldsymbol{R_P}$ and $\boldsymbol{R_Q}$ are not set to zero in any of the prescribed rules. Considering reference voltage of OLTC as the cheapest control action, $\boldsymbol{R_{V_{tap}}}$ is kept constant for all the scenarios ($\boldsymbol{R_{V_{tap}}} = 1$). Some operators might feel OLTC action more

expensive than reactive power modulation due to their limited number of usability. The weights need to be adjusted according to the desired needs. Hence, $\boldsymbol{R}$ varies in the range from (0, 1000).

- Weights of slack variables: The slack variables are used with the output constraints to omit the option of infeasibility in any case. To minimize the use of slack variables, the weighing factor, $\boldsymbol{S}$ is weighted the maximum (1000). $\boldsymbol{S}$ can be any large value. Once the voltages reach the desired limits, $\boldsymbol{S}$ is set to zero as there is no use of slack variables.

The upliftment of the bus voltages is due to the high penetration of PV during day time. As power generation by PV is a function of solar irradiance, the voltages are within the desired limits during most of the time. The rule-based MPC is formulated to enhance its effectiveness during that period of time by introducing minimization of active power distribution loss as one of the main objectives of MPC. While the bus voltages cross the emergency limit (0.9, 1.1) p.u, the MPC strictly makes an attempt to firstly bring the voltage within [0.9, 1.1] p.u and finally within the desired limits. Moreover, as the voltages come nearer to the desired limits, the MPC starts penalizing the costly control actions and include minimization of energy loss as the most important objective. When the voltages are out of emergency limits, the MPC, without taking into consideration the cost of control actions, explicitly makes an attempt to regulate the bus voltages without delay.

Special attention should be given to the constraints of the objective function. In the case of PV, as active power production depends upon weather conditions, the controller cannot request the PV to generate more than the power that is being produced at any instant. However, it can request active power reductions by partial curtailment. While the active power is limited in the upper bounds, the reactive power of PV sources is considered fully controllable, provided the capacity constraint is maintained at every step of the iteration as in eq. (2.22). Eqs. (2.19)-(2.22) describe the constraints associated with control inputs (reference voltage of OLTC, active and reactive power set-points of PV inverters). Moreover, there should be constraints on the rate of change of control inputs to protect the inverters as well as the OLTC from fast transitions of ramping up or ramping down movements. The constraints in eqs. (2.16)-(2.18) are used to limit the ramp movements of the control inputs. The equality and inequality constraints are defined from equations (2.16)-(2.24)

$$\Delta V_{tap}^{min} \leq \Delta V_{tap}(k+i) \leq \Delta V_{tap}^{max} \tag{2.16}$$

$$\Delta Q_{PV}^{min} \leq \Delta Q_{PV}(k+i) \leq \Delta Q_{PV}^{max} \tag{2.17}$$

$$\Delta P_{PV}^{min} \leq \Delta P_{PV}(k+i) \leq \Delta P_{PV}^{max} \tag{2.18}$$

$$V_{tap}^{min} \leq V_{tap}(k+i) \leq V_{tap}^{max} \tag{2.19}$$

$$Q_{PV}^{min} \leq Q_{PV}(k+i) \leq Q_{PV}^{max} \tag{2.20}$$

$$P_{PV}^{min} \leq P_{PV}(k+i) \leq P_{PV}^{max} \tag{2.21}$$

$$P_{PV}^2 + Q_{PV}^2 \leq S_{PV}^2 \tag{2.22}$$

$\forall i = 0, 1, ...N_C - 1.$

The output constraints are softened by application of soft constraints σ as in eq. (2.23). Here, σ_1 and σ_2 are the slack values that are added to the output constraints such that the MPC operation does not stop at any instants of time due to infeasible results. Here, 1 denotes the unitary vector. Eq. (2.24) represents the equality constraint that is maintained at each sampling instant.

$$-\sigma_1 1 + V^{min}(k+i) \leq V(k+i|k) \leq V^{max}(k+i) + \sigma_2 1 \tag{2.23}$$

$$V(k+i|k) = V(k+i-1|k) + \frac{\delta V}{\delta V_{tap}{}^T}\Delta V_{tap}(k+i-1) + \frac{\delta V}{\delta Q_{PV}{}^T}\Delta Q_{PV}(k+i-1) + \frac{\delta V}{\delta P_{PV}{}^T}\Delta P_{PV}(k+i-1) \tag{2.24}$$

$\forall i = 1, 2, ..., N_P.$

The sensitivity matrices $\boldsymbol{\delta V / \delta V_{tap}{}^T}$ are evaluated by running Newton Raphson power flow analysis twice with single tap position difference. $\boldsymbol{\delta V / \delta Q_{PV}{}^T}$ and $\boldsymbol{\delta V / \delta P_{PV}{}^T}$ are obtained from inverse of the Jacobian Matrix.

The proposed approach with the MPC algorithm is described in Fig. 2.4. The flowchart of the proposed approach is depicted in Fig. 2.4(a). Fig. 2.4(b) describes the MPC algorithm and the methodology of problem formulation.

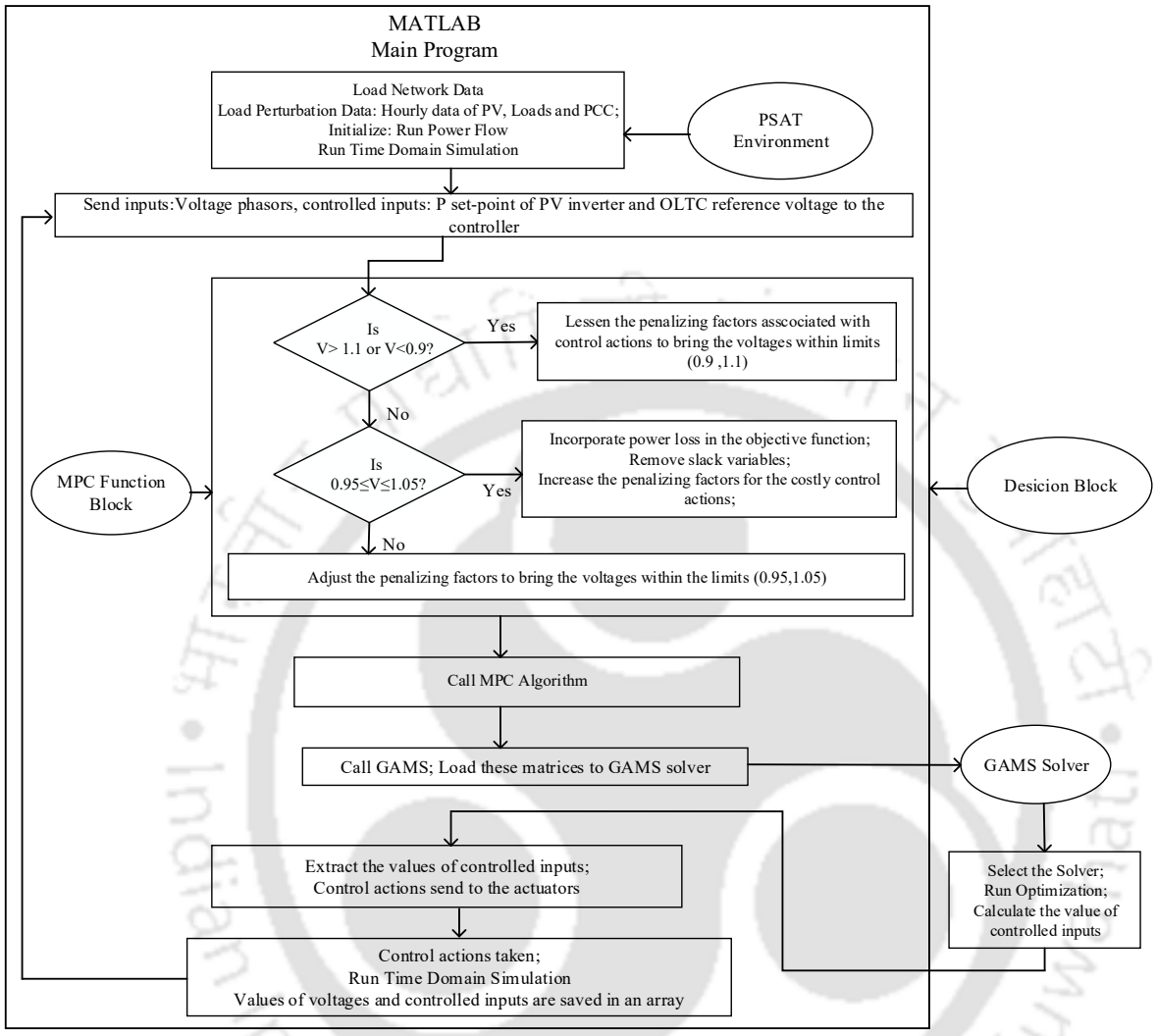

(a)

Algorithm: Model Predictive Control

Inputs: Voltage phasor, OLTC reference voltage, active and reactive power set-points of PV
Outputs: Changes in control inputs, voltage phasor

Begin
1. Determine the control and prediction horizon
2. Set the dimensions of control inputs, controlled outputs and output reference
3. Set the limits: control inputs, change of control inputs, controlled outputs
4. Set the weights of the associated objectives according to the predefined rules
5. Prepare the weight vectors
6. Build up the matrices A, B and C of the prediction model
7. Load the sensitivity matrices to prepare the B matrix
8. Update the controller with new set of measurements
9. Formulate the Prediction matrices (state and output variables) as
$y_P = Fx(k) + \Phi\Delta u$ from the state space equations: $x(k+1) = Ax(k) + B\Delta u(k)$, where $\Delta u(k) = u(k) - u(k-1)$
10. Express the equations of constraints in compact form:
$$u_{min} \leq C_1 u(k-1) + C_2 \Delta u \leq u_{max}$$
$$-\sigma_1 1 + y_{min} \leq Fx(k) + \Phi\Delta u \leq y_{max} + \sigma_2 1$$
11. Formulate the Quadratic Problem
End

(b)

Figure 2.4: (a) Flowchart of proposed method (b) MPC algorithm.

Table 2.2: Ratings of PV and microgrid.

Transformer	PV Inverter Rating	Microgrid Rating	Penetration Level of PV
10 MVA	347 kVA	1 MW	100%

2.4 Simulation results and analysis

This section shows the effectiveness of the proposed rule-based MPC strategy in 33-bus distribution network as depicted in Fig. 5. The simulations are conducted in MATLAB R2018a and modelled using power system analysis toolbox (PSAT) [54]. The optimization problem is then solved by the CONOPT solver in the GAMS optimization platform [55]. The experimental computations are carried out on PC with Intel core i5-6500 processor running at 3.20 GHz and 8 GB of RAM. The network data of the test system are taken from [56] with 10 MVA and 12.6 kV as base. For analysis, IEEE 33-bus system is modified to accommodate photovoltaic generators and the loads, evenly distributed in all the buses as in Fig. 2.5(a). Besides, three microgrids are integrated into the distribution network at bus 13, 15 and 33 as shown in Fig. 2.5(b). The power profiles of PV units, loads and PCC (as microgrids) are shown in Fig. 2.1. The reference voltage of OLTC along with the PV active and reactive power set-points are considered as the control inputs to the MPC. The minimum and maximum change in active power generation and reactive power generation/consumption are taken as 10% of the total capacity of generation [6]. Here, OLTC reference voltage is varied between [0.9, 1.1] p.u for all the simulation studies. The bus voltages are the controlled variables in the MPC model and also considered as states of the system. In the MPC computations, the length of the prediction horizon steps is chosen same as the length of control horizon steps so that the computational burden is reduced. With a sampling interval of 10 seconds, the control and prediction intervals of MPC are chosen as 30 seconds. Furthermore, it is presumed that the system is equipped with a well-established communication infrastructure for uninterrupted information exchange. The ratings of the different elements of ADN are listed in Table 2.2.

The considered model is simulated initially assuming PV units (output varied hourly) and loads in the absence of a controller. Fig. 2.6 shows the voltage profile of the radial network with and without microgrids. As discussed above, microgrids represent distributed generators, loads, and distributed storages and represented as PCC power as shown in Fig. 2.1(c). It is clearly observed that voltages at

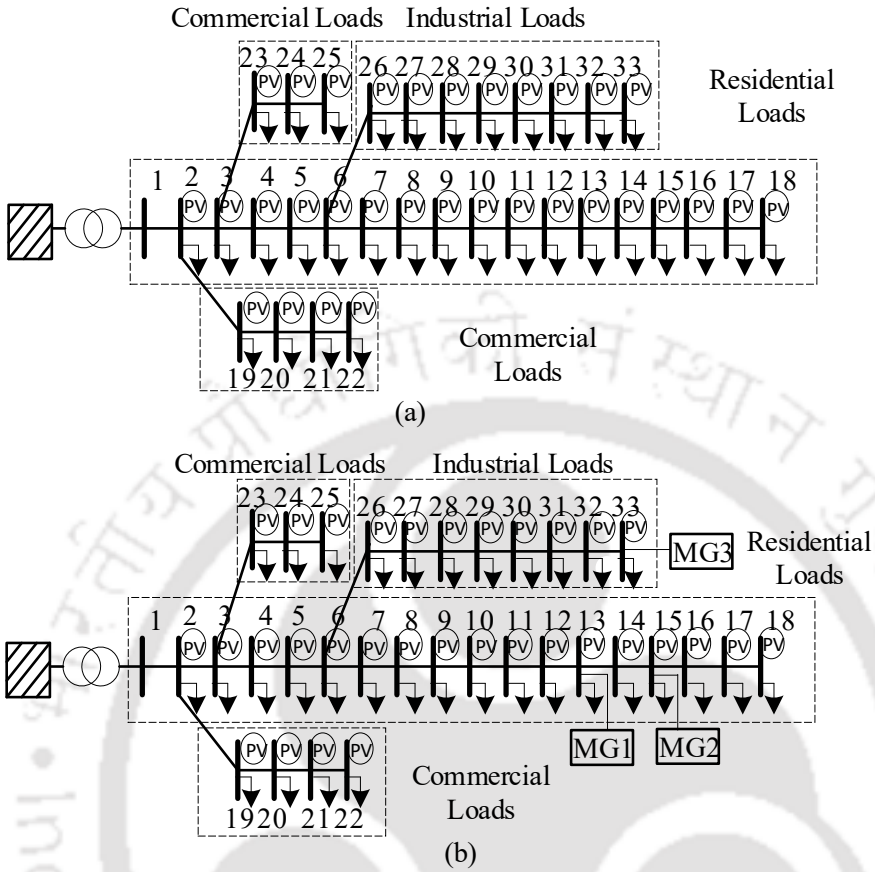

Figure 2.5: Test network: 33-bus distribution systems with time-varying loads and generations (a) without microgrids (b) with microgrids

certain buses are more affected by penetration of PV units than rest of the buses. The adverse effects of high PV penetration are seen on the voltage profile around mid-day. This overvoltage is result of over-generation due to high PV penetration (100%) and load variations in the network. Moreover, PV inverters are injecting finite amount of reactive power to the system even at 100% of active power rating, thereby, increasing the voltage. Integration of additional microgrids into the radial network further aggravates the system voltage as the microgrids are in dispatch mode for most of the time. Besides, the control of these microgrids is not considered here. It is noteworthy that the integration of microgrids at PCC is to worsen the system condition. Furthermore, energy losses are calculated for the above system and tabulated in Table. 2.3.

Next, to regulate the bus voltages effectively, central RBMPC is placed to coordinate OLTC and power set-points of PV inverters. Here, MPC tries to regulate the bus voltages using *if-then-else* rules, where the objectives of the controller are altered with respect to the magnitude of bus voltages. It is

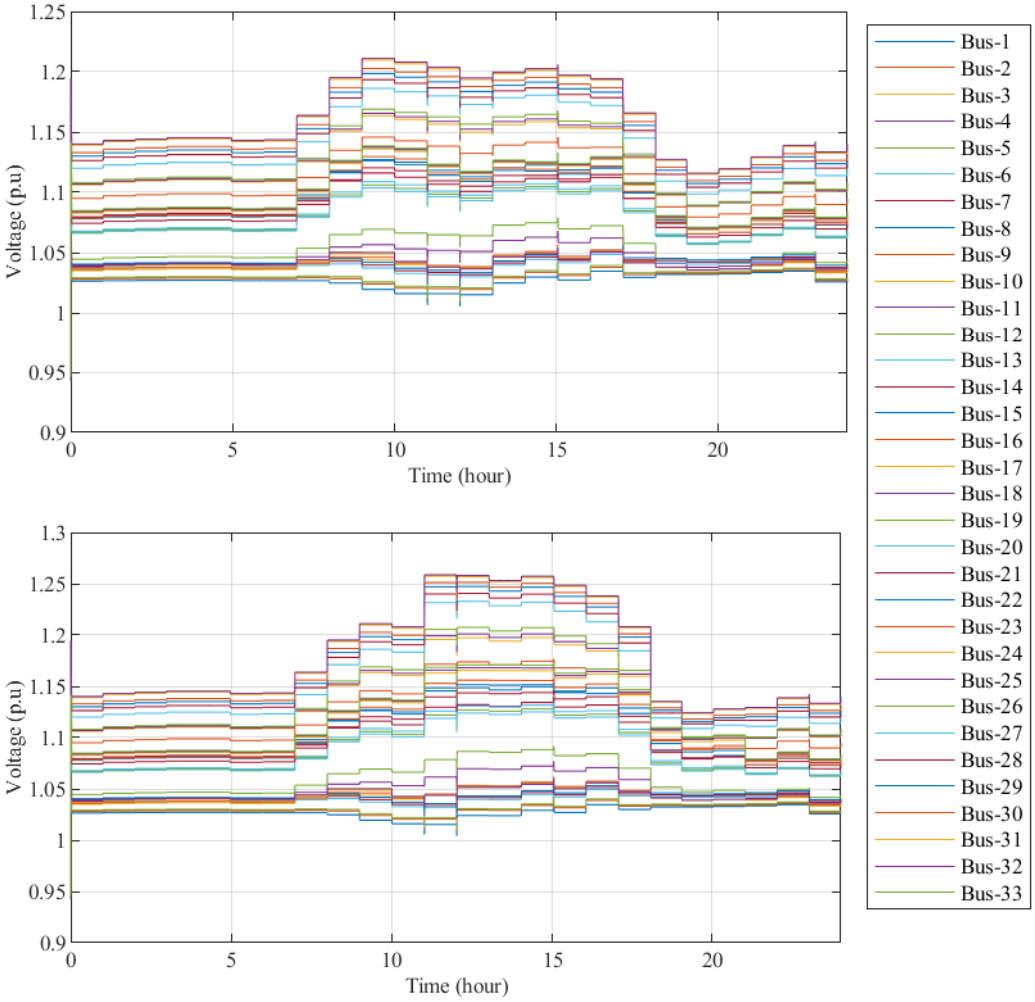

Figure 2.6: Plots of voltage profile in absence of controller: (a) without microgrids (b) with microgrids for 33-bus distribution networks

seen that out of 33 buses, voltages at buses 13, 14, 15, 16 and 17 show similar profiles (maximum value compared to the rest of the buses) owing to less electrical distance and therefore, further analysis is carried out for only bus-15. Fig. 2.7 shows the voltage, active power and reactive power profiles at bus-15 for a typical day. It can be observed that, without microgrids in the network, the voltage at bus-15 rises to a maximum value of 1.189 p.u at the 13th hour. Now, since the voltage magnitude is beyond 1.1 p.u, the MPC with rule-1 tries to bring the voltage of that bus within the defined limits (0.9, 1.1) p.u by utilizing the available control inputs. Following the action, voltage at bus-15 reduces to 1.1 p.u within 32.4 seconds. Once the bus voltage reaches 1.1 p.u, MPC follows rule-2 immediately to bring the voltages within the limits (0.95, 1.05) p.u by penalizing the expensive control actions by

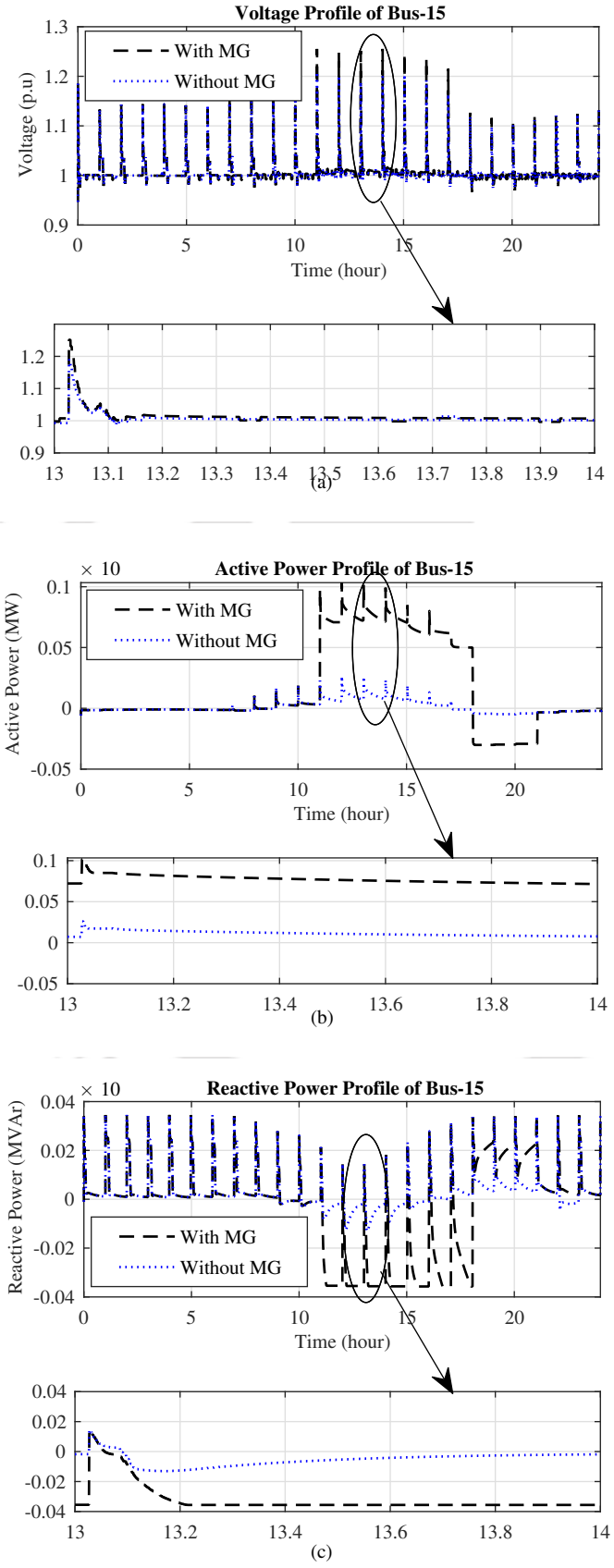

Figure 2.7: Plots of: (a) voltage profile at bus-15 (b) active power profile at bus-15 and (c) reactive power profile at bus-15 for 33-bus distribution networks

Table 2.3: Comparison of energy loss obtained without controller and with RBMPC in the presence and absence of microgrids for 33-bus distribution networks.

	Curtailed Energy, E_{cur} (kWh)	Energy loss, E_{loss} (kWh)
Without Controller:		
Without MG	-	18980
With MG	-	21092
RBMPC:		
Without MG	116	3337
With MG	166	3939

a larger amount than in rule-1. Thereafter, voltage reaches to 1.05 p.u from 1.189 p.u within 75.6 seconds. Once the bus voltages are within the prescribed limits, i.e., [0.95, 1.05] p.u, the proposed controller follows rule-3 to minimize active power losses in the distribution network. It is to be noted that, as the maximum contribution of PV units occurs around mid-day, the analysis is conducted for those instants. Therefore, it can be concluded that performance of the proposed controller is satisfactory. The optimal curtailment of active power and modulation of reactive power using the proposed controller are quite evident from Fig. 2.7. The simulation also shows the effectiveness of RBMPC in minimizing energy losses. Table 2.3 represents the energy loss values due to both energy curtailment (E_{cur}) and active power distribution losses (E_{loss}).

Further, investigations have been carried out with penetration of microgrids at bus 13, 15 and 33 in addition to PV units for the same 33-bus distribution network (same operating conditions). The power profiles of these microgrids are displayed in Fig 2.1(c). In this case, microgrids are assumed to operate mostly in dispatch mode, which in turn, adversely impact the system's operating conditions and results in further increase in overvoltage. The controller arrangement is kept same as previous case. Fig. 2.7 clearly shows that with integration of microgrids, the voltage at bus-15 rises to 1.25 p.u at the 13th hour and reaches 1.05 p.u in 86.4 seconds. As observed from Fig. 2.7, the active power injection due to microgrid penetration at bus-15 is significantly high, thereby increasing the voltage magnitude. At that instant, proposed controller performs actions such as curtailment of active power and absorption of reactive power more effectively to bring the voltages within the desired limits, in comparison to the case when microgrids are not considered as shown in Fig. 2.7 (b) and 2.7(c). Moreover, the overall energy loss is found to be more considering microgrids. It is found that E_{cur} and E_{loss} increase by 43% and 18%, respectively, with the penetration of microgrids in the radial system.

Table 2.4: Comparison of energy loss obtained with RBMPC and existing MPC for 33-bus distribution networks.

	Curtailed Energy E_{cur}, (kWh)	Energy loss, E_{loss} (kWh)
Without MG		
With MPC [6]:	78	11251
With RBMPC:	116	3337

Furthermore, with RBMPC, E_{loss} is evaluated as 3939 kWh which is lesser than 21092 kWh, obtained without any centralized controller. The comparisons of energy losses obtained are tabulated in Table 2.3. Fig 2.7 also shows the comparison of voltage profile of the test system with/without microgrids.

In this subsection, comparative analysis between conventional MPC [6] and proposed controller is presented. For analysis, bus-17 of the radial distribution network is considered. Fig. 2.8 represents the voltage, active power and reactive power profile of corresponding bus of the network using conventional MPC and proposed RBMPC at the 14^{th} hour of the day. Both approaches are compared in the absence of microgrids. It is to be noted that in conventional MPC, same weights at every step of the iteration is considered. However, in the proposed controller, weights of the objective function are updated at every sampling point based on the severity of the voltage control problem. Fig. 2.8 clearly shows the superiority of RBMPC in controlling bus voltages and effectively bring the voltage back to 1 p.u. Moreover, with conventional MPC, voltage at bus-17 settles close to 1.03 p.u, instead of 1 p.u. The corresponding active and reactive power injections are shown in Fig. 2.8(b) and 2.8 (c), respectively. Furthermore, E_{loss} reduces significantly by 70% compared with the conventional MPC due to the inclusion of the power loss objective and inclusion of reactive power capability of PV inverters. Nonetheless, during control operation, minimization of active power curtailment is compromised to some extent, which is not significant. The energy losses obtained for both the approaches are tabulated in Table 2.4.

To check the computational benefit of the proposed approach, the average elapsed time to solve the objective function for one sampling period is compared with [10]. The average elapsed time for the current work is found as 0.7 seconds, while for [10], the elapsed time varies between 0-32 seconds. In [10], the minimization of deviations of reactive power from DG units and slack variables is considered as the only objective. Whereas, in the present work, the objectives are to minimize energy loss and voltage deviations in addition to the minimization of the deviations in the control variables (active

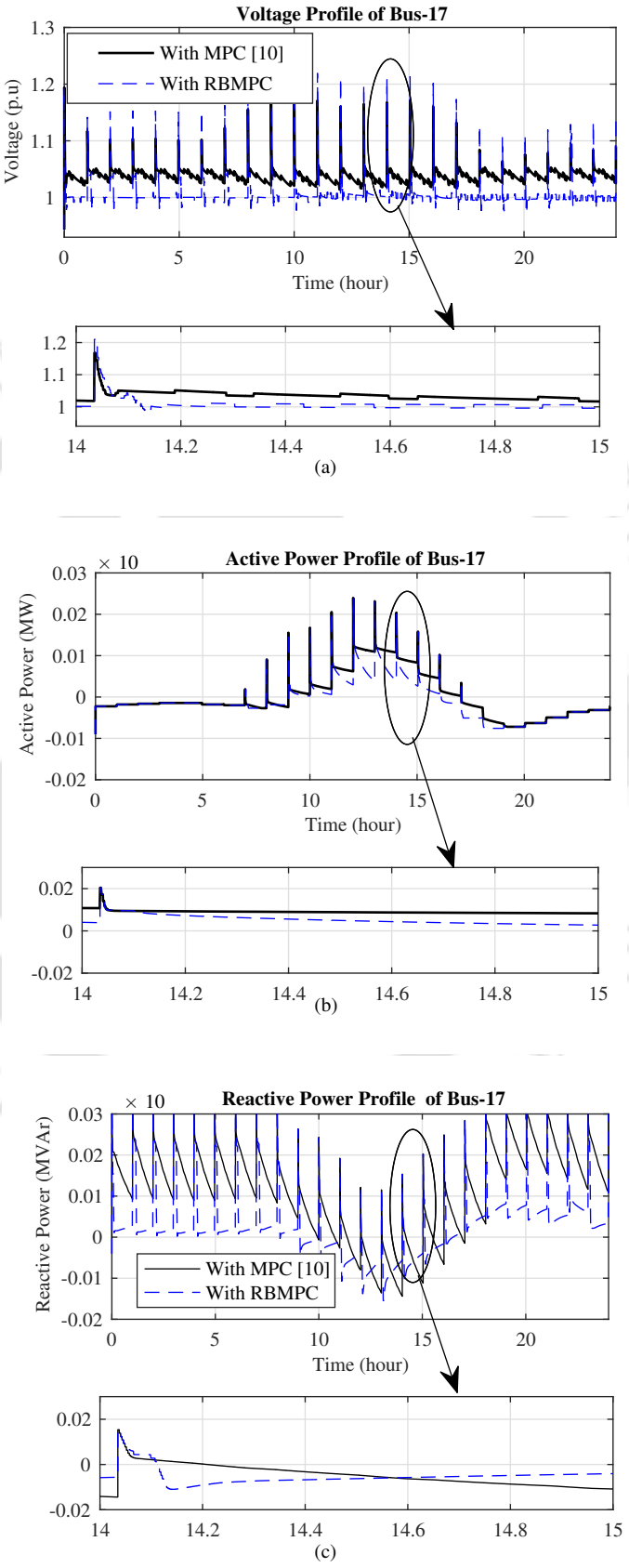

Figure 2.8: Plots of: (a) voltage profile at bus-17 (b) active power profile at bus-17 (c) reactive power profile at bus-17 for 33-bus distribution networks

Table 2.5: Voltage error values between 14th to 15th hour at bus-17.

Time Instants (hour)	Voltage error (p.u) [Proposed Approach]	Voltage error (p.u) [6]
14.2	0.008	0.051
14.4	0.005	0.038
14.6	0.003	0.035
14.8	0.002	0.026

and reactive power of PV units, reference voltage of OLTC) and slack variables. The average CPU time required by the controller in executing the simulations for 24 hours is around 8 seconds with Intel core i5-6500 processor running at 3.20 GHz and 8 GB of RAM.

Further, to demonstrate the effectiveness of the proposed controller, steady state voltage error (SSVE) is computed using a performance index as defined in Eq. 2.25 [21].

$$SSVE = \sum_{t=1}^{24*60} ||V_{\Omega}(t) - V_{ref}|| \tag{2.25}$$

The performance evaluation is carried out for instants between 14th to 15th hour at bus-17 and the corresponding errors are tabulated in Table 2.5. It is clearly observed that the voltage error has been minimized considerably in comparison to conventional MPC described in [6].

2.4.1 Validation of the Proposed Method in 38-bus distribution networks

The proposed control scheme is also validated in a 38-bus balanced distribution system. The test network with accommodation of PV units, microgrids, and loads is shown in Fig. 2.9. The data associated with the network is taken from [57]. The placement of PV plants, microgrids, and loads are kept same as in 33-bus distribution networks. The sampling time is 60 minutes for the first stage and 1 minute for the second stage.

Fig. 2.10 depicts the bus voltage, active and reactive power profiles of the considered test system. The bus-17 is chosen for further analyses. It can be observed that the bus voltage magnitudes of bus-17 cross the desired limits both in the presence and absence of microgrids. However, the proposed scheme successfully brings the voltages within desired limits within few seconds. The time interval from 13^{th} to 15^{th} hours are further shown for better clarity. Similarly, the active and reactive powers of PV are changing dynamically throughout the day depending on the variations in loads and generation. The energy loss calculated during the 24-hour simulation is depicted in Table 2.6. Since the microgrids are

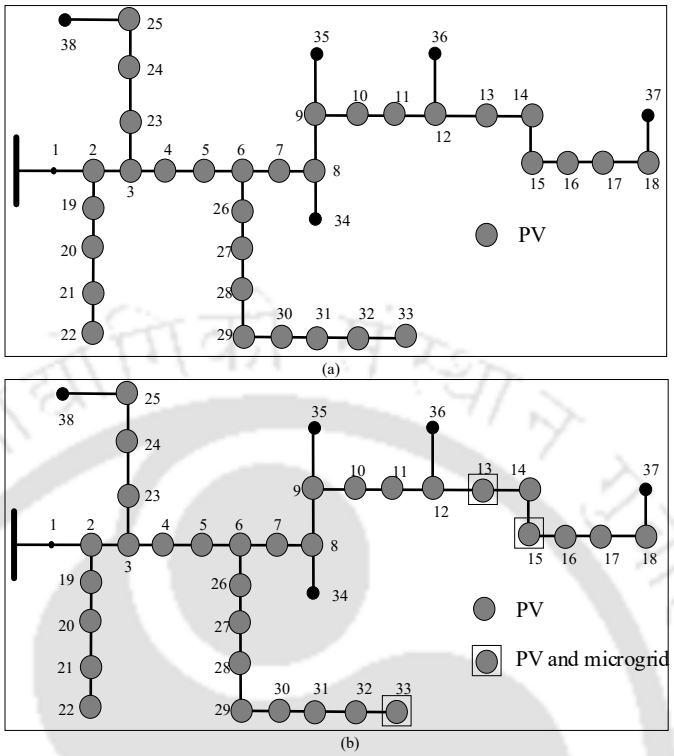

Figure 2.9: Test network: 38-bus distribution networks; (a) without microgrids, (b) with microgrids.

Table 2.6: Comparison of energy loss obtained in the presence and absence of microgrids for 38-bus distribution networks.

	Curtailed Energy, E_{cur} (kWh)	Energy loss, E_{loss} (kWh)
Without MG	161	1946
With MG	197	2400

in dispatch mode during most time intervals, overvoltages, energy loss and PV active power curtailment are more in the presence of microgrids. Thus, the results obtained with this test network are found to be consistent and similar to the 33-bus distribution network.

2.5 Conclusion

A novel rule-based MPC has been presented in this chapter. Three different levels of voltage magnitudes are considered as the basis of the pre-defined rules for MPC. These rules are formulated in such a manner that MPC alters the weights associated with the objectives according to the severity of the voltage control problem. MPC computes a set of optimal control actions to maintain the voltages of the buses within acceptable limits in the presence of high PV penetration and hourly variations of

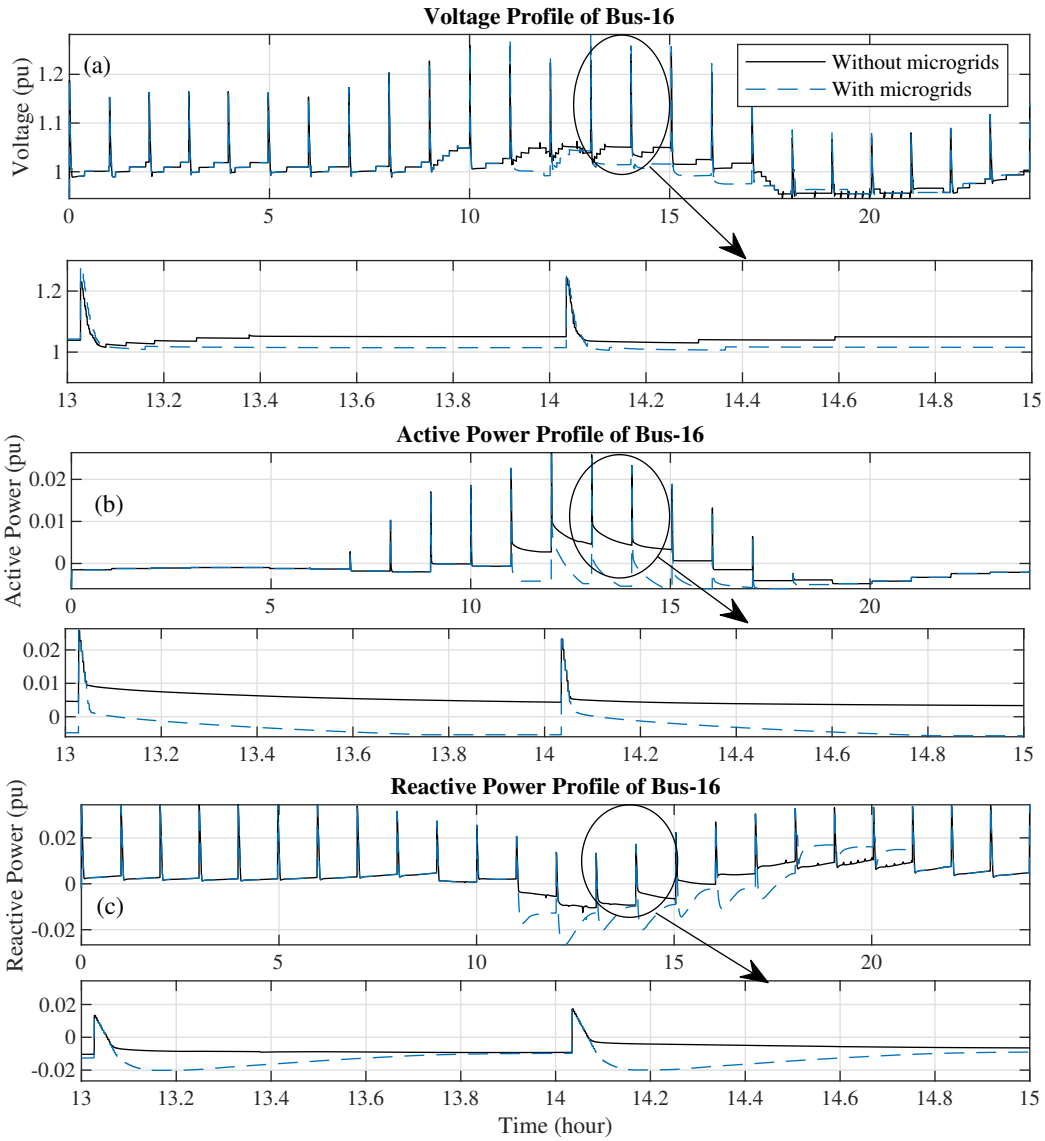

Figure 2.10: Plots of: (a) voltage profile at bus-16 (b) active power profile at bus-16 (c) reactive power profile at bus-16 for 38-bus distribution networks.

loads. As soon as the voltages are within feasible range, minimization of power loss is considered as the main objective of MPC. Simulation results show that, in addition to regulating the voltages within prescribed limits, the rule-based MPC described in this chapter is successful in significantly reducing energy loss. The energy curtailment, as well as active power distribution losses throughout the day, are computed and compared. The energy loss is moderately higher in the case of microgrids integrated ADN, as the microgrids inject power to the buses during most of the time of the day. Furthermore, it is observed that energy loss gets drastically reduced with the incorporation of RBMPC when compared to an existing MPC approach. Besides, the proposed controller is also compared with an advanced MPC approach in terms of computational burden for one sampling period in solving optimization problem. Furthermore, control performance is evaluated using steady state voltage error performance index.

3

Model Predictive Control-Based Coordinated Voltage Control in Active Distribution Networks Incorporating CVR and DR

Contents

In the last chapter, a rule-based voltage control methodology has been developed that coordinates the actions of on-load tap changer and PV units to maintain the voltages within defined limits. This chapter proposes a model predictive based voltage control that optimally coordinates the reference voltage of distribution static synchronous compensator, OLTC, and PV inverters' active and reactive powers set points to maintain network voltages within the operating limits. To manage the different voltage regulation devices with different temporal characteristics, two-timescale based coordinated algorithm has been developed. Moreover, the two functionalities of active distribution management system (ADMS): demand response (DR) and conservation voltage reduction (CVR) are explored in this voltage control methodology to enhance energy efficiency of the distribution networks. The proposed methodology is implemented in 33-bus and 38-bus distribution networks to verify its effectiveness for different cases. Furthermore, simulation results demonstrate the benefits of CVR and DR on the proposed methodology.

3.1 Introduction

The paradigm shift from passive to active distribution networks has been possible with the massive penetration of distributed energy resources (DER), such as, energy storage systems, solar photovoltaics (PV), wind turbine generators, etc. [58]. The rising number of distributed generations (DG) could impact the operation and control of distribution networks in a negative manner. One of the serious issues is the effective coordination of various DGs with conventionally used voltage regulation devices such as, shunt capacitors, on-load tap changers (OLTC), etc. for voltage control purposes [47].

Volt/var control (VVC) is an important aspect of the active distribution management systems (ADMS) [59]. The VVC aims to maintain the voltages within the operating limits set by American National Standard Institute (ANSI) C84.1 and confine to the interconnection reliability standards. The VVC in active distribution networks (ADN) is usually performed either in decentralized [8,26,60] or centralized manner [6,14,21]. Both offline [6,8,60,61] and online [6,14,21,26] VVC methods are available in literature. Recently model predictive controller (MPC) has been used widely as an online voltage control [6,14,21,26]. MPC principles can be applied either in single-timescale [6,14] or multi-timescale [21]. Ref. [6] proposes a centralized MPC to regulate voltages in ADN by coordinating DG units and OLTC in single-timescale. Authors in [21] have developed a voltage control algorithm for distribution networks, coordinating both slow and fast VVC devices.

The smart inverters interfaced to DG units with their reactive power absorption and generation capabilities can participate in voltage regulation. These devices act as fast controllable resources and have been explored in [10, 14, 21, 21, 62]. They either follow commands obtained from control algorithm or any autonomous volt/var curve. In ref. [14], an MPC-based voltage control methodology is presented that coordinates energy storage systems, OLTC, and DG units in preventive and corrective modes of operation. Ref. [62] proposes a centralized MPC to correct the locally obtained reactive power set-point of DG units. All the aforementioned works have considered reactive power capabilities of DG units in their voltage regulation approaches. However, these smart inverters interfacing DG units are slightly oversized to enable their participation in voltage regulation, even with 100% active power production. The usage of custom power devices in VVC is witnessed in recent literature. A voltage control strategy has been developed in [43] utilizing OLTC and distribution static synchronous compensator (DSTATCOM) in an ADN. Although custom power devices have been used with other voltage regulation devices to fulfill different objectives for distribution network operator (DNO) in several literature, very few of them have explored the reactive power capabilities of DSTATCOM in an optimal coordinated voltage control scheme. Moreover, most of the aforesaid works have not explored other features, such as, reduction of energy loss, energy consumption, peak demand or peak power loss.

Conservation voltage reduction (CVR) is another aspect of volt/var optimization (VVO) strategy where the supply voltage to consumers is lowered but within the ANSI standard to reduce the energy consumption of consumers [43, 63, 64]. A considerable amount of studies has been done on this technique. Several authors have studied VVO deployed with CVR and other objectives in presence of DER. Reference [43] has described the model predictive based multi-timescale coordinated operation of CVR in ADN with electric vehicle (EV) integration. Authors in [63] have increased the energy savings from CVR in PVs integrated ADN by coordinating smart inverters with traditional voltage regulating devices. The trade-off between energy conservation and loss minimization with CVR has been studied in [64].

Similarly, demand response (DR) is another technique to improve energy efficiency. DR implies shifting the load behavior from a particular time instant to another to gain economic benefits, or curtailment of certain loads with the coordination of the customers' choices [30,61,65–67]. DR techniques are mainly classified into price based DR and incentive based DR. Authors in [61] aim to formulate

a DR control algorithm considering energy pricing limits for a residential PV storage system. In [65], DR is implemented by reducing demand for a specified time duration in a microgrid. A model based predictive control has been discussed in [65] to schedule flexible resources (heating systems and energy storage systems) in presence of solar photovoltaics.

This chapter presents a model predictive based voltage control scheme, that coordinates OLTC, DSTATCOM and reactive power capability of PV inverters to maintain bus voltages. Curtailment of PV power is used as an emergency control action. This work is an extension of Chapter 2, where the preliminary works on coordinated VVC have been described. In this work, unlike Chapter 2, the VVC is allowed to operate in double-timescale. Further, the CVR and DR functionalities are integrated into the VVC separately by incorporating DSTATCOM, voltage dependent loads and flexible loads, respectively into the network and the effects of DR and CVR techniques on VVC have been analyzed. Moreover, instead of considering all the PV units as controllable resources, PV units at specific buses are considered to be controllable. This is done to reduce computation burden and the necessity of oversized PV inverters for voltage regulation purposes.

In recent survey, CVR and DR both are integrated simultaneously to fulfill different objectives. In [29], CVR and DR have been used to minimize energy consumption cost in a day-ahead market. In [68], authors have considered a two-stage optimization structure to determine the size and location of soft open point (SOP) and battery energy storage system (BESS) considering both CVR and DR schemes. While Ref. [29] discusses the economic aspects, i.e., determination of the optimal pricing scheme for every individual customer to participate in the DR, Ref. [68] formulates a planning problem. However, the online coordinated voltage control structure is missing in [29] and [68].

Unlike previous works on VVC, CVR and DR have been deployed in this work in coordination with the VVC. The VVO objectives are formulated in an MPC-based coordinated framework. Moreover, the proposed scheme considers timescale decomposition of VVC devices. Table 3.1 points out the differences in the approach described in this work with other works from previous literature. Considering the above cited works, the major contributions of this work are:

(i) To develop a two-timescale MPC-based coordinated VVC strategy to enhance energy efficiency along with CVR and DR techniques;

(ii) To propose a load-shifting based DR technique in the MPC-based coordinated voltage control framework.

Table 3.1: Literature survey.

Attributes Consideration	Timescale Decomposition	Reactive power support from DSTATCOM	Reactive power support from PV	CVR	DR	Energy Loss Analysis
Chapter 1	×	×	✓	×	×	✓
Ref. [21]	✓	×	✓	×	×	×
Ref. [43]	✓	×	✓	✓	×	✓
Ref. [67]	×	×	×	×	✓	×
Ref. [29]	×	×	×	✓	✓	×
Ref. [68]	×	×	✓	✓	✓	✓
Present Work	✓	✓	✓	✓	✓	✓

The remainder of this work is organized as follows: Section 3.2 describes the system investigated in this chapter. The modeling of voltage dependent loads and flexible loads are also discussed in Section 3.2. Section 3.3 discusses the voltage control model incorporating CVR and DR objectives. The voltage control problem is formulated in Section 3.4. The simulation results and discussions are presented in Section 3.5. Section 3.6 presents the conclusions of this work.

3.2 System description

In this section, the network and the components that constitute the distribution network are modeled. The physical description of the components to be included in the form of constraints and variables in the problem formulation are further discussed.

Fig. 3.1 depicts the active distribution network considered in this work. Let, Ω be the set of buses of the network. The distribution lines of the network, represented by set of edges, $\epsilon = (i, j) \subset \Omega \times \Omega$ are modeled in the form of series admittances $Y_{ij} = 1/(R_{ij} + j\omega \mathrm{L}_{ij})^{-1}$. Here, R_{ij}, L_{ij}, ω represent the line resistance, inductance and system frequency, respectively. The system data is provided in Appendix. The OLTC, loads, DSTATCOM and PV inverters constitute the network. It is assumed that, like Chapter 2, all the network operations are carried out for a balanced three-phase system. Newton Raphson power flow method has been done for the network initialization and extraction of sensitivity matrix. Since the sensitivity matrix for a given network topology needs to be extracted only once, the power flow is run once at the beginning of the simulation. The results of the power flow are extracted as the initial points for the time domain simulations. Considering sampling time of the controller as 10 seconds, the time-domain simulation is run every 10 seconds. For the first interval,

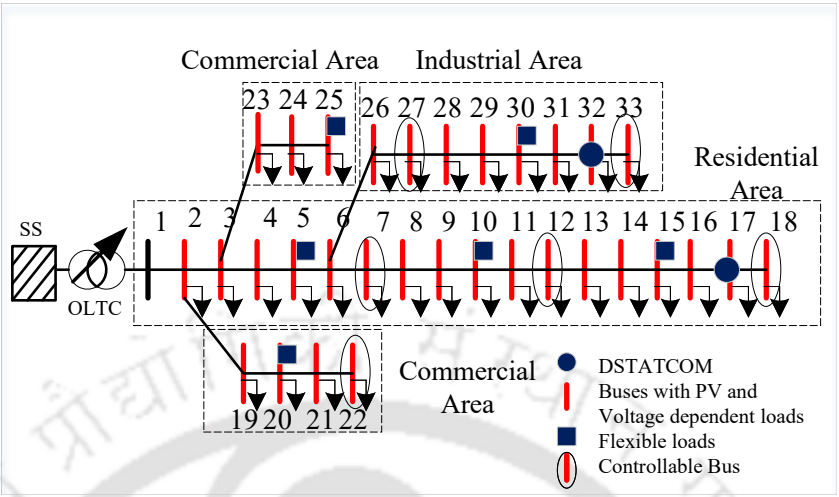

Figure 3.1: 33-bus radial distribution network.

simulation is run with the values taken from the power flow method. Let, Ω_{PV} be the set of buses with PV generators. Being the power injectors, the PV power profile is shown in Fig. 3.2. The PV active power injection is a function of inverter size and solar irradiation. Thus, the reactive power at any time instant t is estimated from (3.1).

$$Q_{PV,t}^{m}{}^{2} = S_{PV}^{m}{}^{2} - P_{PV,t}^{m}{}^{2}. \tag{3.1}$$

The loads with residential, commercial and industrial characteristics are connected to the distribution network. The power profiles of these loads are depicted in Fig. 3.2 [8]. For the CVR operation, the loads with exponential parameter are used. Eqs. [(3.2) and (3.3)] represent the exponential loads that relates load power to bus voltages. The exponential parameter is defined by the CVR factor as described in [63].

$$P_L^m = P_L^{m,nom} V^m(t)^{CVR_{g(kW)}}, \forall m \in \Omega_{VDL} \tag{3.2}$$

$$Q_L^m = Q_L^{m,nom} V^m(t)^{CVR_{g(kVAr)}}, \forall m \in \Omega_{VDL} \tag{3.3}$$

For DR scheme, certain loads of the network are modeled as flexible loads. The objective of the DR scheme in this work is to shift the active power demand based on voltage magnitudes and the real-time price of electricity. The profile of electricity consumption cost is shown in Fig. 3.3 [31]. The demand is shifted instead of curtailment in such a manner that the overall energy requirement

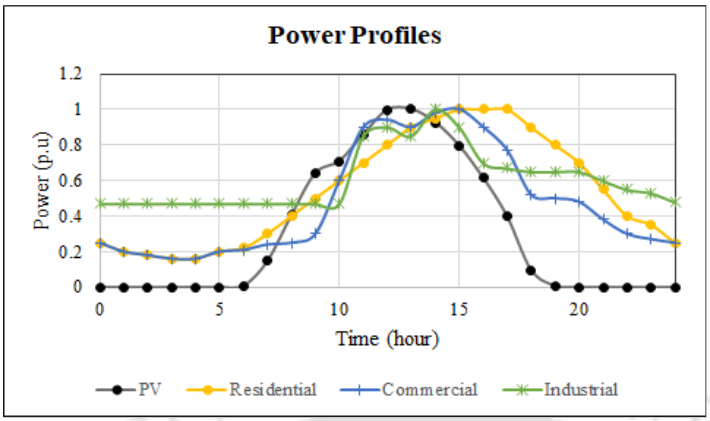

Figure 3.2: PV and loads power profiles.

at a particular bus remains the same over the entire day. Let, λ be the factor to represent demand flexibility. The equations describing the flexible loads are:

$$\sum_{t=1}^{T} P_{L,t}^{m} \Delta t = \sum_{t=1}^{T} P_{L,t}^{nom,m} \Delta t, \forall m \in \Omega_{FL} \tag{3.4}$$

$$P_{L,t}^{m} = P_{L,t}^{nom,m}.\lambda_{t}^{m}, \forall m \in \Omega_{FL} \tag{3.5}$$

where, $(1 - \lambda_t^{m,min}) \leq \lambda_t^m \leq (1 + \lambda_t^{m,max})$

The DSTATCOMs in the distribution networks are modeled as current injectors [refer to Fig. 3.4], in which the current is always in quadrature to the bus voltage. Equations (3.6) and (3.7) represent the model of DSTATCOM.

$$\dot{i_{st}} = \frac{K_{st}(v_{st} - v_m) - i_{st}}{T_{st}} \tag{3.6}$$

$$Q_{st} = i_{st} v_m \tag{3.7}$$

where, m is the bus at which DSTATCOM is connected. K_{st} is the gain and T_{st} is the time constant of the DSTATCOM regulator. A non-windup limiter is further integrated to the DSTATCOM model to lock the DSTATCOM current when one of its limits is reached. The reactive power injected or absorbed at the bus m is denoted by Q_{st}.

3.3 Voltage control model for ADN

Fig. 3.5 depicts the voltage control problem framework. The active distribution management system (ADMS) regularly monitors the voltage profile of ADN with the help of advanced metering

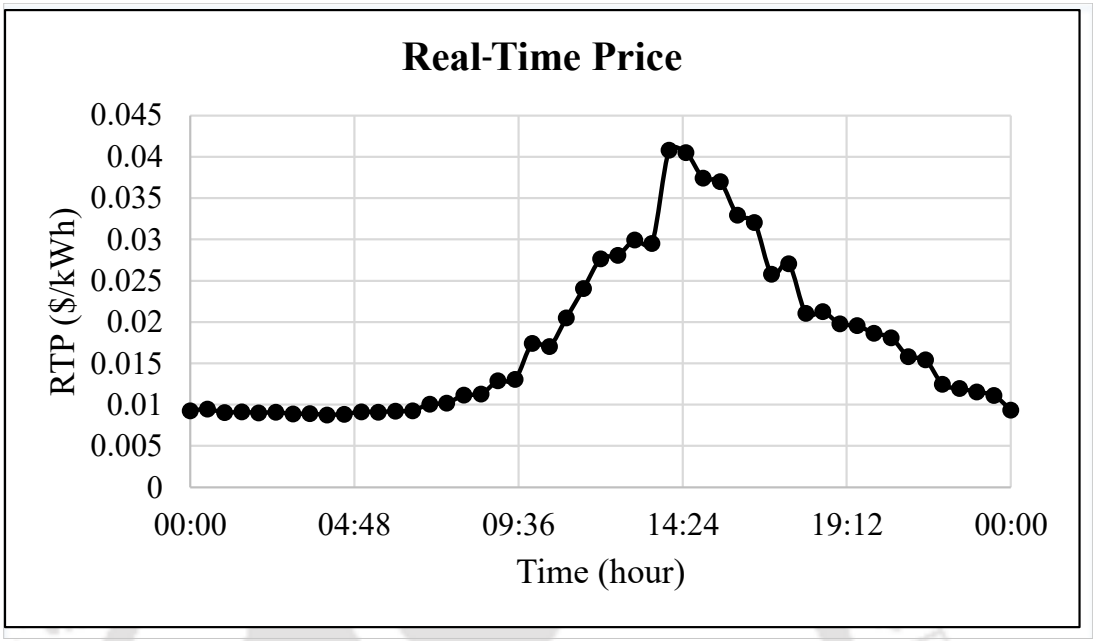

Figure 3.3: Real-time price of electricity.

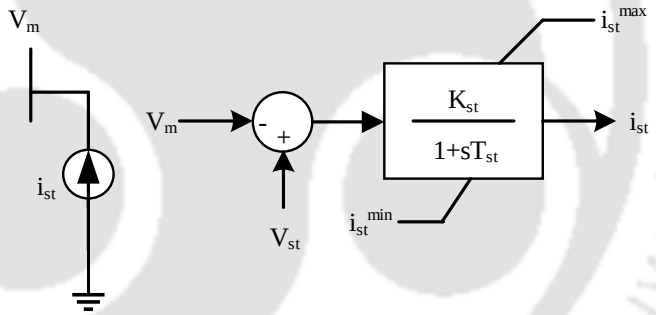

Figure 3.4: Model of DSTATCOM.

infrastructure (AMI), and supervisory control and data acquisition (SCADA). The necessary data obtained from SCADA are processed by the central VVC for optimization. The VVC calculates the optimal set-points for the available volt/var devices in coordination with the CVR and DR. At each sampling point k, MPC-based voltage control problem is formulated and solved. The optimal plan to be applied at any sampling point $k = 1, 2, ..., k + N_c - 1$ is the solution of the MPC problem. The first control actions obtained for time k are applied. The MPC problem is then solved again but for a shifted prediction horizon, with consideration of updated measurements (voltages and active and reactive powers, etc.) and initial conditions. The receding horizon principle of MPC ensures that the controller considers any uncertainties/disturbances instantaneously. If at any instant, uncertainties get detected, the updated information gets reflected in the next sampling instant. Thus, the accuracy

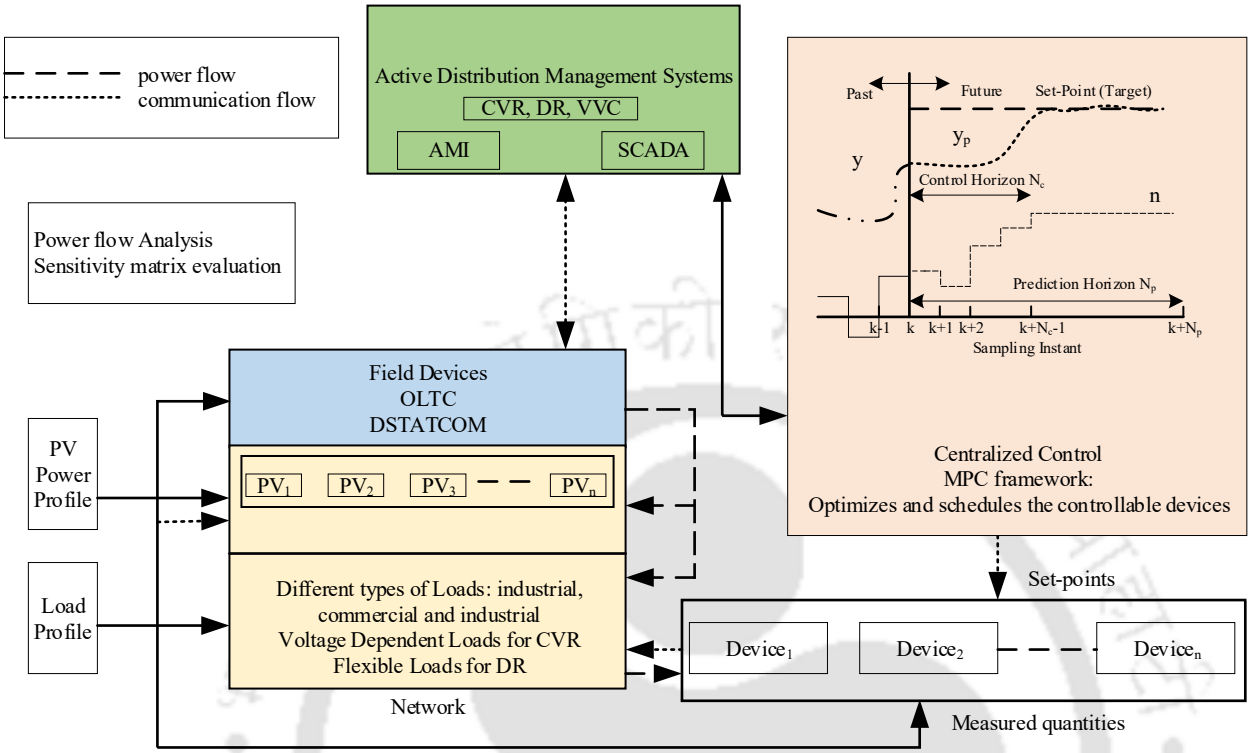

Figure 3.5: Block diagram of the proposed VVC.

of calculations of control actions is not compromised. MPC formulation generally requires difference equations and are represented as given in Chapter 2 [refer to eqs. (2.3) and (2.4)]. In eq. (2.3), $\Delta u(k) = u(k) - u(k-1)$ indicates the set of control input (control variables). $y(k)$ and $x(k)$ represent the output and the states of the control system, respectively. $\boldsymbol{A}$, $\boldsymbol{B}$ and $\boldsymbol{C}$ are the system, input and output matrices, respectively. The input and predicted output along the control and prediction horizon are denoted by Δu and y_p, respectively as in eqs. (2.5)-(2.6). Thus, the state variables at instants $k = k, ..., k + N_C - 1$ can be calculated sequentially from the basic difference equations as in eqs. (2.7)-(2.8). Similarly, the predicted output at instants $k = k + 1, ..., k + N_P$ can be derived as in eqs. (2.9)-(2.11). The final form of predicted output matrix can be written as provided in eqs. (2.12)-(2.14). Similarly, the control inputs are represented in the matrix form. These matrices are further used to represent the objective problem in the form of standard programming. The voltage sensitivity model is used as the prediction model for the MPC problem. The sensitivity matrices of the voltage sensitivity model, $\boldsymbol{\delta V / \delta u}$ are calculated from the inversion of the Jacobian matrix. The sensitivity matrix is seldom updated if there is any change in network configuration. The sensitivities of bus voltages with respect to the reference voltage of OLTC and DSTATCOM are obtained as the ratio of

variations of the controlled bus voltages to the bus voltage associated with OLTC and DSTATCOM due to a single tap and reference voltage difference, respectively as described in Chapter 2.

3.4 Problem formulation

The VVO problem is formulated as a quadratic programming problem as given in eq. (3.8).

$$min \sum_{i=1}^{N_P} [\{V_{ref}(k+i) - V(k+i)\}^T \boldsymbol{Q} \{V_{ref}(k+i) - V(k+i)\}] + \sum_{i=0}^{N_C-1} [\Delta u(k+i)^T \boldsymbol{R} \Delta u(k+i)] + \sigma^T \boldsymbol{S} \sigma \tag{3.8}$$

The VVO problem aims to minimize the voltage errors and to limit the usage of control and slack variables in such a manner that the magnitudes of the bus voltages remain within desired bounds [0.95, 1.05] p.u. Further, the reference voltage for the VVO is kept at 1.0 p.u to obtain minimum power loss. Q, R, and S are the weighing matrices associated with the objectives: minimization of voltage error, control variables, and slack variables, respectively. These weights are selected heuristically as described in Chapter 1. Based on the timescale of operation of devices, the MPC-based VVO is operated in the slow and fast timescale as shown in Fig. 3.6. The change in control inputs in the slow and fast timescale are: $\Delta u(k)_{slow} = [\Delta V_{tap}(k)^T]^T$ and $\Delta u(k)_{fast} = [\Delta P_{PV}(k)^T, \Delta Q_{PV}(k)^T, \Delta V_{st}(k)^T]^T$. The objective function is subjected to inequality constraints as follows:

$$\Delta u^{min} \leq \Delta u(k+i) \leq \Delta u^{max} \tag{3.9}$$

$$u^{min} \leq u(k+i) \leq u^{max} \tag{3.10}$$

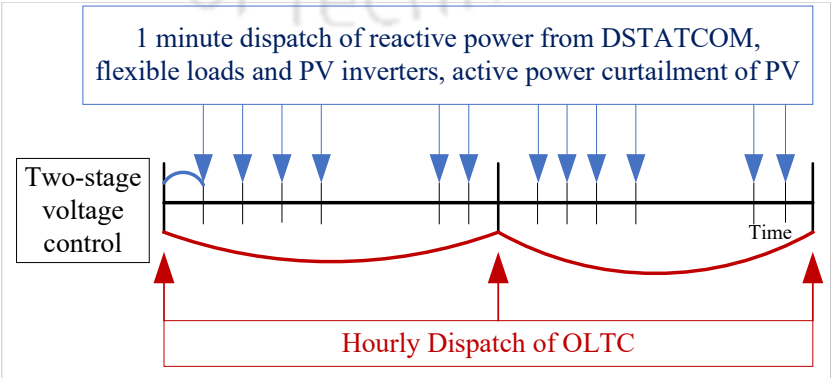

Figure 3.6: Timescale decomposition of VVC devices.

$$-\sigma_1 1 + V^{min}(k+i) \leq V(k+i|k) \leq V^{max}(k+i) + \sigma_2 1 \tag{3.11}$$

The objective function is further subjected to the equality constraint as follows:

$$V(k+i|k) = V(k+i-1|k) + \frac{\delta V}{\delta u}\Delta u(k+i-1) \tag{3.12}$$

Eq. (3.9) represents the constraints on manipulated variables or inputs of the MPC-based model. The inputs differ according to the stages of operation. Eq. (3.10) describes the limits on the ramp movements of the manipulated variables. The constraint on the output variable, bus voltage magnitudes, as described in eq. (3.11) is softened by usage of slack variables. The equality constraint, described in eq. (3.12) is the prediction model used for MPC and thereby, handled at every sampling instant.

Further, eq. (3.8) is modified for CVR operation and represented in eq. (3.13).

$$min \sum_{i=1}^{N_P}[\{V_{cvr}(k+i) - V(k+i)\}^T \boldsymbol{Q}\{V_{cvr}(k+i) - V(k+i)\}] + \sum_{i=0}^{N_C-1}[\Delta u(k+i)^T \boldsymbol{R}\Delta u(k+i)] + \sigma^T \boldsymbol{S}\sigma \tag{3.13}$$

The objective of the CVR operation aims to maximize the energy saving by minimizing the sum of the square of the deviation of bus voltages from the expected CVR voltage in all buses at each sampling point. V_{cvr} is the expected CVR voltage. The expected CVR voltage is chosen as 0.98 p.u. Eq. (3.13) is subjected to constraints described from (3.9)-(3.12).

For the DR operation, some loads are modeled as flexible loads. While the optimization function remains same as in (3.8), it is subjected to additional constraints, as given in eqs. (3.15)-(3.18). Here, $\Delta u(k)_{slow} = [\Delta V_{tap}(k)^T]^T$ and
$\Delta u(k)_{fast} = [\Delta P_{PV}(k)^T, \Delta Q_{PV}(k)^T, \Delta V_{st}(k)^T, \Delta P_{FL}(k)^T]^T$.

The voltage magnitudes as well as the energy demand at every sampling point are the states and output of the MPC model equipped with DR, i.e., $y = [V(k+i|k), E(k+i|k)]$.

$$min \sum_{i=1}^{N_P}[\{y_{ref}(k+i) - y(k+i)\}^T \boldsymbol{Q}\{y_{ref}(k+i) - y(k+i)\}] + \sum_{i=0}^{N_C-1}[\Delta u(k+i)^T \boldsymbol{R}\Delta u(k+i)] + \sigma^T S_\sigma \sigma + \mu^T \boldsymbol{S_\mu}\mu \tag{3.14}$$

The weighting factor for the change of power consumption by flexible loads is derived from market

price signal and is bounded between [0, 1].

$$E(k+i|k) = E(k+i-1|k) + \Delta t P_{FL}(k+i-1) \tag{3.15}$$

$$-\mu_1 1 + E^{min}(k+i) \leq E(k+i|k) \leq E^{max}(k+i) + \mu_2 1 \tag{3.16}$$

Eq. (3.16) describes the constraint on output variable, energy demand at buses connected to flexible loads. This constraint is further softened by adding slack variable, μ.

Moreover, in eq. (3.15), the energy demand from the flexible loads shall reach the desired (original) demand by time t_{out}, as described in (3.17)

$$E(t_{out}) \geq E_{orig} \tag{3.17}$$

This is assured with the manipulation of lower bound constraint, $E^{min}(k)$ of (3.16).

$$E^{min}(k) = max[E_{req} - max(0, (k_{out} - k)P_{FL}^{max}\Delta t)] \tag{3.18}$$

3.5 Results and analysis

The MPC-based VVC has been implemented on a PC with specifications: Intel Core i5-6500 processor, 3.20 GHz, and 16 GB RAM. MATLAB R2018a is used as simulation platform. The components of the network are modeled with the help of power system analysis toolbox (PSAT) [54]. The optimization problem is formulated as QP and solved by CPLEX solver of IBM ILOG community edition.

The performance of the proposed methodology is tested in a 33-bus distribution network (refer to Fig. 3.1). The line and load data are taken from [56]. The single line diagram of the ADN is depicted in Fig. 3.1 describing the locations of PV generators, DSTATCOM, OLTC and different types of loads. The normalized load profiles in the residential, commercial and industrial areas are considered for simulations. The daily power profiles of loads and PV units are derived from the product of the peak power of each load or PV units with the multiplying factor as depicted in Fig. 3.2. Exponential load model coefficients are taken from [63]. The OLTC is connected between the substation and bus-1. The DSTATCOMs are placed at bus-17 and bus-32. The permissible limits of voltage are considered to lie within [0.95, 1.05] p.u, i.e., ±5% of the nominal voltage. The PV units are installed at all the buses except bus-1. The capacity of each PV unit is chosen as 347 kVA. The PV units at buses 7, 12, 18, 22, 27, and 33 are considered controllable. It is assumed that the smart inverters interfaced to PV

Table 3.2: Different cases considered for simulation

S. No.	MPC-based VVC	CVR	DR
Case 1	×	×	×
Case 2	✓	×	×
Case 3	✓	✓	×
Case 4	✓	×	✓
Case 5	✓	✓	✓

units have some excess reactive power capability and thus participate in voltage regulation. For the DR scheme, it is assumed that load demands at bus 5, 10, 15, 20 25 and 30 act as flexible loads. The range of flexibility of the demands participating in DR program is assumed as 20%.

The sampling time of the control strategy is 10 seconds. The controller parameters, prediction horizon N_P is equal to control horizon N_C for all the considered cases, i.e., equal to three. Active power curtailment (APC) from PV units is used only if the voltage magnitude of any bus crosses the upper desired limit.

Five different cases have been considered for simulations as illustrated in Table 3.2. Case 1 corresponds to the scenario, where there is no MPC framework or any control to regulate voltages, but there are PV units and DSTATCOM. Case 2 corresponds to MPC-based coordinated control framework with PV inverters, OLTC and DSTATCOM. In Case 3, CVR operation is studied in VVC framework that is described in Case 2. Case 4 considers DR scheme in the MPC-based VVC operation. Case 5 integrates both DR and CVR operation with the VVC scheme.

Tables 3.3 and 3.4 tabulate the most relevant variables (maximum voltage rise and drop, energy loss, energy consumption, peak demand and resource utilization) for comparison among different cases. Fig. 3.7 depicts the voltage profile of bus-18 for all the cases. The voltage profile of bus-18 exhibits the highest voltage drop for all the scenarios and is thus considered for analysis. Simulations are run with time-varying generation and loads.

3.5.1 Voltage profile analysis for different Cases

In Case 1, the voltage magnitude of bus-18 drops down to 0.87 p.u as observed from Fig. 3.7. However, the voltage magnitude could not be restored to the desired level due to absence of any type of control. Since, power absorption by loads being greater than power injection by the PV generators, under voltage is more prevalent. In Case 2, MPC-based VVO optimally determines the

Table 3.3: Numerical results for different cases considered for simulation

Case. No.	Maximum voltage rise (p.u)	Minimum voltage drop (p.u)	PV/DSTATCOM reactive power injection/absorption (MVAr)
1	1.056/_	0.87/_	_
2	1.053/1.05	0.91/0.96	PV(0.122/-0.072), DSTATCOM1 (2.875/-1.814), DSTATCOM2(1.424/-0.619)
3	1.012/1.012	0.87/0.92	PV(0.161/-0.082), DSTATCOM1 (2.675/-1.548), DSTATCOM2(1.375/-0.310)
4	1.05/1.05	0.92/0.97	PV(0.120/-0.072), DSTATCOM1 (2.879/-1.840), DSTATCOM2(1.424/-0.613)
5	1.015/1.015	0.87/0.94	PV(0.173/-0.092), DSTATCOM1 (2.980/-1.324), DSTATCOM2(1.407/-0.344)

Table 3.4: Comparison of energy loss, consumption and peak demand for all the cases

S. No.	Energy loss (MWh)	Energy consumption (MWh)	Peak demand at 15^{th} hour (MW)	Power loss at peak time (MW)
Case 1	4.582	95.712	0.5825	0.266
Case 2	4.227	96.552	0.5865	0.224
Case 3	4.134	95.045	0.5715	0.176
Case 4	4.262	96.865	0.566	0.221
Case 5	4.053	96.077	0.569	0.168

reference voltages of DSTATCOM and OLTC, and reactive power set-points of PV inverters to correct the voltages that have crossed the prescribed limits. The voltage magnitudes reach the desired level within a few seconds with the optimal amount of reactive power injection and absorption from PV inverters and DSTATCOM, and OLTC tap operations.

When CVR is employed in Case 3, the voltage magnitudes remain at the lower end of the prescribed limits. Further, the voltage magnitudes could not be brought back to the desired limits at few instants. With DR in Case 4, better voltage performance is observed, since the voltage deviation with respect to 1 p.u is less than the other cases. Thus, DR technique acts as an additional support to voltage regulation by balancing the injection and absorption of power in response to market price signals. The voltage profile in Case 5 is almost similar to the voltage profile in Case 4 due to implementation of DR. However, the CVR technique in Case 5 keeps the voltage magnitudes at the lower end of the desired voltage level.

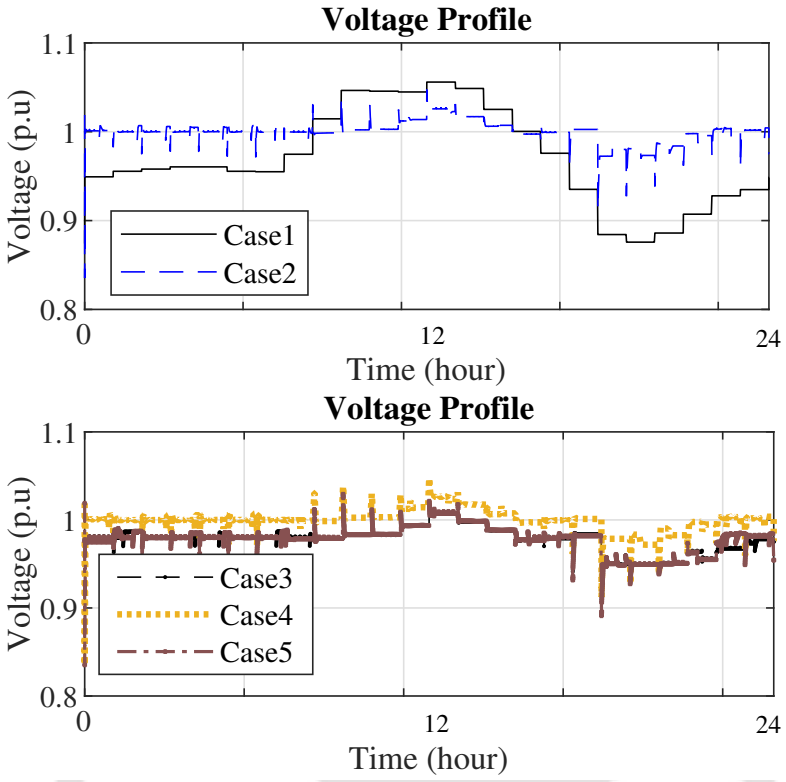

Figure 3.7: Voltage profile of bus-18 for all the cases.

3.5.2 Energy loss and energy consumption for different Cases

Fig. 3.8 shows the power loss profiles for Case 1 and Case 5 for comparative analysis. The least values of energy loss as well as power loss at peak time are noted in Case 5 as shown in Table 3.4. Further, it is observed that with the proposed method, the energy loss throughout the day has been decreased by 529 kWh (unit), that amounts to 1,93,085 units in a year. As compared to Case 1, it is seen that there is 6.9% to 11.54% of energy loss reduction in the other four cases. With the consideration of voltage dependent loads for all the cases, the energy consumption during the day is function of voltage magnitude. Thus, it is observed that energy consumption is least in Case 3. The energy consumption during the day in Case 3 has been reduced by 1.56% compared to Case 2. However, less the CVR voltage, more is the amount of reduction in energy consumption. Moreover, the reactive power extraction and injection from DSTATCOM are relatively less in Case 3 than the other cases as shown in Table 3.3. Here, positive value represents injection and negative value represents absorption of reactive power. Although the energy consumption is more in Case 5 than Case 3, it has been decreased by 0.5% and 0.8% when compared to Case 2 and Case 4, respectively.

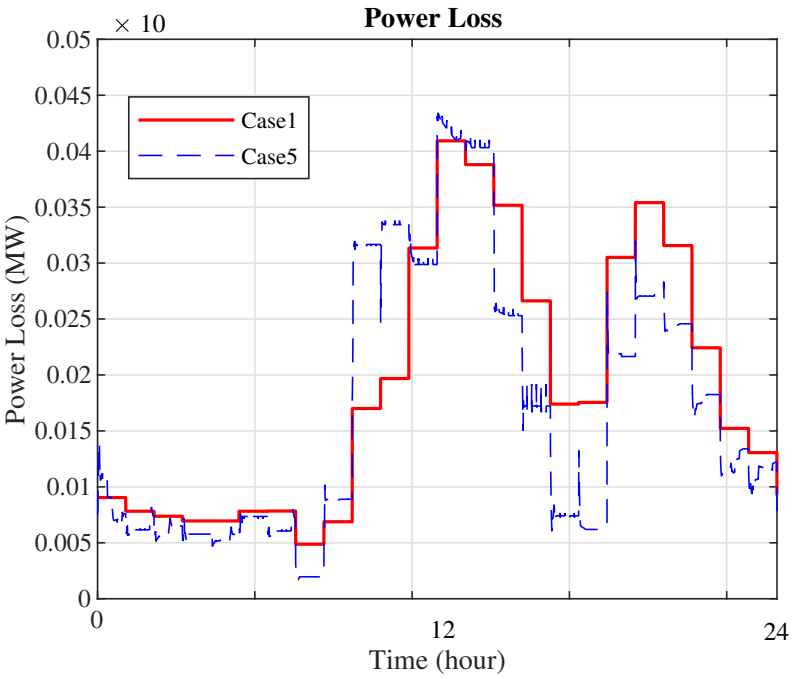

Figure 3.8: Power loss profile during the day.

In terms of peak reduction, the power profile of bus-25 at 15^{th} hour is considered for analysis, since adverse effect of peak loading is observed in bus-25 at hour 15. Thus, the market price is also high at this hour. Fig. 3.9 depicts the active power profile of bus-25. It is observed that the active power consumption is modulated with the help of DR operation. However, the MPC tries to keep the overall energy consumption same throughout the day at bus-25. This flexibility in energy consumption further helps in reduction of peak energy demand at the considered hour and thus in reduction of energy cost. Thus, the demand at hour 15 has been reduced by 2.55%, 3.49%, and 2.98% in Case 3, Case 4 and Case 5, respectively compared to without DR technique (Case 2). This can be seen from Fig. 3.9. Thus, while CVR helps in minimizing energy consumption and energy loss, with additional DR scheme, peak demand reduction and smoother voltage profile can be achieved by altering the demands at peak and off-peak times.

3.5.3 Effect of smart inverters in CVR operation

To show the effectiveness of smart inverters interfaced PV units in CVR operation, voltage profiles are shown in Figs. 3.10 and 3.11. Fig. 3.10 represents the voltage profile with coordinated operation of OLTC and DSTATCOM, whereas Fig. 3.11 depicts the voltage profile with coordinated operation

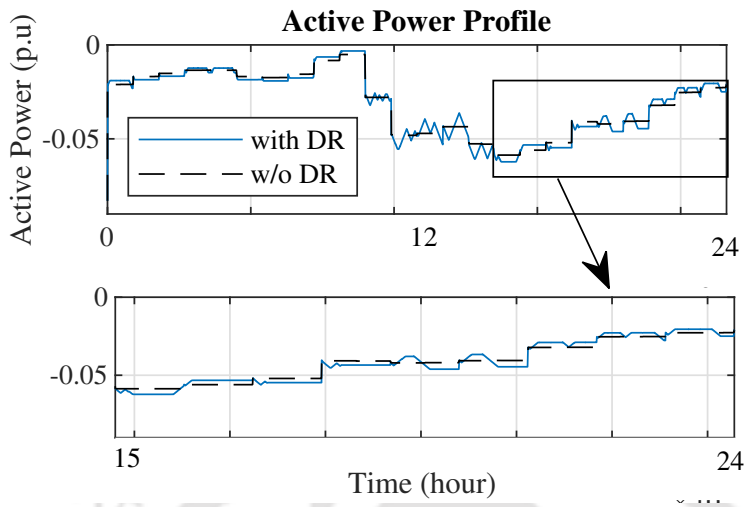

Figure 3.9: Active power profile of bus-25.

of PV inverters along with OLTC and DSTATCOM. For more clarity, voltage profiles of bus-12 and bus-18 are shown. It can be observed from Fig. 3.10 that with 0.98 p.u as CVR voltage, the voltage magnitudes could not be brought back to their desired limits [0.95, 1.05] for several time instants. The minimum voltage noted after application of control action is 0.92 p.u. However, the support from PV inverters in Fig. 3.11 helps in maintaining the desired voltage levels with more energy conservation. Moreover, deeper voltage reduction (0.95 p.u) for energy conservation without violating the lower limits can be attained with the help of reactive power support from PV inverters.

3.5.4 Effect of timescale decomposition of voltage control devices

Next, to study the effect of timescale decomposition of voltage control devices, simulations have been run to compare the single-timescale and dual-timescale voltage control in the test system. In the single-timescale operation, the OLTC, PV inverters and DSTATCOM operate at every 10 seconds duration. The tap operations of the dual-timescale and single-timescale have been shown in Figs. 3.12 and 3.13, respectively. It can be observed from the two figures that the dual-timescale coordinated voltage control algorithm mitigates the number of tap operations significantly and thus, reduces the possibility of occurrence of multiple operations in the network. Moreover, the energy loss is 6.152 MWh with single-timescale coordinated voltage control scheme, which is 45.54% more than the dual-timescale.

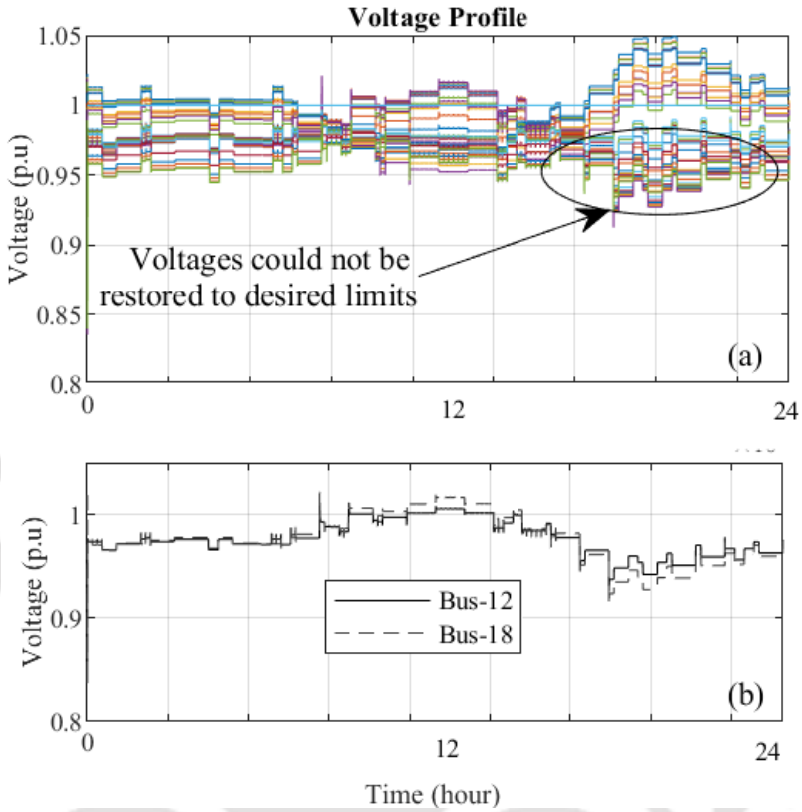

Figure 3.10: Voltage profile with reactive power support from DSTATCOM and OLTC.

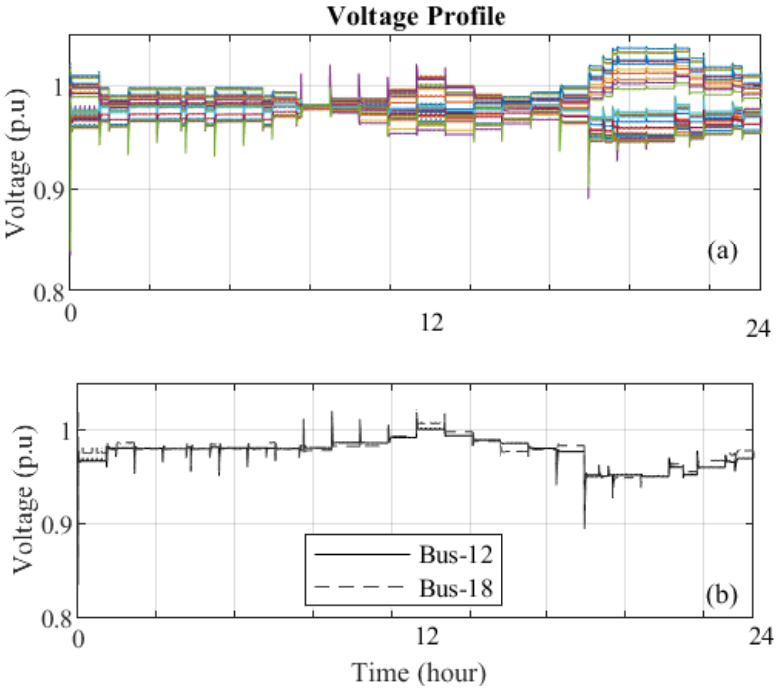

Figure 3.11: Voltage profile with reactive power support from DSTATCOM, PV inverter and OLTC.

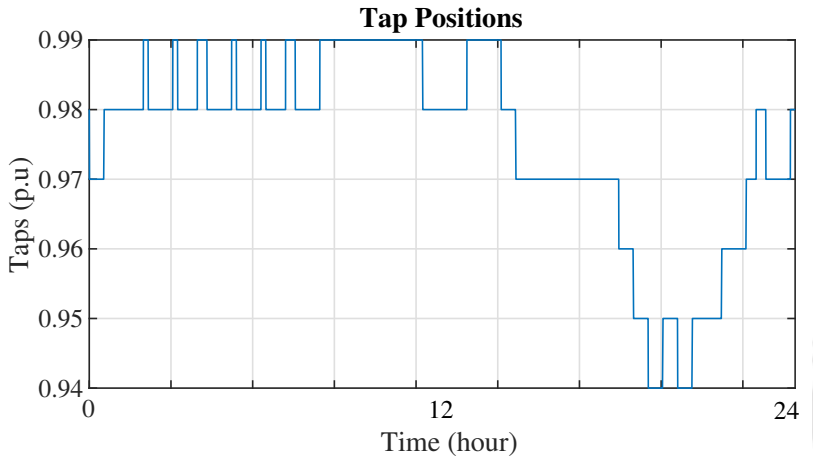

Figure 3.12: Tap positions corresponding to the proposed voltage control scheme.

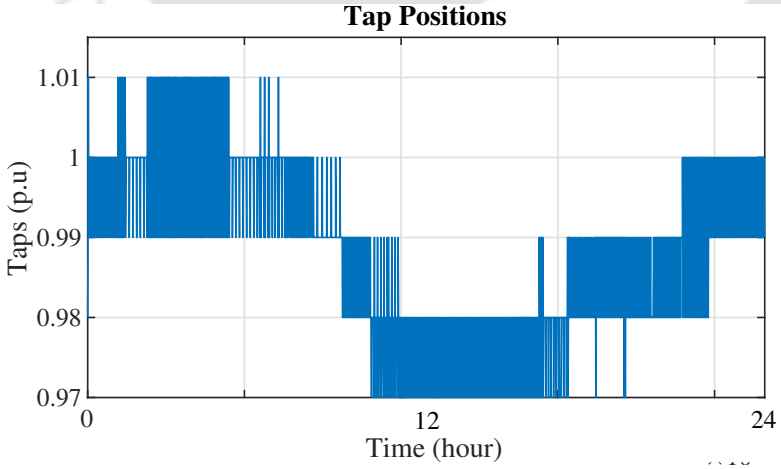

Figure 3.13: Tap positions corresponding to the single-timescale voltage control scheme.

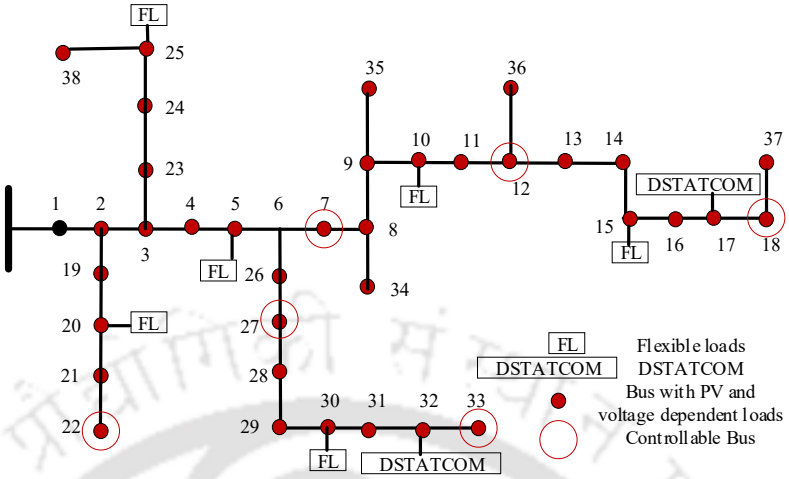

Figure 3.14: Test network: 38-bus distribution network.

Table 3.5: Comparison of energy loss, consumption and peak demand for all the cases

S. No.	Energy loss (MWh)	Energy consumption (MWh)	Peak demand at 15^{th} hour (MW)	Maximum/minimum voltage before control(pu)
Case 1	7.207	136.826	0.5901	1.051/0.88
Case 2	6.531	137.108	0.5898	1.059/0.9081
Case 3	6.343	135.849	0.5833	1.048/0.8741
Case 4	7.909	136.956	0.5712	1.062/0.896
Case 5	6.066	136.428	0.5805	1.043/0.8759

3.5.5 Validation of proposed method in 38-bus distribution networks

The proposed control scheme is further validated in a 38-bus balanced distribution system. The test network with allocation of PV units, DSTATCOM, flexible and voltage dependent loads, is shown in Fig. 3.14. The voltage profile of bus-18 is illustrated in Fig. 3.15 for Cases 3, 4, and 5. As observed from Fig. 3.15, voltage magnitudes are outside the prescribed limits at few time instants. However, with the help of the proposed scheme, the voltages are brought back to their desired limits within few seconds. The energy losses calculated during the 24-hour simulation are 6.343, 7.909, and 6.006 MWh for Cases 3, 4, and 5, respectively. Moreover, the consumption of energy for Cases 3, 4 and 5 are 135.849, 136.956, and 136.428 MWh, respectively. Table 3.5 depicts the numerical results with 38-bus distribution networks. The results obtained with this test network are found to be consistent and similar to the 33-bus distribution network.

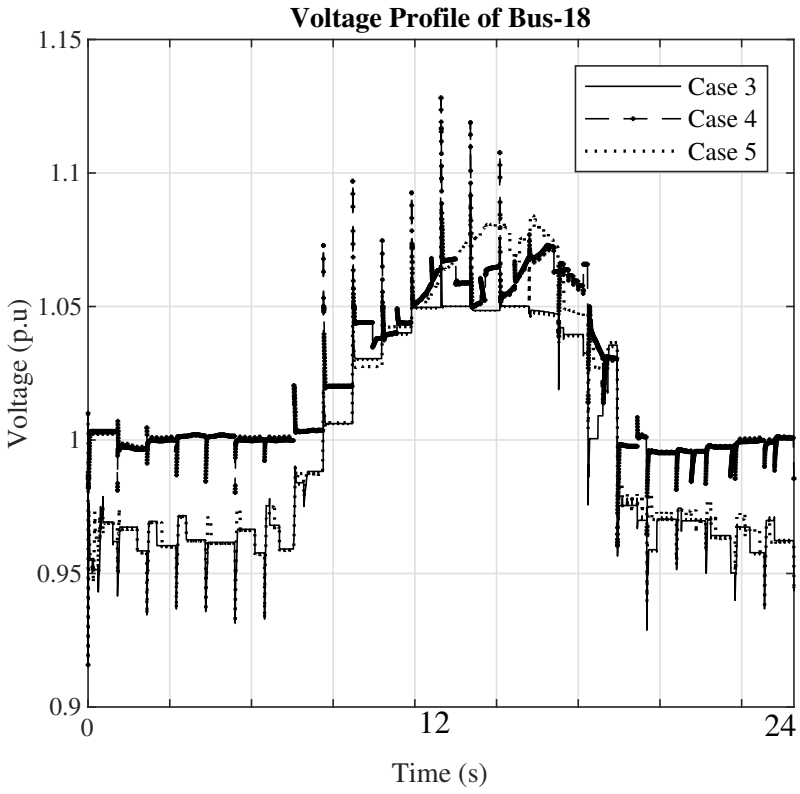

Figure 3.15: Voltage profile of bus-18 for Cases 3, 4, and 5 in 38-bus distribution network.

3.6 Conclusion

In this chapter, a voltage control framework has been developed that coordinates the OLTC operation on hourly basis, and smart inverters interfaced PV units and DSTATCOM operations every one minute. This dual-timescale coordinated algorithm effectively reduces power loss as well as OLTC tap operations. The two functionalities (CVR and DR) of ADMS have been explored further in this framework. Different cases have been studied and compared on the basis of a few variables, such as, energy loss, voltage profile, energy consumption and peak demand. Simulation results depict that the integration of these two functions in the MPC-based VVC helps in reduction of energy loss, peak demand, energy consumption and controllable resource utilization. The CVR operation with PV inverters' reactive power capability yields better results in terms of higher reduction in energy consumptions, system losses, and deeper voltage reduction within ANSI standard in comparison with only CVR (absence of PV inverter).

4

Coordinated Volt/Var Control of PV and EV Interfaced Active Distribution Networks Based on Dual-Stage Model Predictive Control

Contents

In the last Chapter, a dual-stage MPC-based approach has been developed to coordinate different volt/var devices with different temporal characteristics for regulating voltages. This chapter presents a dual-stage coordinated control approach for voltage regulation and congestion management of ADN in the presence of PV generators and electric vehicle charging stations (EVCS). The proposed scheme operates on rule-based model predictive control (RBMPC) to optimally manage the settings of the regulating devices, i.e., OLTC, DSTATCOM, PV generators, and EV inverters that possess different temporal characteristics. The first (hourly timescale) and the second (one-minute timescale) stages of the dual-stage coordinated control mechanism are designed to correct the long-term and short-term voltage fluctuations, respectively. The objectives of the proposed approach are to minimize the number of OLTC operations (first stage) and changes in set-points of PV and EV inverters, and DSTATCOM (second stage) in addition to minimization of slack variables, energy loss, and voltage error at EV charging stations. In both the stages, pre-defined rules are set for MPC to optimize different objectives on the basis of the magnitudes of bus voltages. Simulations are performed on 33-bus and 38-bus distribution networks to test the efficacy of the control approach. It is observed that the proposed approach could mitigate the voltage variations as well as line congestion for different scenarios.

4.1 Introduction

Power distribution networks are undergoing fundamental changes due to the rapid progression of PV units and EV [69], [31]. The high surge in the penetration of intermittent renewables and EV would not only affect the voltage profile but also add more stress to the power system's aging infrastructure [6,20]. Hence, an effective control strategy is necessary to overcome the concurrent over/under voltage issues arising due to the integration of PV generators/EVCS in distribution networks.

Several control schemes are discussed in the literature to regulate bus voltages in active distribution networks (ADN). The voltage regulation is generally performed either in decentralized [8, 26, 70], distributed [11, 16, 27], or centralized [6, 10, 14, 20, 28, 71–73] manner.

- *Decentralized control scheme:* In decentralized control schemes [8, 26, 70], the voltage regulating devices utilize local measurements to control their local buses in a predefined manner. Peng Li. et al. [26] have proposed a model predictive control (MPC) based local strategy to alleviate voltage violations and power losses across the distribution network with reduced computation burden. Despite being easy to implement and require less infrastructure, decentralized approaches

are likely to over-exploit specific controllable devices rather than coordinating all devices in a network.

- *Distributed control scheme:* Distributed control schemes [11, 16, 27] are based on a multi-agent system, in which each agent receives information from their neighbouring agents and collaborate to reach a consensus. A cooperative voltage control strategy has been developed for MV distribution networks consisting of an EV charging station and PV units [27]. Although distributed control schemes enable information sharing between control agents to achieve voltage regulation, it is more like a case-specific approach and mostly lacks optimal coordination [20].

- *Centralized control scheme:* The centralized control schemes [6, 10, 14, 20, 28, 71–73] can achieve optimal voltage control effect by using either an online or offline optimization approach. Moreover, these control schemes provide more controllability. However, they need high investment in communication and remote terminal units to dispatch controllable resources optimally to regulate voltages. In [6], MPC is used as an online corrective controller, placed centrally to correct the voltage deviations by minimizing changes in reactive/active power of the DG units and tap positions of on-load tap changing (OLTC) transformers. A non-linear program with three consecutive stages is formulated in [20] as a voltage regulation problem. MPC is used in [28] as a centralized voltage control strategy considering uncertainties from load demands and PV generations. The coordinated operation between OLTC and battery energy storage system is ensured through weighted average approximation in [71]. MPC approach is used in [72] and [73] to schedule different volt/var devices in presence of wind energy generators. In [14], preventive and corrective control modes are designed to coordinate the economic operation and voltage regulation. An MPC-based centralized corrective controller is developed in [10] to refine the corrections obtained from local control. In Chapter 2, several rules are devised on the basis of voltage magnitudes to effectively utilize the single-timescale MPC approach.

Despite considerable work on centralized coordinated voltage control, very few of them have focused on multi-timescale coordination of regulation devices that possess different temporal characteristics [21, 74, 75]. Guo et al. [21] have proposed a double timescale control framework based on MPC principles. Authors in [74] aim to utilize multiple volt/var devices in different time scales to overcome the effects of uncertain voltage fluctuation and deviation. However, it will be interesting to investigate the multi-timescale volt/var control in presence of EV charging stations. Subsequently, the capabilities

Table 4.1: Comparison of the proposed approach with similar approaches.

Attributes Consideration	This Chapter	Ref. [6]	Ref. [14]	Ref. [10]	Ref. [21]	Ref. [43]
Timescale decomposition of VR devices	✓	×	×	×	✓	✓
Reactive power support from DSTATCOM	✓	×	×	×	×	×
Reactive power support from EV	✓	×	×	×	×	✓
Line Congestion Analysis due to large EV demand	✓	×	×	✓	×	×

of EVCS for conservation voltage reduction (CVR) on different timescales is explored in [43]. However, in their work, the timescale decomposition is not based on the operation time characteristics of different volt/var devices.

Although the DG units' capabilities in providing fast reactive power support are explored in [10, 10, 14, 21, 72], such arrangement might involve oversized inverters leading to the increased overall cost and divert from the primary aim, i.e., energy harvesting. On the contrary, distribution static synchronous compensators (DSTATCOMs) are dedicated reactive power compensating devices that regulate the voltages independently and can reduce the utilization of over-sized PV inverters [60,70,76]. Particularly, in [60] local control algorithm has been developed to allocate DSTATCOM in distribution networks to coordinate the power electronics interfaced devices.

Furthermore, due to the availability of on-board chargers, opportunities emerge for EV to provide services to the distribution network operators (DNO) through vehicle-to-grid (V2G) technology. Recently, few works have been reported that explore the potential of EVs in providing reactive power services to the network [20, 31, 77, 78]. EV chargers can provide reactive power at different state-of-charge (SoC) without degrading the battery life cycle [20]. Although EV infrastructure benefits the distribution system through V2G services, the increasing number of EVs creates congestion in the feeders, resulting in network overloading [14, 79, 80]. In [79], an EV charge scheduling problem has been investigated to reduce line congestion in the distribution system. Nevertheless, their study lacks coordination between EVs and traditional compensating devices.

The comparison of the proposed approach with similar approaches is described in Table 4.1. The comparison has been done considering four different attributes as mentioned in Table 4.1. However, only a few reported works have considered all these four attributes. In view of the above discussion, an

attempt has been made to develop a dual-timescale based centralized coordinated control algorithm that follows the principles of MPC. The proposed MPC-based control scheme optimally coordinates the volt/var devices (EVCS, PV inverters, OLTC, and DSTATCOM) with different temporal characteristics to regulate the voltage profile of the network, while performing the congestion management. The proposed problem is formulated as a multi-objective optimization problem that includes energy loss and voltage error minimization, while maintaining the voltage magnitudes and branch currents within desired limits. To this end, the objectives of the current work are as follows:

(i) To develop a model predictive control scheme based on dual-timescale coordinated algorithm to maintain voltages and branch currents within desirable limits, with minimum use of control elements.

(ii) To manage line congestion in the distribution network due to increased penetration of EVs, while regulating the OLTC tap positions and dispatch of active power from PV, reactive power from DSTATCOM, EVCS, and PV units.

(iii) To perform sensitivity analysis to confirm the effectiveness of the coordinated MPC-based approach.

The rest of this work is organized as follows: Section 4.2 describes the modeling of ADN and its components, Section 4.3 illustrates the MPC-based dual-stage coordinated approach, Section 4.4 discusses the problem formulation, Section 4.5 presents the simulation results, and Section 4.6 concludes this chapter.

4.2 Active distribution network modeling

A radial distribution network with N number of buses is considered as in previous chapters. The set of buses and the distribution lines of the network are modeled as in Section 3.2 of Chapter 3. It is assumed that all the operations are carried out for a three-phase balanced network. Newton Raphson method is used for the initialization of the network. The active distribution network comprises OLTC, PV generators, loads, DSTATCOM, and EVCS.

The power profiles of residential, commercial, and industrial types of loads are depicted in Fig. 4.1(a). The active and reactive power (P_L and Q_L) absorptions by loads are some specific percent of the base loads [8]. The PV units are modeled as power injectors. The energy generation by PV

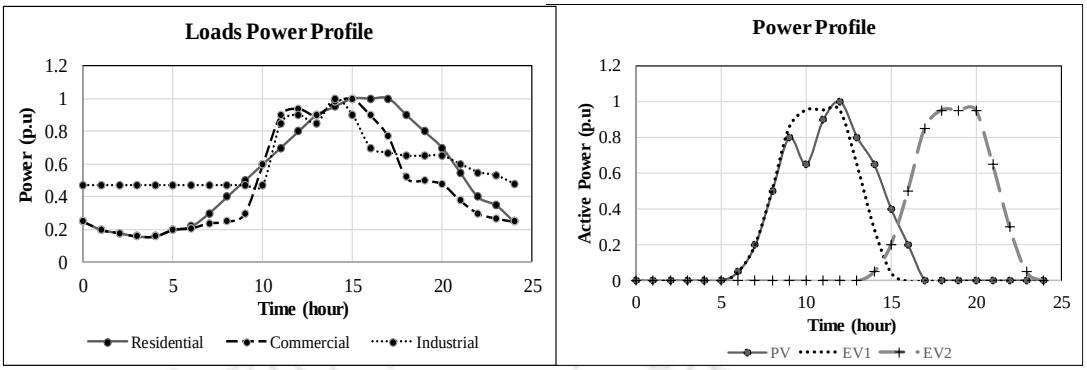

(a) (b)

Figure 4.1: Power profiles of (a) loads (b) PV units and EV charging station.

units is dependent on physical characteristics, such as, solar irradiance and ambient temperature. The active power generations of PV on a fifteen minutes timescale, P_{PV} based on irradiance are shown in Fig. 4.1(b) [20].

The charging power profiles of EVCS located in industrial [20] and residential [78] areas of the distribution network are depicted in Fig. 4.1(b). The charging stations are assumed to be an uncontrolled charging load, i.e., charging begins as soon as the EVs are plugged into the charging point. The information of each EV, such as state of charge, number of incoming vehicles, number of outgoing vehicles, etc. are shared by each EV owner with the EV aggregator of an area. The aggregator further conveys/receives necessary information of EV to/from the DNO. The EVs have the capability to inject/absorb reactive power to/from the network while charging process. The reactive power support is one of the vehicle-to-grid services provided by EVs to the network. This service is an added advantage, since it can be provided without degradation of battery life. The reactive power support could be provided in the first and fourth quadrants of the P-Q quadrant charging scheme, as demonstrated in Fig. 4.2(a) [77]. The profiles of the number of incoming vehicles to the charging station located in the industrial and residential areas are shown in Fig. 4.2(b).

A current injection model is used to model DSTATCOM as in Chapter 3. The current is always kept in quadrature with respect to the bus voltage. Thus, only reactive power is exchanged between the DSTATCOM and the ADN. The dynamic model of DSTATCOM, described by the differential equation is shown in Fig. 3.4 and represented by eqs. (3.6)-(3.7). The controller is employed with a non-windup limiter to ensure the DSTATCOM current gets locked if one of its limits is reached and

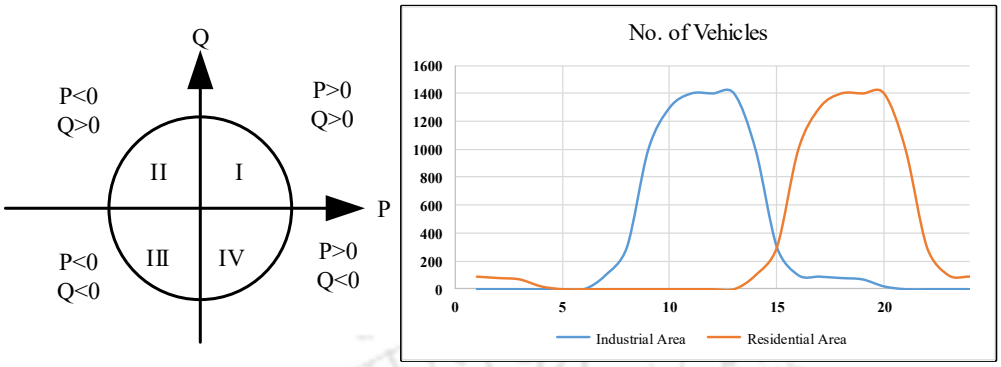

(a) (b)

Figure 4.2: (a) P-Q quadrant of EV (b) number of incoming vehicles to EV charging station.

the first derivative is set to zero.

4.3 Proposed voltage control approach

The control elements considered in this work are the reference voltage of OLTC and DSTATCOM, active power set-point of PV units, and reactive power set-points of PV and EV inverters. The OLTC, being discrete and slow, shows different temporal characteristics than the fast PV and EV inverters and DSTATCOM. Moreover, change in the OLTC tap position shall not exceed a specific limit so as to enhance its lifetime. Nevertheless, with power variations in loads and PV units, and the number of vehicles in a charging station, frequent oscillations of tap positions occur. Therefore, these different control elements need a coordination strategy based on different time scales.

As illustrated in Fig. 4.3, an MPC-based centralized dual-stage coordinated voltage control scheme is presented in this work. The DNO collects all the necessary data (voltage measurements, set-points of control devices) through the data acquisition system. The MPC processes this information and dispatches the optimal set-points to these control devices. In the first stage, the traditional device, such as, OLTC reference voltage is set assuming that PV sources are operating at maximum power point tracking mode. The reference voltage of OLTC is kept fixed for that hour of the day. In the second scale of operation, the active power of PV inverters, reactive powers of PV and EV inverters, and the reference voltage of DSTATCOM are controlled in an optimal manner to reduce the fast voltage variations. These control actions are repeated every 1 minute in this multi-step optimization based control scheme. In this dual-stage based operation, a set of pre-defined *if-then-else* rules is devised to have effective control. The active power of PV inverters is modulated only when the voltages are

outside the upper bound of the desired limits.

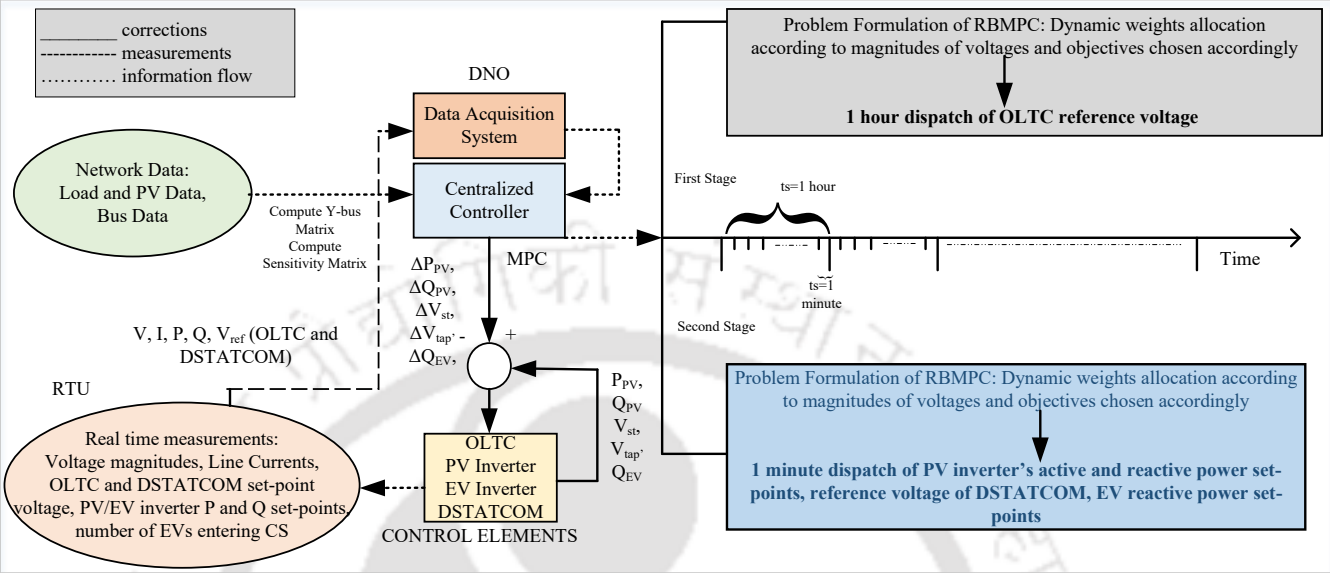

Figure 4.3: Block diagram of the proposed control strategy.

4.4 Problem formulation

A prediction model of the plant is the foremost requirement for MPC operation. The linear model can be represented by a state space model as in eq. (2.3). Further, the output equation can be represented as in eq. (2.4). In eqs. (2.3)-(2.4), $\boldsymbol{B}$ is the sensitivity matrix that represents the sensitivity of the monitored variables with respect to the control variables. $\boldsymbol{A}$ and $\boldsymbol{C}$ are the system matrix and output matrix, respectively.

It is to be noted that the voltage magnitudes of specific buses and branch currents of the ADN are the states of the network as well as the outputs of the prediction model. The reference voltage of OLTC is the controllable resource for the first stage, the active as well as reactive power of PV units, reactive power of EV inverter, and the reference voltage of DSTATCOM are the control inputs in the second stage, i.e.,

$$\Delta u_{first}(k) = [\Delta V_{tap}(k)]^T \tag{4.1}$$

$$\Delta u_{second}(k) = [\Delta P_{PV}, \Delta Q_{PV}, \Delta Q_{EV}, \Delta V_{st}]^T \tag{4.2}$$

The active power set-points of the PV inverters are used as emergency control action. The sensitivities of the bus voltages with respect to control variables are extracted from the Jacobian matrix, obtained through offline power flow [6]. The sensitivities of the branch currents with respect to control

variables are evaluated at each sampling point [80].

Let, the prediction and control horizon be N_P and N_C, respectively. Then, the prediction and control steps are N_P/t_s and N_C/t_s, where t_s represents the control period. The length of the prediction horizon, N_P is generally equal to or greater than the control horizon length, N_C. Moreover, $\Delta u(k+i) = 0$ is considered for $i \geq N_C$. It is assumed that there exists a communication infrastructure for the free-flow of information in the system. Suppose, the set of predicted input and output variables at each time instant be represented by Δu and y_p as in eqs. (2.5)-(2.6), respectively. Here, $y_P = [V(k+i|k), I(k+i|k)]^T$. The predicted outputs can be calculated sequentially with the help of eqs. (2.3) and (2.4).

For example, the predicted output at time instant $k+1$ can be calculated as:

$$y_p(k+1) = \boldsymbol{C}[\boldsymbol{A}x(k) + \boldsymbol{B}\Delta u(k)] \tag{4.3}$$

which implies,

$$y_p(k+1) = \boldsymbol{CA}x(k) + \boldsymbol{CB}\Delta u(k) \tag{4.4}$$

Similarly, $y_p(k+2)$ can be written as:

$$y_p(k+2) = \boldsymbol{CA}^2x(k) + \boldsymbol{CAB}\Delta u(k) + \boldsymbol{CB}\Delta u(k+1) \tag{4.5}$$

Thus, the output prediction matrix y_p can be formulated as in eqs. (2.12)-(2.14). Further, the inputs in a control horizon are written in terms of the previous input and change in input as in eqs. (4.6)-(4.7).

$$u(k) = u(k-1) + \Delta u(k) \tag{4.6}$$

Similarly,

$$u(k+1) = u(k) + \Delta u(k+1) = u(k-1) + \Delta u(k) + \Delta u(k+1) \tag{4.7}$$

Similarly, in concise form, control input matrix u can be written as:

$$u = \boldsymbol{G}u(k-1) + \boldsymbol{\Lambda}\Delta u \tag{4.8}$$

where $\boldsymbol{G} = [\boldsymbol{I} \quad \boldsymbol{I} \quad \boldsymbol{I}....\boldsymbol{I}]^T$ and $\boldsymbol{\Lambda} = \begin{bmatrix} \boldsymbol{I} & \boldsymbol{0} & \boldsymbol{0}.... & \boldsymbol{0} \\ \boldsymbol{I} & \boldsymbol{I} & \boldsymbol{0}.... & \boldsymbol{0} \\ \boldsymbol{I} & \boldsymbol{I} & \boldsymbol{I}.... & \boldsymbol{0} \\ \boldsymbol{I} & \boldsymbol{I} & \boldsymbol{I}.... & \boldsymbol{I} \end{bmatrix}$

Here, $\boldsymbol{I}$ is identity matrix and $\mathbf{0}$ is null matrix.

A quadratic programming problem is formulated for both the stages to minimize the utilization of controllable resources and slack variables, energy loss, and voltage deviations from the reference voltage. A set of pre-defined rules is devised on the basis of magnitudes of voltages. The objectives of MPC are changed dynamically during the simulations by changing the weight matrices associated with these objectives. Moreover, the output weighing matrix is chosen in such a manner that the voltage magnitudes of the buses connected to the charging stations reach 1 p.u. When magnitudes of voltages are within the desired limits, the objective function is:

$$min \sum_{i=1}^{N_P} [\|V_{ref}(k+i|k) - V(k+i|k)\|_Q^2 + \|\sigma 3\|_S^2 + \|P_{loss}\|_T^2] + \sum_{i=0}^{N_C-1} [\|\Delta u(k+i)\|_R^2] \tag{4.9}$$

Here, $\sigma 3$ represents the slack variable associated with the branch currents. When magnitudes of voltages are outside the desired limits the objective function is:

$$min \sum_{i=1}^{N_P} [\|\sigma\|_S^2] + \sum_{i=0}^{N_C-1} [\|\Delta u(k+i)\|_R^2] \tag{4.10}$$

Here, the control variables of MPC, $\Delta u(k)$ will be changed based on the stage of operation as shown in eqs. (4.1) and (4.2). The maximum number of OLTC operations during the day depends on the lifetime of OLTC. The OLTC reference voltage, being changed hourly during the day ensures the limited tap operation (< 24). The input constraints of the first stage are described by

$$\Delta u^{min} \leq \Delta u(k+i) \leq \Delta u^{max} \tag{4.11}$$

$$u^{min} \leq u(k+i) \leq u^{max} \tag{4.12}$$

$$Q_{PV} = \pm\sqrt{{S_{PV}}^2 - {P_{PV}}^2} \tag{4.13}$$

$$Q_{EV} = \pm\sqrt{{S_{EV}}^2 - {P_{EV}}^2} \tag{4.14}$$

for $i = 0, 1, ...N_C - 1$

The output constraints are further described in eq. (4.15)-(4.16)

$$-\sigma_1 1 + V^{min}(k+i) \leq V(k+i|k) \leq V^{max}(k+i) + \sigma_2 1 \tag{4.15}$$

$$I(k+i|k) \leq I^{max}(k+i) + \sigma_3 1 \tag{4.16}$$

for $i = 1, 2, ..., N_P$.

The equality constraints that have been used to design the optimal control problem are

$$V(k+i|k) = V(k+i-1|k) + \frac{\delta V}{\delta u^T}\Delta u(k+i-1) \tag{4.17}$$

$$I(k+i|k) = I(k+i-1|k) + \frac{\delta I}{\delta u^T}\Delta u(k+i-1) \tag{4.18}$$

for $i = 1, 2, ..., N_P$.

4.5 Simulation results and analysis

The proposed dual-stage coordinated control scheme is tested on a 33-bus balanced distribution network, as shown in Fig. 4.4. The IEEE 33-bus test system is modified to accommodate nine PV units and two EV charging stations. The PV units are located at buses numbered 4, 6, 12, 18, 20, 22, 25, 29, and 33. The EV charging stations are located at buses numbered 14 and 31. The rated capacities of the PV units and EV charging stations are taken as 1 MW. The loads are assumed to be residential, commercial, or industrial. For the sake of analysis, the time-varying profiles of loads, PV generation, and EV charging stations as represented in Fig. 4.1 are considered. While the profiles of loads and EVCS vary hourly over the day, the PV unit power is considered to vary at every 15 minutes interval. Furthermore, the test network is equipped with DSTATCOM as well as OLTC. The DSTATCOM is placed at bus-17 of the test network. Bus-1 is at the secondary side of the OLTC transformer. The parameters of OLTC and DSTATCOM are provided in Table 4.2. The DSTATCOM gain, K_{st} is chosen based on trial-and-error method. After a series of trials, K_{st} is set to 50. The system base is considered as 10 MVA, 12.6 kV, and the test data are taken from [81]. The simulations are carried out on a computer with specifications: Intel Core i5-6500 processor, 3.20 GHz, and 8 GB RAM with simulation platform: power system analysis toolbox (PSAT) in MATLAB R2018a. The optimization problem is solved by CPLEX solver.

The targeted limit of the voltages is kept as [0.95,1.05] p.u. Table 4.3 provides the controller parameters used for numerical simulations. All the simulations are run for 24 hours. The curtailment

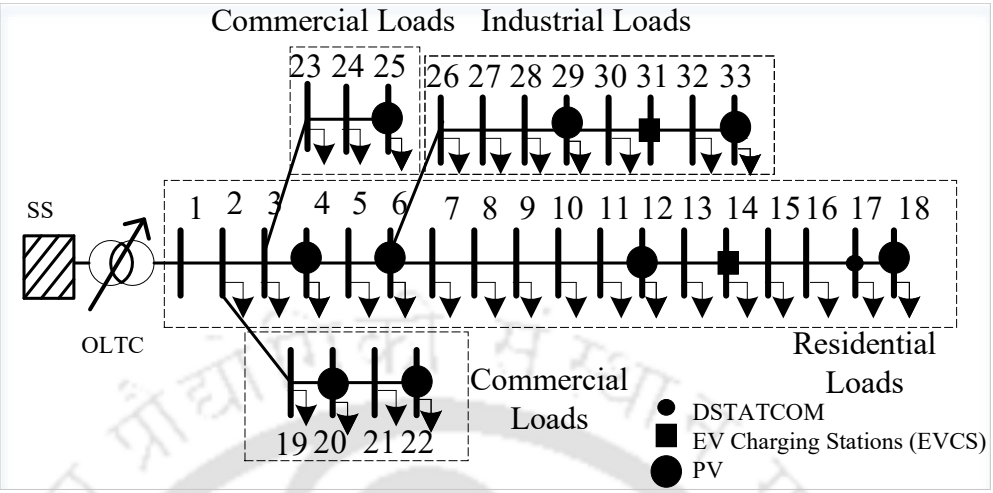

Figure 4.4: Test network: 33-bus distribution systems with allocation of loads, PV, DSTATCOM and EVCS.

Table 4.2: Parameters of OLTC and DSTATCOM.

OLTC		DSTATCOM	
Parameter	Value	Parameter	Value
Voltage rating	63.3/12.6kV	K_{st}	50
Number of taps	21	T_{st}	0.5
Deadband	2%	I_{max}	0.2 p.u
Step change	1% of V_{rated}	I_{min}	-0.2 p.u

of active power is chosen as the control variable only when the voltages' magnitudes are outside the targeted voltage's upper limit. The rules for MPC that are designed to change the weights associated with the objectives are described in Table 4.4.

4.5.1 Performance analysis of the proposed approach considering placement of EV charging station

Three cases are considered based on the placement of EV station in a distribution network. The cases are as follows:

- Case A: EV Charging Station in industrial area (Bus-31)

Table 4.3: Parameters of MPC.

First-stage	Second-stage
$N_C = 3$; $N_P = 15$	$N_C = N_P = 3$
$\Delta u = \Delta V_{tap}$	$\Delta u = [\Delta Q_{PV}, \Delta P_{PV}, \Delta Q_{EV}, \Delta V_{st}]$
t_s= 1 hour	t_s=1 minute

Table 4.4: Weights of rule-based MPC.

Voltage Range (p.u)	Weights (first stage)	Weights (second stage)
$V > 1.1$ or $V < 0.9$	$R_{V_{tap}} = 1$, $Q = 0$, $S = 1000, T = 0$	$R_P = 10, R_Q = 1$ $R_{st} = 1, R_{EV} = 1$ $Q = 0$, $S = 1000, T = 0$
$0.9 \leq V < 0.95$ or $1.05 < V \leq 1.1$	$R_{V_{tap}} = 5$, $Q = 0$, $S = 1000, T = 0$	$R_P = 50, R_Q = 5$ $R_{st} = 5, R_{EV} = 5$ $Q = 0$, $S = 1000, T = 0$
$0.95 \leq V \leq 1.05$	$R_{V_{tap}} = 10$, $Q = 1000$ $S = 0, T = 1$	$R_P = NA, R_Q = 10$ $R_{st} = 10, R_{EV} = 10$ $Q = 1, Q = 1000$ $S = 0, T = 1$

- Case B: EV Charging Station in residential area (Bus-14)
- Case C: EV Charging Station in both industrial (Bus-31) and residential areas (Bus-14)

Figs. 4.5, 4.6 and 4.7 show the corresponding simulation results representing voltage profiles, voltage profile at EVCS, branch current profile of line-1, and OLTC operation for 24 hours for Case A, Case B, and Case C, respectively. It can be observed that the bus voltages in all the cases reach their desired limits in due course of time. The voltage levels of EV charging stations at the 14^{th} and 15^{th} hours are selected to be shown in an enlarged view. The line-1, connected between bus-1 and bus-2 is chosen for line congestion analysis.

In Case A, the vehicles are parked and charged at the EV charging station during the daytime, since the location of EVCS is at the industrial lateral. As PV generation is available during EV charging, the voltage magnitudes are mostly within their limits. Unlike Case A, most of the vehicles enter the residential EV charging station during evening hours and begin charging their vehicles (Case B). Here, both over and under voltage scenarios are more prevalent than Case A. The reason behind this is the difference in charging hours from PV generation hours. The voltage magnitude drops down to 0.88 p.u in Case B, following which the control scheme initiates operation. Furthermore, the maximum voltage without any control is observed to be 1.062 p.u during the daytime, which is higher than the other two cases. This leads to utilization of more controllable resources, namely, active power curtailment, tap operations, and reactive power support from PV inverters, as observed from Table

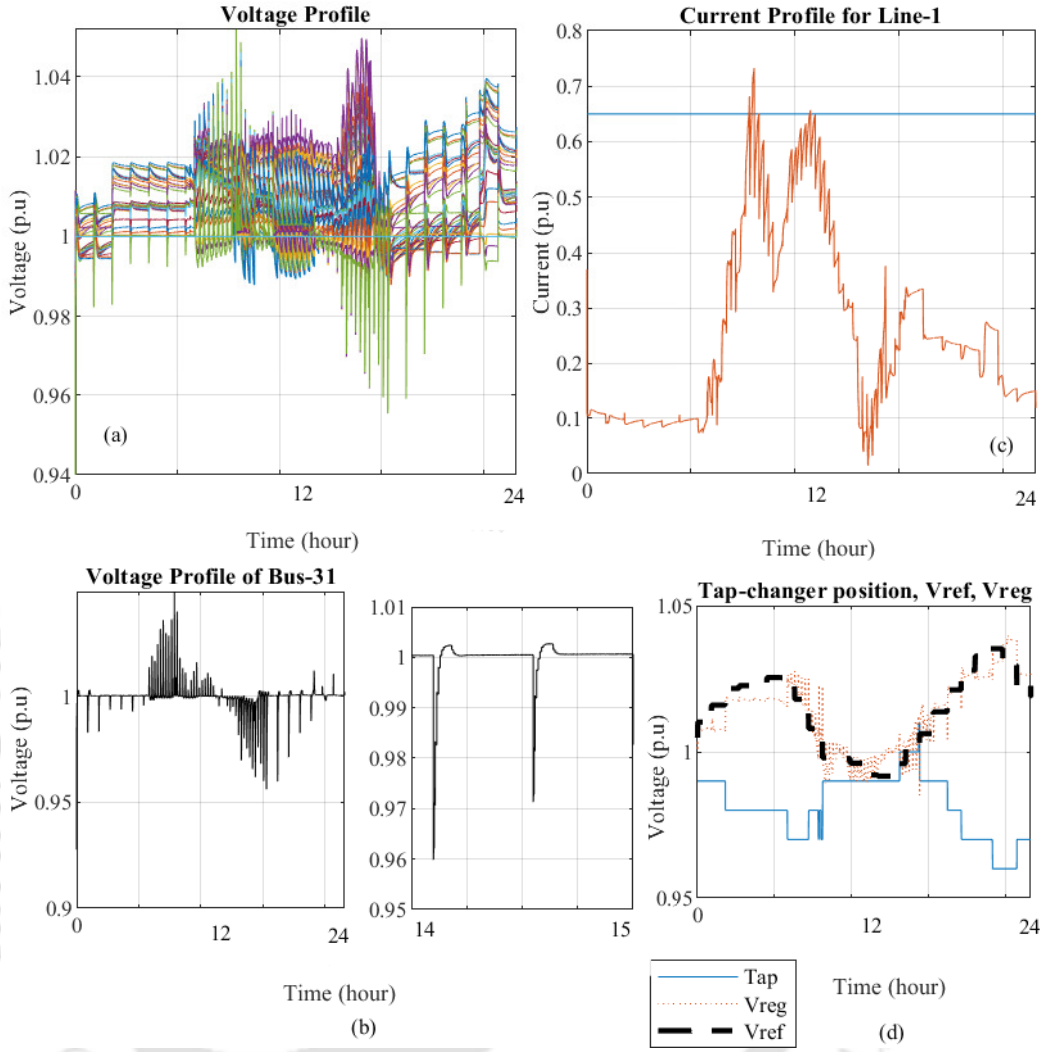

Figure 4.5: Simulation results with Case A for 33-bus distribution network: (a) voltage profile (b) voltage profile at EVCS, (c) current profile of line-1, (d) tap positions, V_{tap} and bus-1 voltage.

4.5. In Case C, the proposed approach is examined with EV charging stations both in the industrial and residential zones. In spite of more charging demand in this case, the controller performance, in terms of voltage magnitudes, energy loss, and resource utilization is better than Case B. This is due to the availability of more reactive power support from EVs. Thus, the reactive power absorption and injection from EVCS are greater in this case compared to Case A and Case B, as evident from Table 4.5. Although the branch current in line-1 exceeds the thermal limits in all the cases as in Figs. 4.5-4.7(c), the proposed scheme brings them within its bounds by utilizing the controllable resources effectively. The performance of the proposed controller for the three cases is provided in Table 4.5. It is observed that the number of taps is within the tap constraint (< 24) for all the cases.

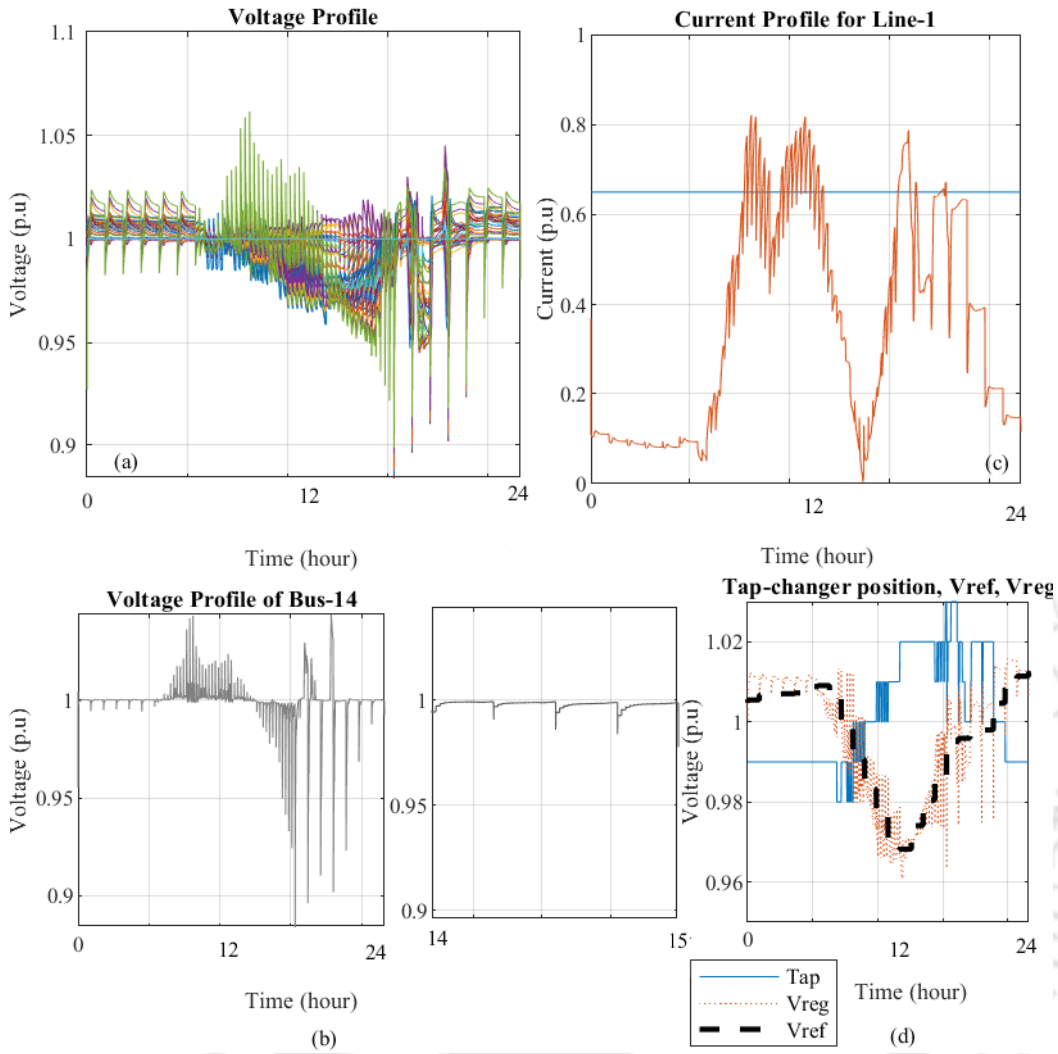

Figure 4.6: Simulation results with Case B for 33-bus distribution network: (a) voltage profile (b) voltage profile at EVCS, (c) current profile of line-1, (d) tap positions, V_{tap} and bus-1 voltage.

4.5.2 Comparative analysis

In this sub-section, the performance of the proposed approach is compared with RBMPC and MPC approaches reported in [14]. For the sake of comparison, the operating conditions are kept the same as Case C, and the corresponding results are depicted in Fig 4.8. Here, the voltage profile of the buses connected to EV charging stations, and tap positions of OLTC are analyzed for comparison purposes. Since the line connected between bus-24 and bus-25 shows overloaded condition, it has been considered to validate the congestion analysis. It is to be noted that line congestion is determined by the line congestion ratio (LCR), which is defined as the ratio of branch current (I) to the thermal limit (I_L^{max}). The numerical results of the comparative study are tabulated in Table 4.6.

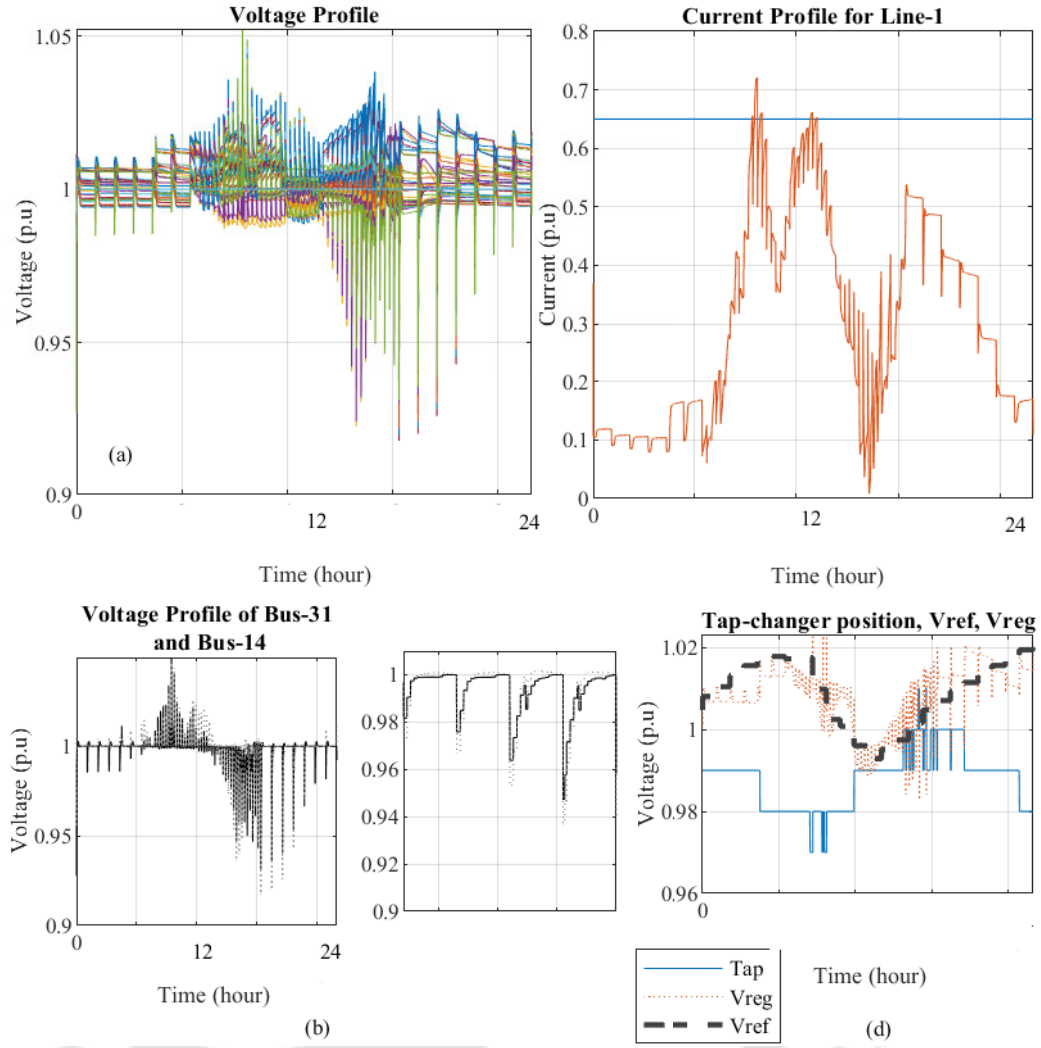

Figure 4.7: Simulation results with Case C for 33-bus distribution network: (a) voltage profile (b) voltage profile at EVCS, (c) current profile of line-1, (d) tap positions, V_{tap} and bus-1 voltage.

The results, shown in Fig. 4.8(a) and (b), indicate that the performance outcomes of the proposed controller are similar, or even improved to the ones obtained by the approaches used in [14] and Chapter 2. Due to the consideration of the reactive power support from DSTATCOM in the proposed approach, the maximum and minimum bus voltages observed during the day are almost near to the permissible limits. Besides, the voltage magnitudes at the buses connected to EV charging stations, deviate from the reference voltage (1 p.u) by a large amount using the MPC approach reported in Chapter 2 as shown in Fig. 4.8. Further, it is seen that the line-24 exceeds its thermal limits most of the time in 24-hour simulation using the strategies in [14] and Chapter 2. It is to note that the LCR of line-24 in the proposed approach is less than 1. However, LCR of line-24 is greater than 1 for the

Table 4.5: Numerical results obtained with different cases for 33-bus distribution network.

Cases	Energy loss (MWh)	Energy curtailed (MWh)	PV reactive power injection/absorption (MVArh)	EV reactive power injection/absorption (MVArh)	Maximum and Minimum Voltage before and after control (pu)	Taps
A	2.331	0.422	1.565/-2.067	0.295/-0.102	1.052/1.018 0.9559/0.9949	17
B	6.118	0.682	1.926/-2.350	0.365/-0.024	1.062/1.016 0.885/0.95	19
C	4.004	0.467	1.784/-1.805	0.450/-0.134	1.052/1.018 0.91/0.99	14

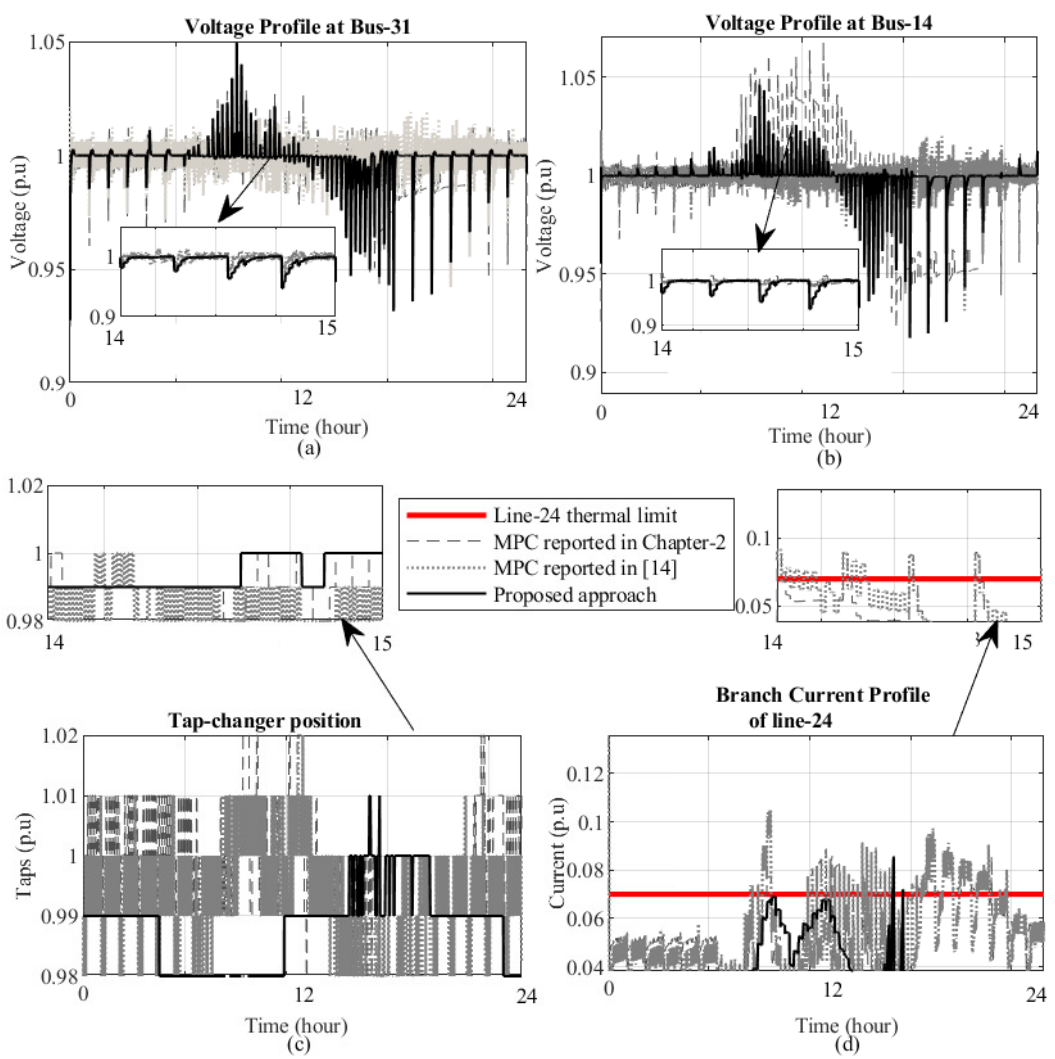

Figure 4.8: Simulation results for comparative studies (a) voltage profile of bus-31, (b) voltage profile of bus-14, (c) OLTC tap position and (d) branch current profile of line-24.

Table 4.6: Comparison of the proposed approach with other MPC approaches reported in literature.

Approach	PV active power curtailment (MWh)	PV reactive power injection/absorption (MVArh)	EV reactive power injection/absorption (MVArh)	Maximum and Minimum voltage before and after control (p.u)	No. of of taps	LCR of line-24
Proposed	0.467	2.023/-1.805	0.450/-0.134	1.052/1.018 0.91/0.99	14	<1
MPC in [14]	0.000	2.677/-2.060	0.510/-0.257	1.045/1.02 0.935/0.99	>24	>1
RBMPC Chapter 1	0.279	1.361/-1.024	_	1.083/1.05 0.92/0.95	>24	>1

other approaches.

The achievements of the proposed controller are further highlighted in terms of the number of tap changes. As observed from Table 4.6, it is clearly evident that the coordination based on timescale decomposition reduces the undesired oscillations of the discrete control devices, such as, OLTC. Comparatively, the proposed approach optimally harnesses the controllable resources to regulate voltages and branch currents. Whereas, the approach at [14] tries to minimize the voltage error of all the critical buses at every sampling point, resulting in extensive resource usage, such as, reactive power support from PV and EV inverters.

4.5.3 Sensitivity analysis

Sensitivity analysis has been performed in this sub-section to check the impacts of controllable resources on the proposed voltage regulation scheme. For this purpose, three scenarios are demonstrated considering the same test system as in Case C. The inference from these scenarios are as follows:

- Scenario 1: In this scenario, reactive power support from only PV and EV inverters (without DSTATCOM) are considered. As observed from Fig. 4.9(a), the voltage magnitudes of the buses rise to a greater value before initiation of control operation. This results in a high amount of PV power curtailment, and reactive power absorption from PV and EV inverters to bring down the voltages within the desired limits, as depicted in Table 4.7.

- Scenario 2: In this scenario, reactive power support from only EV inverters and DSTATCOM are considered. Reactive power compensation from PV inverters is not taken into consideration. The voltage profiles in Fig 4.9(b) show that although the penalty factor associated with voltage error is kept the same for all the scenarios, deviations from the reference voltage (1 p.u) is the

Table 4.7: Numerical results obtained with Scenarios 1, 2, and 3 for 33-bus distribution network.

Scenario No.	Energy loss MWh	PV active power curtailment MVArh	PV reactive power injection/absorption MVArh	EV reactive power injection/absorption MVArh	DSTATCOM reactive power injection/absorption MVArh	Maximum/Minimum voltage before control pu
1	3.672	0.685	2.160/-3.818	0.812/-0.356	_	1.113/ 0.88
2	3.955	0.000	_	0.599/-0.257	1.878/-12.412	1.04/0.88
3	3.926	0.009	2.471/-2.476	_	3.154/-7.626	1.06/0.91

largest in this scenario. Moreover, there is an increment of 7.7% in energy loss in this scenario as compared to Scenario 1. A large amount of reactive power is absorbed by DSTATCOM in order to limit the maximum voltage magnitude and maintain the bus voltages within the prescribed limits.

- Scenario 3: This scenario considers the reactive power support from only PV inverters and DSTATCOM. Here, EVs are acting as loads and do not provide V2G services. As observed from Fig 4.9(c), without reactive power support from industrial and residential EV inverters, the variations in the voltage profiles of bus-31 and bus-14 are less than the other scenarios. There are 14.4% and 67% increase in reactive power injection by PV inverters and DSTATCOM as compared to Scenario 1 and Scenario 2, respectively. This results in a considerably higher minimum voltage magnitude observed during the day compared to the other scenarios. The combined reactive power absorption from PV inverters and DSTATCOM help to maintain the bus voltage magnitudes.

Thus, it is evident that each control action in the proposed control approach has a role to play in voltage regulation and each of them needs coordination among them for better performance.

4.5.4 Performance of the proposed control scheme in 38-bus distribution system

The proposed control scheme is also validated in a 38-bus balanced distribution system. The test network with accommodation of PV units, DSTATCOM, loads, and EVCS is shown in Fig. 4.10. The data associated with the network is taken from [57]. The placement of PV plants, EVCS and DSTATCOM are kept same as in 33-bus distribution networks. The sampling time of the controller is 60 minutes for the first stage and 1 minute for the second stage.

As observed from Fig. 4.11, the bus voltage magnitudes for the three cases are well maintained

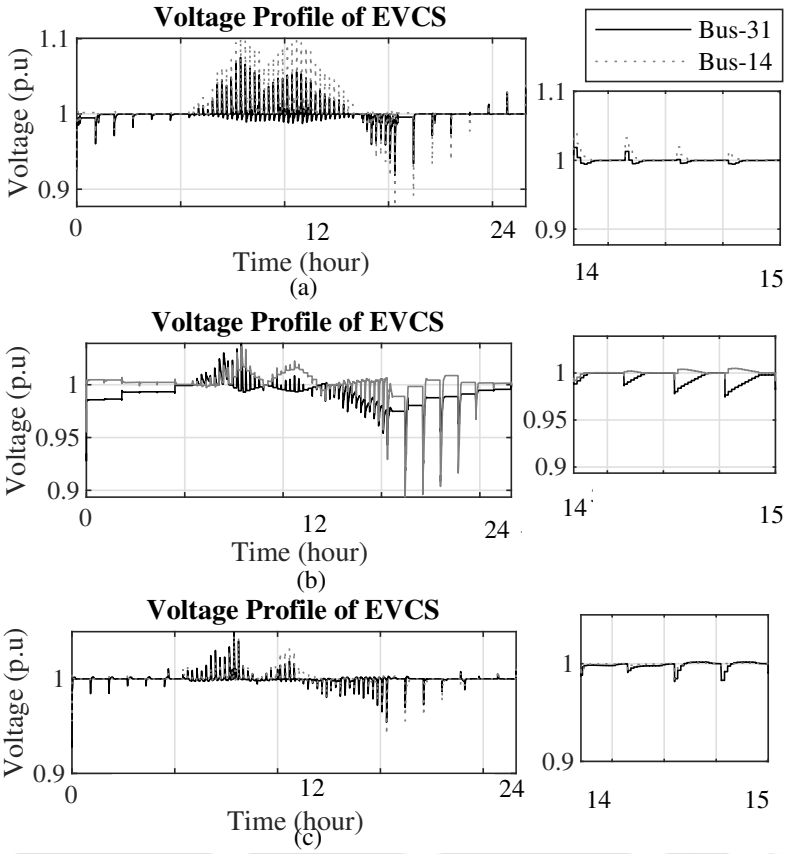

Figure 4.9: Simulation results for 33-bus distribution network: voltage profile of EVCS for (a) Scenario 1, (b) Scenario 2, (c) Scenario 3.

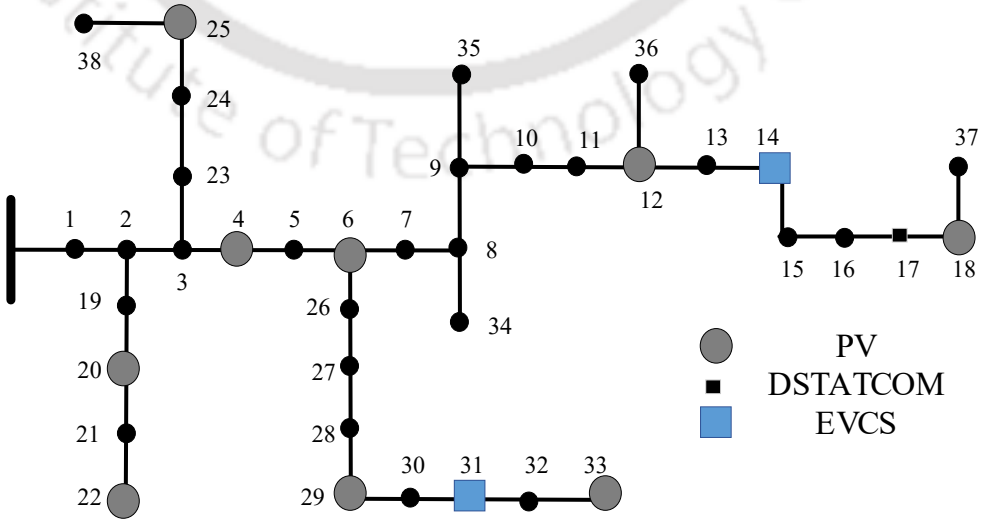

Figure 4.10: 38-bus distribution network.

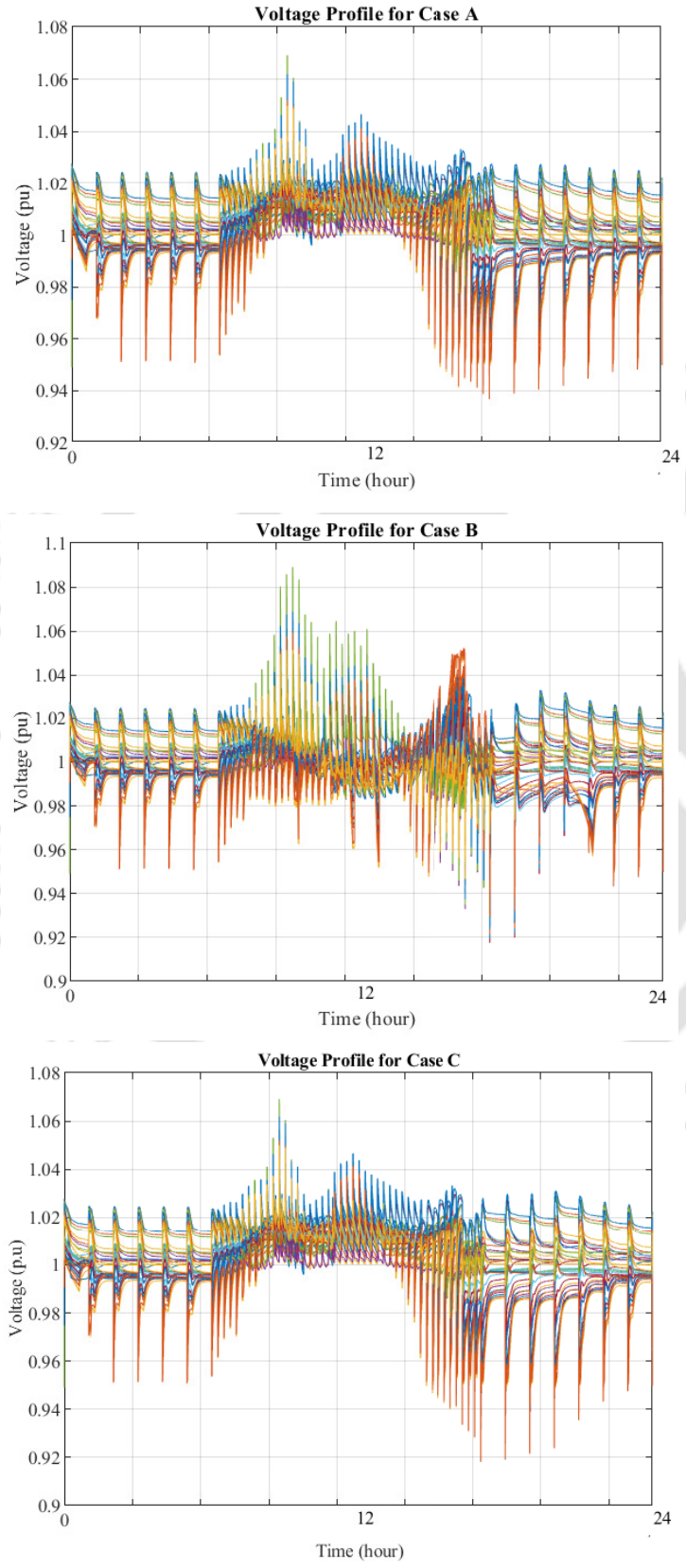

Figure 4.11: Voltage profile with the proposed control scheme in 38-bus distribution network: (a) Case A (b) Case B, (c) Case C.

within the desired limits during the day. Although at certain time instants, the bus voltages are out of the desired bounds, the proposed scheme successfully brings the voltages within desired limits. The reactive powers of PV and EVCS are changing dynamically throughout the day depending on the variations in loads and generation. Moreover, the tap positions of OLTC are changed, but within the tap constraint. The numerical results of this test network are depicted in Table 4.8. Although the charging demand is more in Case C compared to Case A and Case B, the controller performs better in Case C than Case B. This is due to the increased availability of reactive power support from on-board chargers of EVs. Moreover, energy loss is less in Case C as compared to Case B. It can be thus inferred that the results obtained with this test network are found to be consistent and similar to the 33-bus distribution network.

Table 4.8: Numerical results obtained with different cases for 38-bus distribution network.

Cases	Energy loss (MWh)	Energy curtailed (MWh)	PV reactive power injection/absorption (MVArh)	EV reactive power injection/absorption (MVArh)	Maximum/Minimum voltage before and after control (pu)
A	3.500	1.288	1.928/-2.947	0.260/-0.153	1.069/1.021 0.9367/0.98
B	5.421	2.329	2.568/-3.221	0.221/-0.002	1.089/1.033 0.91/0.9528
C	4.401	1.288	1.985/-2.887	0.523/-0.154	1.069/1.049 0.92/0.95

4.6 Conclusion

A dual-stage coordinated control mechanism based on principles of MPC has been presented in this chapter to coordinate controllable resources with different temporal characteristics for voltage regulation and congestion management. A set of rules is developed for both the stages to incorporate different weighted objectives on the basis of magnitudes of voltages. The proposed approach is validated in 33-bus and 38-bus distribution networks. The major findings of this study are as follows:

- In Case C, although the charging demand is more than the other two cases with two EVCS, the controller performs better than Case B. This is due to the increased availability of reactive power support from on-board chargers of EVs.
- The number of tap movements and line congestion in the proposed approach are considerably less than the other compared approaches due to the inclusion of timescale decomposition of

volt/var devices and branch current constraint in the proposed scheme.

- It is evident from the sensitivity analysis that the proposed approach, with proper coordination among the control elements, could fulfill the desired objectives. Each control element has a role to play in the voltage regulation scheme. While the DSTATCOM helps to limit the maximum voltage magnitudes, the reactive power support from PV inverters aids in minimizing voltage error and energy loss.

Moreover, the computation time for a particular sampling instant is evaluated to be few milliseconds, which makes the proposed approach compatible for practical use.

5

Coordinated Control Scheme for EV Charging and Volt/Var Devices Scheduling to Regulate Voltages of Active Distribution Networks

Contents

In the last chapter, a dual-stage MPC-based voltage control approach has been developed to coordinate the actions of OLTC, DSTATCOM, reactive power set-points of PV and EV inverters, and active power set-point of PV inverters. In this chapter, a three-stage MPC-based centralized coordinated approach has been developed to schedule charging of EV and volt/var devices. The approach aims at maintaining bus voltage magnitudes and state-of-charge (SoC) of EV battery within desired limits with minimal usage of control resources and cost of electricity consumption. The first stage determines the optimal operating points of traditional discrete control devices on an hourly basis. The second stage dispatches the optimal set-points of power electronics interfaced fast devices [PV and EV inverters] every one minute. The third stage schedules charging/discharging of EV half-hourly with respect to the real-time electricity price. Furthermore, several rules are formulated to adjust the local volt/var curve of PV and EV inverters according to the voltage magnitudes. The combined central and local control approach ensures that EVs attain the desired SoC at the time of their departure from the charging station without violating the voltage limits. The proposed control approach is tested in 33-bus distribution network and 38-bus distribution network with different operating conditions. Simulation results depict that the performance of the proposed control approach is better than uncoordinated charging in terms of reduced voltage deviations, energy loss, and control resources utilization.

5.1 Introduction

5.1.1 Background and motivation

Reducing carbon emissions and reliance on fossil fuels are the two major drivers of transportation electrification and renewable-based energy generation. This has led to a significant increase in the installed capacity of PV generators and the number of EV in the ADN [27]. Consequently, the integration of intermittent renewable-based DG units and uncoordinated charging of EVs have complicated the operation and planning of DNs.

The voltage regulation problem is one of the serious concerns arising out from the integration of DG units and the uncontrolled charging of EVs. Various control methods are proposed in the literature. However, the frequent voltage violations due to the stochastic nature of PVs and EVs increase the operations of certain voltage regulating devices (VRD), such as, OLTC, shunt capacitors, etc, leading to their lifetime degradation [82]. Thus, an advanced voltage control method is needed to coordinate different VRD, and utilize the PV and EV inverters for voltage regulation.

5.1.2 Literature review

With the advent of vehicle-to-grid (V2G) technology, the aggregated control, operation, and economics of EVs in smart grids have gained the attention of the research communities [82]. The coordinated control of EVs has been proposed for frequency [83] as well as voltage regulation [84]. Authors in [31, 85] have discussed several charging strategies for EVs to house a large number of EV penetrations in the DN. The reactive power support from EVs has been explored in [15, 31, 85] to minimize the node voltage variations without degrading the lifetime of the EV battery. In [30], the plug and play charging requests of shapeable loads (EV) are considered. Similarly, PV inverters have a high potential in providing support to the network operators with their control of real and reactive power [30, 51]. The services that can be provided by PV inverters are voltage and frequency regulation, active power controls, fault ride through, etc. [28, 51].

The PV and EV inverters need to work in coordination with other VRD to regulate the system voltages. The voltage regulation methodologies discussed in the literature are mainly categorized into decentralized, distributed, and centralized control schemes. The local or decentralized control approach causes competition among the control units and induces the possibility of oscillations in the network [28]. The distributed and centralized coordinated control approaches, on the contrary, have the potential to overcome the shortcomings of the local control approach and achieve optimal control performance. Ref. [26] has proposed a MPC-based local control strategy to tune parameters of control curves to obtain optimal voltage control performance. A distributed control strategy with two consensus algorithms has been developed in [23] to coordinate the EV battery and PV active power. A distributed MPC-based online EV charge scheduling has been developed in [86] with power flow and voltage constraints satisfied. Authors in [14, 14, 21] have proposed an MPC-based control strategy to coordinate different volt/var devices either on a single timescale or dual timescale to maintain node voltages within desired limits. Although there exists significant literature on centralized coordinated voltage control schemes [10, 14, 21, 28], very little work has been done on EV charge scheduling in addition to scheduling other VRD for voltage regulation. With consideration of the charging constraints of ESS, EVs can be treated as ESS with a particular requirement on the final SoC at a given time. However, detailed modeling of EV charging stations is necessary to analyze the effect of EV charge scheduling in the volt/var control.

From the literature survey, it can be found that coordinated EV charging along with the operation

of other VRD (smart inverters, OLTC) is rarely investigated. In this work, both the real and reactive power of EVs and PVs will be coordinated along with the reference voltage of OLTC in a centralized manner. Therefore, a three-stage coordinated voltage control scheme based on MPC principles has been proposed in this chapter to effectively utilize the multiple units with different temporal characteristics. Besides, EV user's satisfaction (in terms of desired SoC at departure time) is ensured with the coordinated operation of the control units.

5.1.3 Contributions of this chapter

To fill out the research gap as mentioned above, this chapter aims to develop an online control scheme for EV charging and scheduling volt/var devices to deal with the voltage regulation issues caused by high PV and EV penetrations in DN. The major contributions of this work can be summarized as follows:

(i) The volt/var devices are coordinated in two different time scales. At the first stage, the reference voltage of OLTC is set and kept fixed for the next hour. In the second stage, the PV power set-points and reactive power set-points of EV are dispatched to each inverter.

(ii) At the lower level, a local controller receives the reactive power set-points and adjusts according to the volt/var curve.

(iii) The EV charge scheduling is performed in the third stage by taking into consideration the balance between the operating cost and customer satisfaction.

This chapter is structured as follows: the system descriptions including modeling of EV charging stations are discussed in Section 5.2. In Section 5.3, the proposed voltage control strategy is explained explicitly. Simulation results are presented and discussed in Section 5.4. Finally, Section 5.5 draws the conclusion.

5.2 System description

A radial distribution system with N number of buses in the set $N = [1, 2..., N]$ is considered. The set of edges, $\epsilon = (m, n) \subset NXN$ represent the distribution lines of the network. Each line is represented by admittance $Y_{mn} = (R_{mn} + j\omega L_{mn})^{-1}$. The DG units are connected to a set of buses $P \subset N$. The EV charging stations (CS) are connected to buses $H \subset N$. Node-1 is the secondary

side of the substation transformer equipped with OLTC. The loads are modeled as constant power loads that vary hourly over the day. The residential, industrial, and commercial types of loads are distributed in the network.

The EVCS models are developed considering the EV characteristics, such as, initial SoC, time of arrival, and time of departure. Moreover, these EV characteristics change based on their placements in the DN. The EVs are considered to be located in the industrial and residential lateral of the DN. The EV owners are managed and controlled by an EV aggregator of an area. The EV owners of residential and industrial laterals receive the data and accordingly, models of EVs are developed [31,85] as shown in Fig. 5.1. The initial SoC, plug-in and plug-out times of EVs are generated from a normal probability distribution function.

Figs. 5.1 (a), (b) and (c) represent the SoC of EVs at arrival times, plug-in and plug-out times of the EVs in the residential area, respectively. Similarly, Figs. 5.1 (d), (e) and (f) show the initial SoC, plug-in and plug-out times of EVs in the industrial area. Maximum of the EVs' initial SoC, arrival time and the departure time in the residential area are 0.4, 7:00 PM and 7:00 AM. Similarly the maximum number of EVs in the industrial area is found to have SoC of 0.4 while entering the charging station. The time of arrival and departure of the maximum number of EVs in the industrial area are 9:00 A.M. and 6:00 P.M., respectively, according to Fig. 5.1. The data of arrival time of EVs in the residential area follow a normal distribution with a mean of 19:00 hours and a standard deviation of 2.2 hours. Similarly, data of departure time for residential EVs, the arrival and departure of EVs in the industrial area are generated from the mean and standard deviation data. The mean of normal distribution of EVs' arrival SoC for residential and industrial laterals is considered as 0.4.

The final SoC, (soc_{fin}) for all the EVs is considered to be 0.8. It is presumed that there are 1000 and 450 EVs in industrial and residential areas, respectively. It is further assumed that the chargers in the EV charging stations are bidirectional. Both parking as well as charging events occur in the EVCS.

The time for which EVs are parked at the CS is defined as the parking time, t_{park} and is evaluated as

$$t_{park} = t_a - t_d \tag{5.1}$$

where t_a, t_d are the arrival and departure time of EVs to the CS. The EV driver submits the EV data, i.e., initial and final SoC, energy requirement, their parking time, all-electric range, and battery

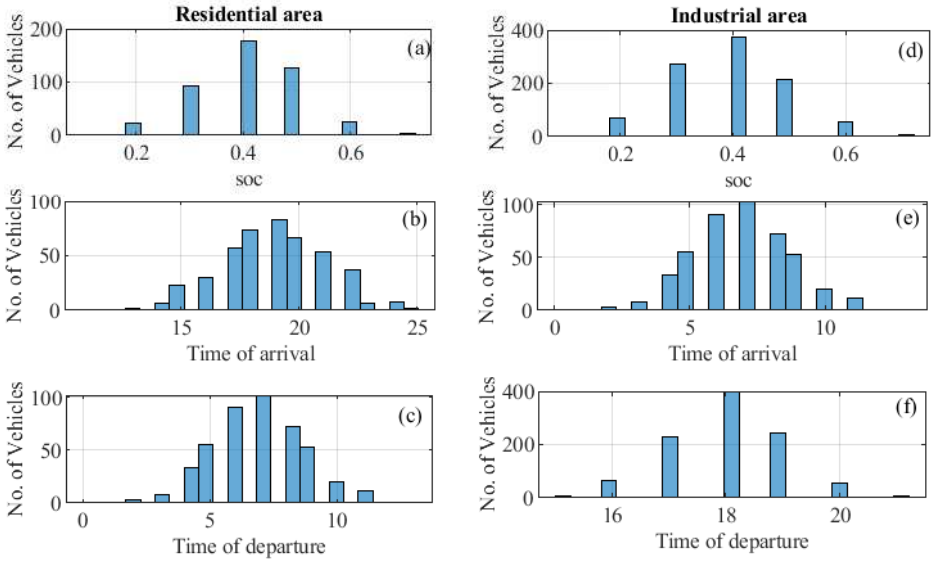

Figure 5.1: Data of EV: (a) initial SoC of EVs in residential area, (b) plug-in time of EVs in residential area, (c) plug-out time of EVs in residential area, (d) initial SoC of EVs in industrial area, (e) plug-in time of EVs in industrial area, (f) plug-out time of EVs in industrial area.

specifications to the EV aggregator of that area as soon as it reaches the charging station.

The required energy for each EV, E_{req} as calculated by aggregator at the arrival time is evaluated as

$$E_{req} = \frac{soc_{req}.B_{cap}}{\eta} \tag{5.2}$$

where B_{cap} and η are the battery capacity of EV and efficiency of the EV charger for charging/discharging, respectively. The soc_{req} is given by

$$soc_{req} = soc_{fin} - soc_{init} \tag{5.3}$$

Moreover, it is presumed that the CS has the capability to provide reactive power support to the network in addition to dispatch of active power to/from the network. The EV charger reactive power absorption/injection is bounded by

$$Q_{EV} = \pm\sqrt{{S_{EV}}^2 - {P_{EV}}^2} \tag{5.4}$$

where S_{EV} and P_{EV} are the charger rating and active power dispatch by the EV charger. The state space model for EVs that fits into MPC framework is expressed as follows:

$$x(k+1) = soc(k+1) = soc(k) + \frac{P_{EV}}{B_{cap}}\eta\Delta t \tag{5.5}$$

where P_{EV} is the charging/discharging power of EV

$$y(k+1) = soc(k+1) \tag{5.6}$$

where $\boldsymbol{A}=\boldsymbol{I}$; $\boldsymbol{B}=\frac{\eta\Delta t}{B_{cap}}$; $\boldsymbol{C}=\boldsymbol{I}$.

Smart PV inverters can affect the feeder voltage with their active as well as reactive power production. This work assumes that the PV inverter is oversized to enable injection of at least 44% PV reactive power, even with 100% active power production. Further, due to economic considerations, the curtailment of PV active power is limited to 20% of its active power production. The reactive power set-points of the PV inverters, obtained from the centralized control are further adjusted according to an autonomous volt/var curve. Depending on the local voltage magnitudes, the volt/var curve determines the reactive power.

5.3 Proposed control scheme

The proposed control scheme aims at realizing two control objectives:

(i) Voltage control: To ensure voltage magnitudes at all the buses remain within bounds

(ii) User's desired SoC: To ensure that the desired energy is provided to all the EVs before departure

An online centralized controller (CC) that follows the principles of model predictive control is chosen to fulfill the desired objectives. The sensitivity model is chosen for prediction purposes. The sensitivity coefficients for the linear model of MPC are evaluated from the inversion of the Jacobian matrix [6]. The sensitivity matrix for a given network topology needs not to be updated frequently, and is extracted only once at the beginning of the simulations. The CC, on receiving the necessary information from the data acquisition system calculates a set of optimal control actions, out of which, only the first set is taken into consideration. The optimizer embedded into CC minimizes the cost function subject to certain constraints. Here, the CC aims at driving the voltages and the SoC of the EV battery to the desired values, with the minimum usage of controllable resources. The controllable resources are tap changing positions of OLTC and power set-points of PV and EV inverters. The proposed control scheme operates in three stages as depicted in Fig. 5.2. There are certain rules to adjust the volt/var curve according to local voltage magnitudes. This section describes the preliminaries of MPC and describes the stages of MPC in detail.

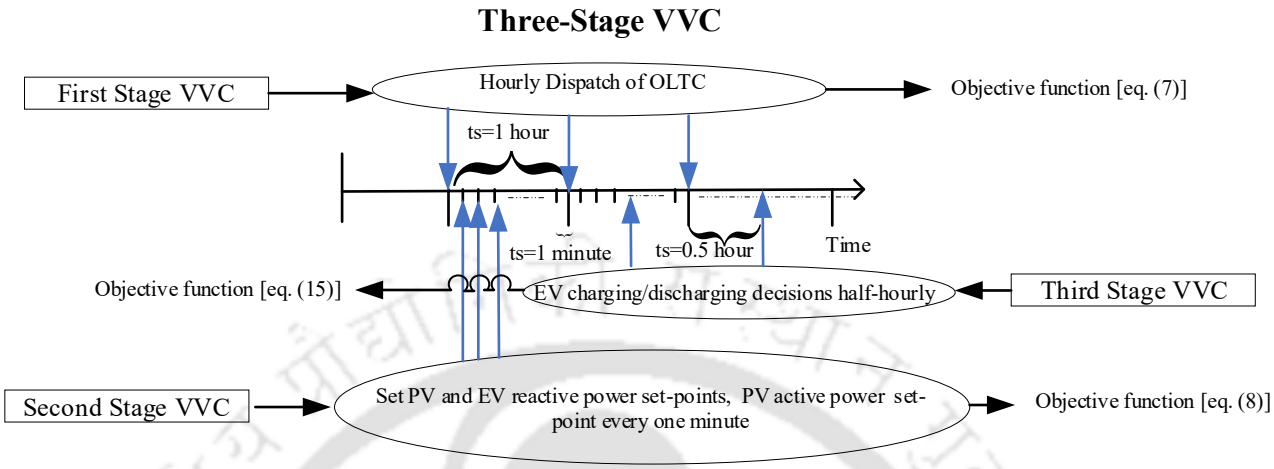

Figure 5.2: Coordinated centralized controller: three-stage MPC.

5.3.1 Three stages of MPC in the proposed scheme

To coordinate different voltage regulation devices with different operation time characteristics, the proposed control scheme is operated at three stages. In the first stage, the slow discrete devices' operation is optimized to bring the voltage levels within the desired limit. The optimal control problem at this stage is solved at every hour to minimize the switching operations of OLTC. The second stage aims at scheduling different fast volt/var devices at every one-minute interval. It is mainly designed to coordinate the reactive and active power injections of power electronics interfaced devices to deal with short-term voltage variations. The third stage deals with the economic charging of EVs to satisfy the EV users' demand. As the real-time electricity price is received by the EV aggregator of each area at half-hour interval, the charging/discharging decisions of EVs are taken half hourly. The optimization problem is formulated in such a way that it fits into the framework of economic MPC.

5.3.2 Problem formulation

Let, the incremental control inputs over the horizon be denoted by

$[\Delta u(k), \Delta u(k+1), ..., \Delta u(k+N_C-1)]$

and inputs be

$[u(k), u(k+1), ..., u(k+N_C-1)]$.

The outputs over the prediction horizon are represented as $[y(k+1), y(k+2), ..., y(k+N_P)]$.

The voltage magnitudes $[V(k)]$ and state-of-charge of the EVs $[soc(k)]$ are the outputs of MPC for all the stages. The OLTC reference voltage $[V_{tap}(k)]$ is input for the first stage, active and reactive power of PV and reactive power of EV $[P_{PV}(k), Q_{PV}(k), Q_{ev}(k)]$ are the second stage inputs, and charging/discharging power of EV $[P_{EV}(k)]$ is input for the third stage.

Similarly, incremental input vectors $[\Delta u(k)]$ for first, second and third stage are:

$[\Delta V_{tap}(k)]$,

$[\Delta P_{PV}(k), \Delta Q_{PV}(k), \Delta Q_{EV}(k)]$,

$[\Delta P_{EV}(k)]$, respectively.

The MPC problem for the first stage can be formulated as

$$min \sum_{i=1}^{N_P} [||V_{ref}(k+i|k) - V(k+i|k)||_Q^2 + ||\sigma||_S^2] + \sum_{i=0}^{N_C-1} ||\Delta V_{tap}(k+i)||_{R_{tap}}^2 \tag{5.7}$$

The MPC problem for the second stage can be formulated as

$$\begin{aligned} min \sum_{i=1}^{N_P} [||V_{ref}(k+i|k) - V(k+i|k)||_Q^2 + ||\sigma||_S^2] + \sum_{i=0}^{N_C-1} [||\Delta P_{PV}(k+i)||_{R_{PV_p}}^2 \\ + ||\Delta Q_{PV}(k+i)||_{R_{PV_q}}^2 + ||\Delta Q_{EV}(k+i)||_{R_{EV_q}}^2] \end{aligned} \tag{5.8}$$

The above objective functions are subjected to the following constraints:

$$\Delta u^{min} \leq \Delta u(k+i) \leq \Delta u^{max} \tag{5.9}$$

$$u^{min} \leq u(k+i) \leq u^{max} \tag{5.10}$$

In eqs. (5.9)-(5.10), u and Δu are changed according to the stage of operation.

$$Q_{PV} = \pm\sqrt{{S_{PV}}^2 - {P_{PV}}^2} \tag{5.11}$$

$$Q_{EV} = \pm\sqrt{{S_{EV}}^2 - {P_{EV}}^2} \tag{5.12}$$

for $i = 0, 1, ...N_C - 1$

It is to be noted that the active power of PV is curtailed to 20% of its rated capacity.

$$-\sigma_1 1 + V^{min}(k+i) \leq V(k+i|k) \leq V^{max}(k+i) + \sigma_2 1 \tag{5.13}$$

for $i = 1, 2, ..., N_P$.

$$V(k+i|k) = V(k+i-1|k) + \frac{\delta V}{\delta u^T}\Delta u(k+i-1) \tag{5.14}$$

for $i = 1, 2, ..., N_P$.

The objective function to be minimized in the third stage is a linear programming problem with economic considerations.

$$min \sum_{i=1}^{N_P}[||V_{ref}(k+i|k) - V(k+i|k)||_Q^2 + ||\sigma||_S^2] + \sum_{i=0}^{N_C-1}[RTP.\Delta P_{EV}(k) + p_y.\nu] \tag{5.15}$$

where, RTP is real-time price of electricity consumption and p_y is the penalty associated with the violation of output variable (SoC of EV battery). Eq. (5.15) is subjected to inequality and equality constraints as in (5.16)-(5.19) along with (5.13) and (5.14).

$$\Delta P_{EV}^{min} \leq \Delta P_{EV}(k+i) \leq \Delta P_{EV}^{max} \tag{5.16}$$

$$P_{EV}^{min} \leq P_{EV}(k+i) \leq P_{EV}^{max} \tag{5.17}$$

$$-\nu_1 1 + soc^{min}(k+i) \leq soc(k+i|k) \leq soc^{max}(k+i) + \nu_2 1 \tag{5.18}$$

$$soc(k+i|k) = soc(k+i-1|k) - \frac{P_{EV}(k+i-1)}{B_{cap}^{max}}\Delta t \tag{5.19}$$

for $i = 1, 2, ..., N_P$.

There are basically three types of MPC constraints: plant manipulated variable (MV); plant output variable (OV), and MV increment constraints. The physical limits on the plant MVs are included in MPC as hard MV bounds. The MV increment bounds are included when there is a known physical limit on the rate of change, or the application requires preventing large increments for some other reason.

Eqs. (5.16) and (5.17) are MV increments and MV constraints, respectively. Here, the charging /discharging power of EV is considered as the MV. They are hard constraints and are handled by the algorithm that the solver uses. However, due to varying charging power available at each sampling instant, the input variables and rate of inputs can be out of bounds. To cope with this situation, several rules are formulated to the MPC problem. They are:

- Rule 1: If at any time, the input constraints are violated due to the sudden changing available charging power from the aggregated EVs, the minimum/maximum value at that sampling instant

is automatically considered as discharging/charging power for the next sampling instant.

- Rule 2: The charging/discharging power is adjusted at every sampling instant to keep the storage constraints within desired bounds.

A popular method for handling state and output constraints in a MPC algorithm is to use "soft constraints", in which penalty terms are added directly to the objective function. Here, eq. (5.18) is the output constraint (*soc* being the OV). Slack variables, μ are added to OV with the aim to soften the constraint so as to diminish the possibility of infeasibility. These variables are heavily penalized by the penalty variable p_y.

Eq. (5.19) is the equality constraint that describes how the SoC of EV battery is updated at each sampling instant. This is the plant model for MPC and is thus, handled at each sampling instant.

Reaching the final SoC by all EVs at time of departure, t_d is one of the important constraints that needs to be satisfied. This is described in eq. (5.20).

$$soc(t_d) \geq soc_{req}. \tag{5.20}$$

Further, with the manipulation of lower bound constraint, $soc^{min}(k)$ of (5.18), constraint (5.20) can be satisfied. $soc^{min}(k)$ needs to be updated at every sampling instant. Using eqs. (5.18) and (5.20), the required constraint can be represented as:

$$soc^{min}(k) = max[soc_{req} - max(0, \{k_{out} - k)\eta \frac{P_{EV}^{max}}{B_{cap}^{max}}\}, soc_{low}] \tag{5.21}$$

Here, soc_{low} is limited to 0.2 due to physical considerations of the EV battery.

5.3.3 Local level control

The reactive power is dispatched by the centralized controller to the local control layer embedded in each DG unit. The PV and EV inverters need to have their local controller as per the recent distributed energy resources integration standards. A piecewise linear Q(V) characteristic is proposed as local control for each DG unit. This local characteristic is adjusted according to the set-points received from the centralized MPC as per Table. 5.1. The reactive power set-point received from the centralized control is denoted by Q_0.

Table 5.1: Adjustment rules of the local-level controller

Rule No.	Voltage Criteria	Adjustment Rules
1	$V < 0.9$	Q^{max}
2	$0.9 < V < 0.95$	$Q_0 + \frac{Q^{max}-Q_0}{0.9-0.95}(0.95 - V)$
3	$0.95 < V < 1.05$	Q_0
4	$1.05 < V < 1.1$	$Q_0 - \frac{Q^{max}+Q_0}{1.1-1.05}(V - 1.05)$
5	$V > 1.1$	$-Q^{max}$

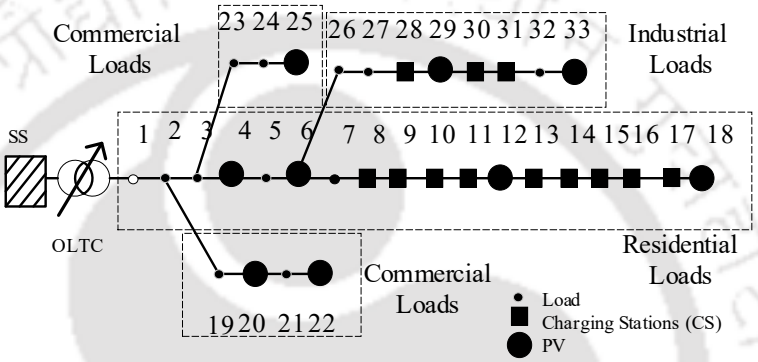

Figure 5.3: Test network: 33-bus radial distribution network

5.4 Results and discussions

To demonstrate the performance of the proposed scheme, the three-stage control method is tested in a 33-bus distribution network with nine PV units, loads, and twelve EV charging stations, as shown in Fig. 5.3. The active distribution network is connected to the substation through a 10 MVA, 66/12.6 kV tap-changing transformer. The configuration of the test network is taken from [56]. The power profiles of the PV units and the loads (residential, industrial and commercial) are depicted in Fig. 5.4. The EVs are placed in two areas, viz., industrial and residential areas. The plug-in and plug-out times and SoC for the EVs in both the areas are depicted in Table 5.2. Buses 1, 31, 4, 6, 9, 12, 15, 18, 20, 22, 25, 26, 29, and 33 are the controllable buses whose voltage magnitudes are sent to the MPC at every sampling instant. The control and prediction interval are designed to be three for all the stages. The sampling times are one hour, one minute, and thirty minutes for the first, second, and third stages, respectively.

To evaluate its performance, the test network is implemented in MATLAB R2018a and power system analysis toolbox (PSAT) on a PC with Intel Core i5-6500 processor running at 3.20 GHz and 8 GB of RAM. For optimization purposes, the CPLEX solver has been used. The two types of EV

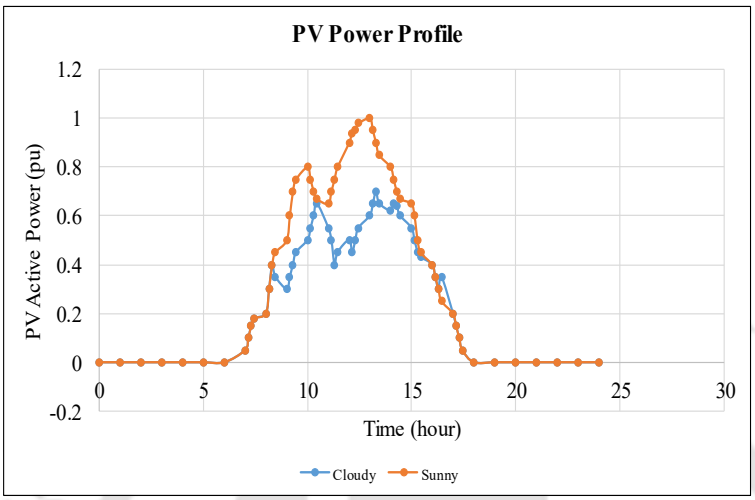

(a)

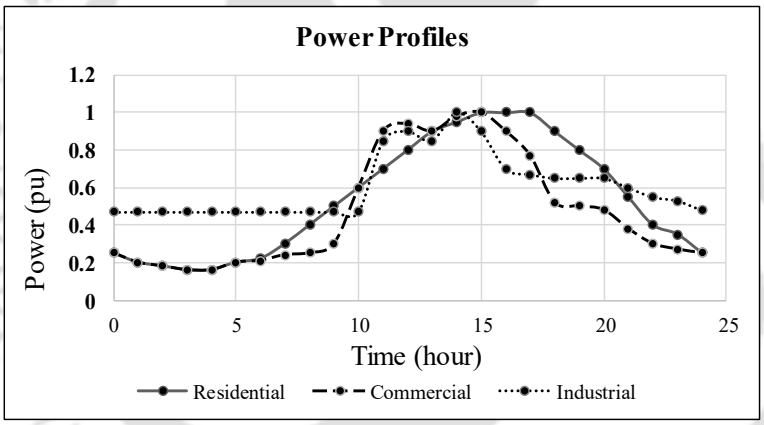

(b)

Figure 5.4: Active power profile of (a) solar PV on sunny and cloudy day, (b) residential, commercial and industrial loads

Table 5.2: Behaviour of EVCS

Type	Location	Mean of Initial SoC	Mean of Final SoC	Mean of Arrival time	Mean of Departure time	Charger rating rating
Industrial	28, 30,31	0.4	0.8	9:00 AM	6:00 PM	2 kW
Residential Residential	8,9,10,11,13, 14,15,16,17	0.4	0.8	7:00 PM	7:00 AM (next day)	4 kW

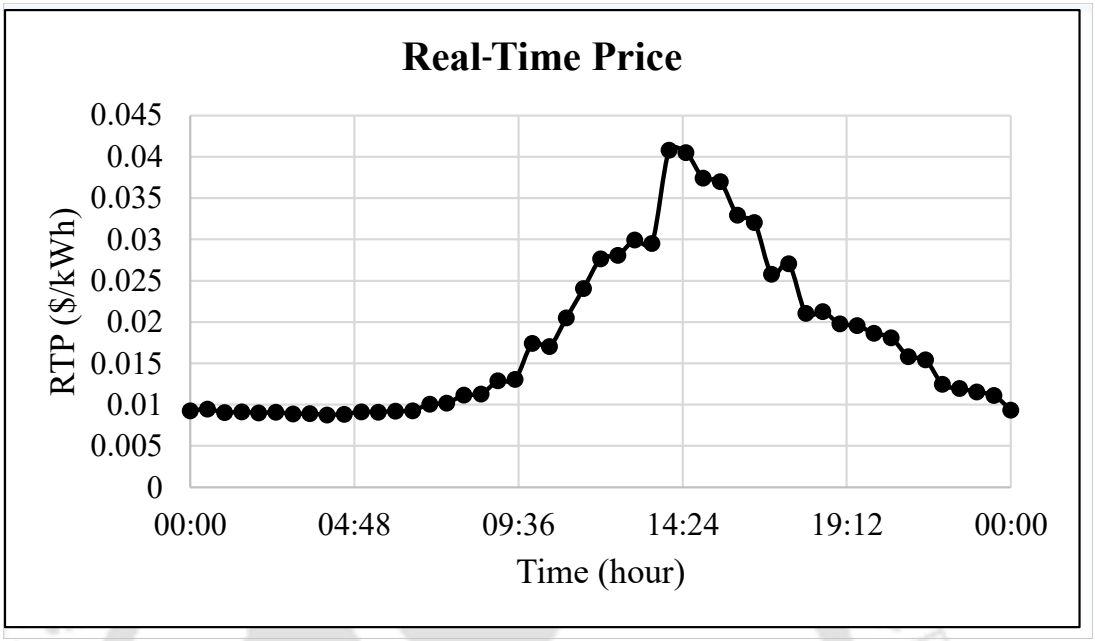

Figure 5.5: Real-time price of electricity consumption.

charging that have been studied in this chapter are:

- Type I: uncoordinated EV charging
- Type II: economic EV charging

In Type I charging, EVs are charged with maximum power once plugged in to the distribution network. On the other hand, in Type II charging, the charging occurs in accordance to eqs. (5.14)-(5.21). The profile of RTP of electricity consumption is shown in Fig. 5.5.

5.4.1 Performance analysis for different types of charging

The voltage profiles with Type I and Type II charging are depicted in Figs. 5.6 and 5.7, respectively. As shown in Figs. 5.6(a) and 5.7(a), both rise and drop in voltage magnitudes occur beyond the desirable voltage limits [0.95 p.u., 1.05 p.u.] due to Type I and Type II charging schemes. However, the voltage drop is more prominent in Type I charging due to the high EV charging load at a particular instant. The voltage profiles at 13^{th} hour are shown in Figs. 5.6(b) and 5.7(b) for further performance comparison. The highest voltage is observed to be around 1.06 p.u, immediately after the departure of all the EVs from the industrial EVCS. The under voltage occurs during charging of EVs. However, with the application of the proposed voltage regulation method, the voltages could be regulated after

a certain time for both types of charging. The active power profiles of the industrial and residential EVs for both types of charging are depicted in Figs. 5.6(c) and (d) and 5.7(c) and (d), respectively. The performance of the proposed control method with Type I and Type II charging is tabulated in Table 5.3. Nevertheless, the performance with Type I charging is found to be poor compared to Type II charging. The energy demand at 15^{th} hour in Type II charging has been decreased by 40.36% compared to Type I charging.

Table 5.3: Performance of Type I and Type II charging

Type	Energy loss (MWh)	PV curtailment (MWh)	PV reactive power injection/absorption (MVArh)	EV reactive power injection/absorption (MVArh)	Maximum voltage (p.u)	Minimum voltage (p.u)	EV energy demand from 13^{th} to 15^{th} hour (MWh)
I	3.234	0.477	2.044/-2.122	1.300/-0.518	1.065	0.9128	1677.9
II	2.582	0.448	1.798/-1.888	1.062/-0.477	1.069	0.9173	1000.648

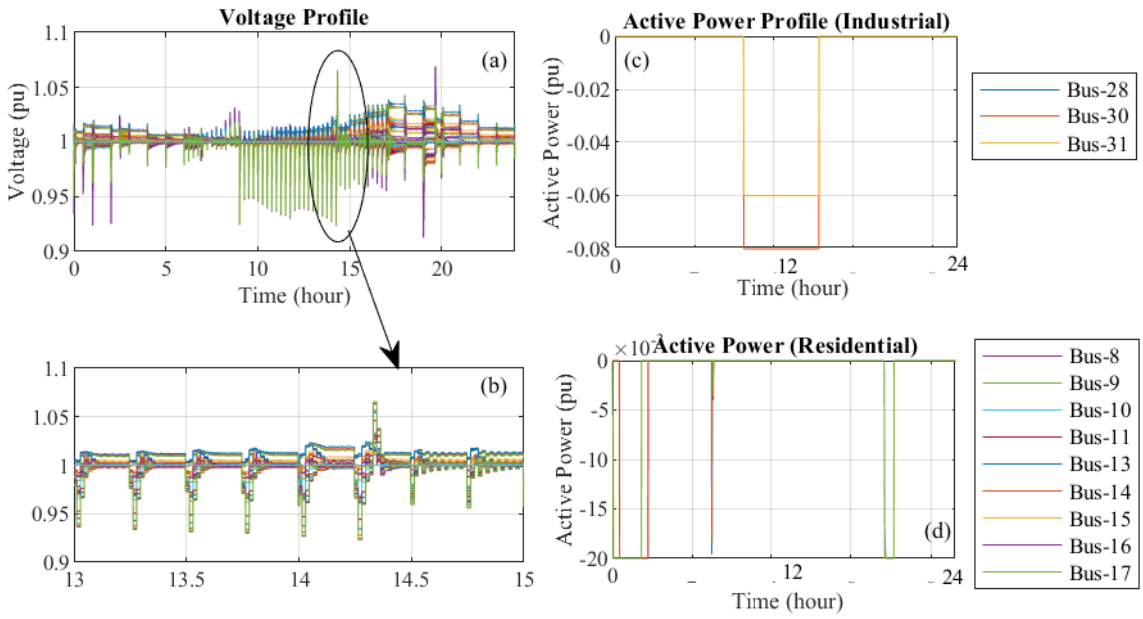

Figure 5.6: Simulation results with Type I charging: (a) voltage profile, (b) voltage profile at 13^{th} hour, (c) active power profile (industrial), (d) active power profile (residential)

5.4.2 Performance analysis during two extreme scenarios

The simulation is then performed under two extreme scenarios:

- Scenario I: light load and sunny condition

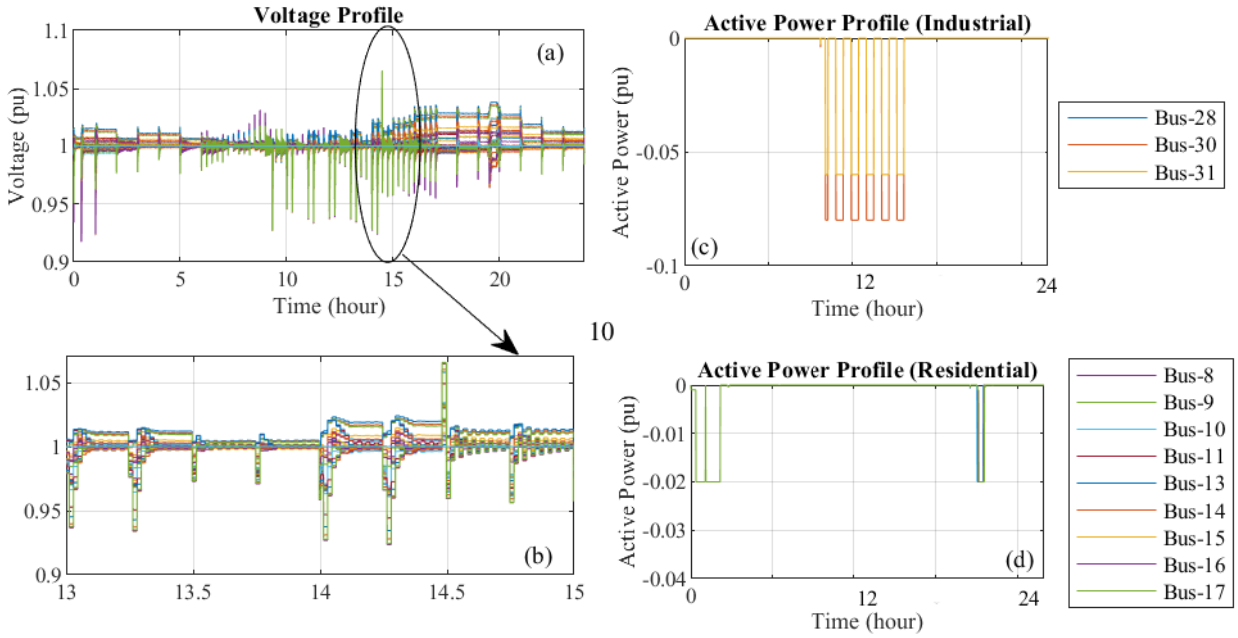

Figure 5.7: Simulation results with Type II charging: (a) voltage profile, (b) voltage profile at 13^{th} hour, (c) active power profile (industrial), (d) active power profile (residential)

- Scenario II: heavy load and cloudy condition.

The voltage and active power profiles of these scenarios are depicted in Figs. 5.8 and 5.9, respectively. It can be observed that the voltage magnitudes in Scenario II exhibit more voltage dips compared to Scenario I. It is further seen that the EVs in the industrial area in Scenario II discharge to lessen the effect of heavy loading and less generation. The lowest voltage measured is 0.9 p.u. Further, the energy loss and utilization of controllable resources (active power of PV, active and reactive power of EV) to regulate voltages increase in Scenario II compared to Scenario I, as depicted in Table 5.4.

Table 5.4: Performance of Scenario I and Scenario II

Scenario	Energy loss (MWh)	PV curtailment (MWh)	PV reactive power injection/ absorption (MVArh)	EV reactive power injection/ absorption (MVArh)	Maximum Voltage (p.u)	Minimum Voltage (p.u)
I	1.672	0.588	1.889/-1.764	1.092/-0.710	1.063	0.9167
II	4.430	0.374	2.134/-2.358	1.505/-0.747	1.068	0.9

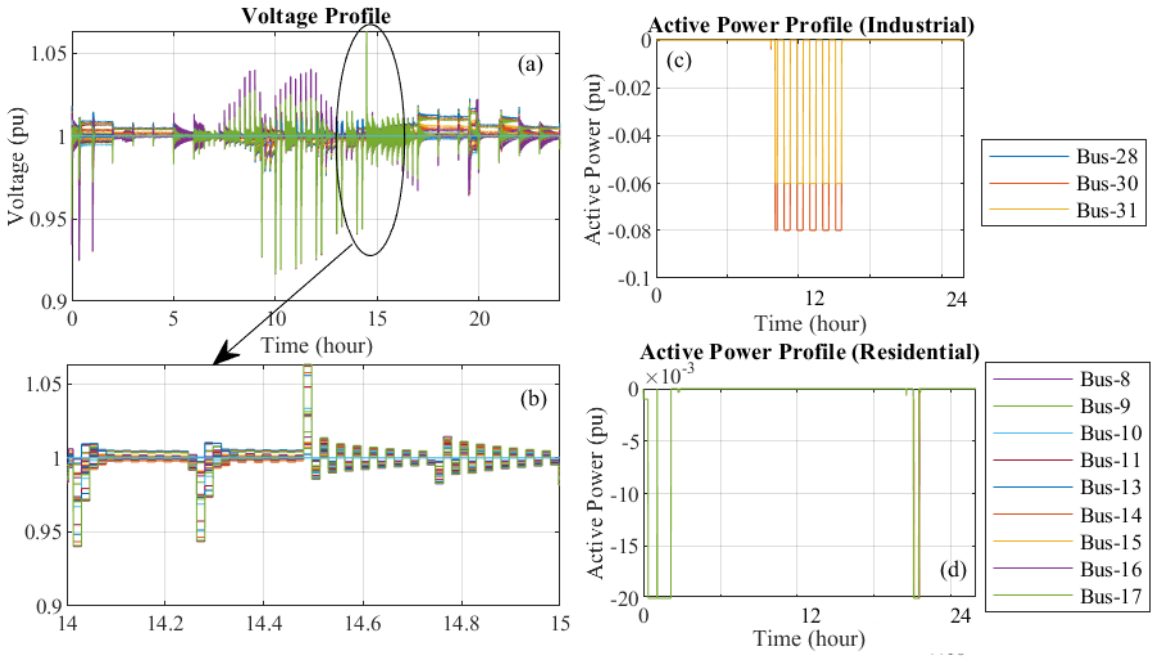

Figure 5.8: Simulation results with Scenario I: (a) voltage profile, (b) voltage profile at 14^{th} hour, (c) active power profile (industrial), (d) active power profile (residential)

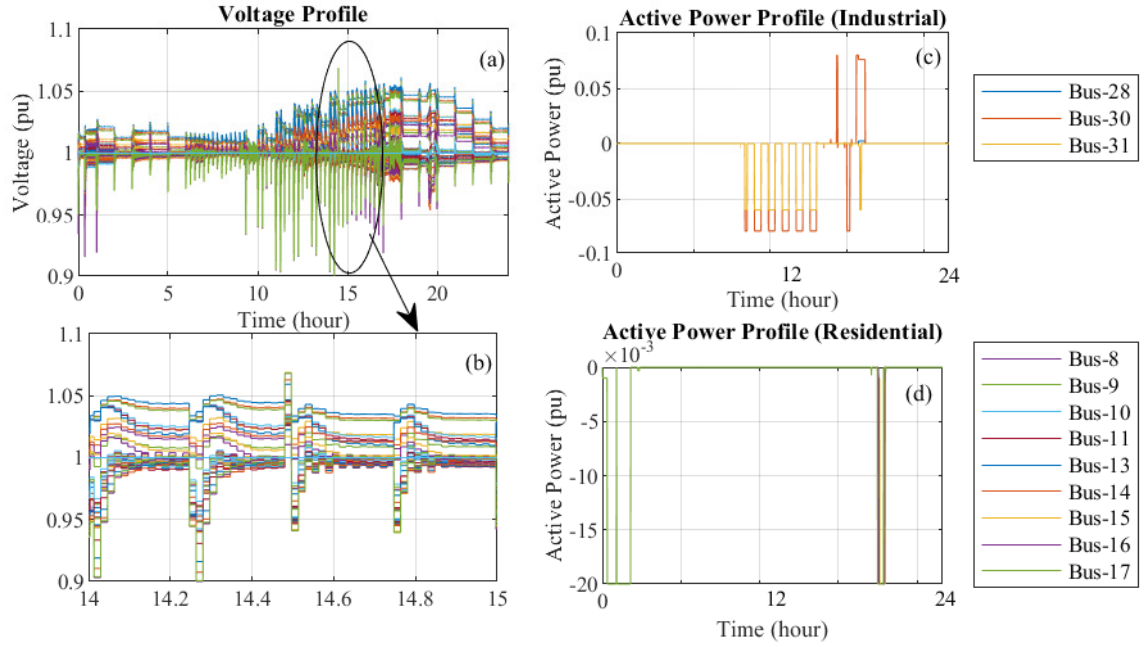

Figure 5.9: Simulation results with Scenario II: (a) voltage profile, (b) voltage profile at 14^{th} hour, (c) active power profile (industrial), (d) active power profile (residential)

Table 5.5: Performance for different percentages of EV penetration

Percentage	Energy loss (MWh)	PV curtailment (MWh)	PV reactive power injection/absorption (MVArh)	EV reactive power injection/absorption (MVArh)	Maximum voltage (p.u)	Minimum voltage (p.u)
50%	1.613	0.429	1.716/-1.826	0.620/-0.283	1.043	0.9534
75%	2.034	0.419	1.758/-1.871	0.867/-0.420	1.06	0.938
100%	2.582	0.448	1.798/-1.888	1.062/-0.477	1.066	0.9173

5.4.3 Performance analysis for different EV penetration

Next, to study the effect of different EV penetration levels, simulations have been performed with 50%, 75% and 100% EV penetration into the network. Fig. 5.10 depicts the voltage profile of bus-31 and bus-17 for the three penetration levels. It is to be noted that EV penetration level represents the ratio of EV loads to the base load of the network. It can be observed that the rise and drop in voltage magnitudes are least with 50% EV penetration. As number of EVs increases, there is increase in voltage deviations. Further, energy loss and utilization of control actions increase as there is growth in EV penetration levels. However, the centralized MPC could bring the voltage magnitudes back to their desired limits within few seconds. Moreover, the current flowing through the substation transformer increases with increase in EV penetration levels as shown in Fig. 5.10(e). The numerical results obtained for different penetration levels have been tabulated in Table 5.5.

5.4.4 Validation of the proposed approach in 38-bus distribution networks

Table 5.6: Performance of Type I and Type II charging in 38-bus distribution networks

Type	Energy loss (MWh)	PV curtailment (MWh)	PV reactive power injection /absorption (MVArh)	EV reactive power injection /absorption (MVArh)	Maximum voltage (p.u)	Minimum voltage (p.u)	EV energy demand from 13^{th} to 15^{th} hour (MWh)
I	4.149	0.389	3.374/-3.553	2.054/-1.269	1.078	0.91	1676
II	3.762	0.361	3.065/-3.228	1.825/-1.292	1.071	0.9145	1126

To further validate the proposed control approach, a 38-bus balanced distribution system is chosen as the test network. The test network with accommodation of PV units, loads, and EVCS is shown in Fig. 5.11. The data associated with the network is taken from [57]. The sampling time is 60 minutes for the first stage; 1 minute for the second stage and 30 minutes for the third stage. Fig. 5.12 depicts

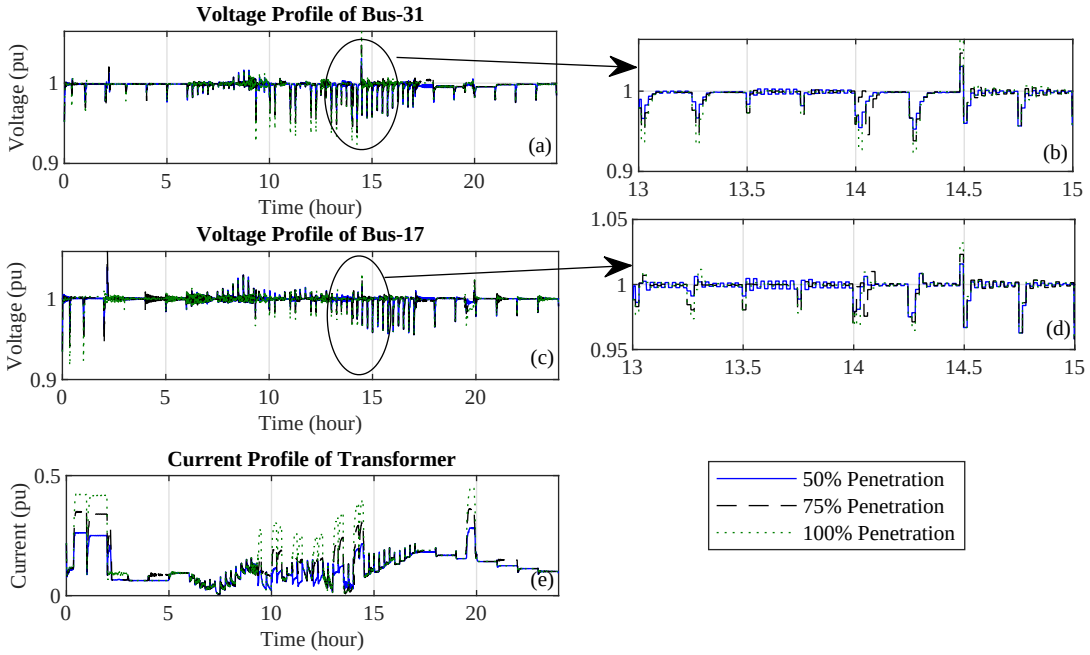

Figure 5.10: Simulation results for different levels of EV penetration: (a) voltage profile of bus-31, (b) voltage profile of bus-31 at 13^{th} hour, (c) voltage profile of Bus-17, (d) voltage profile of Bus-17 at 13^{th} hour, (e) current profile of transformer

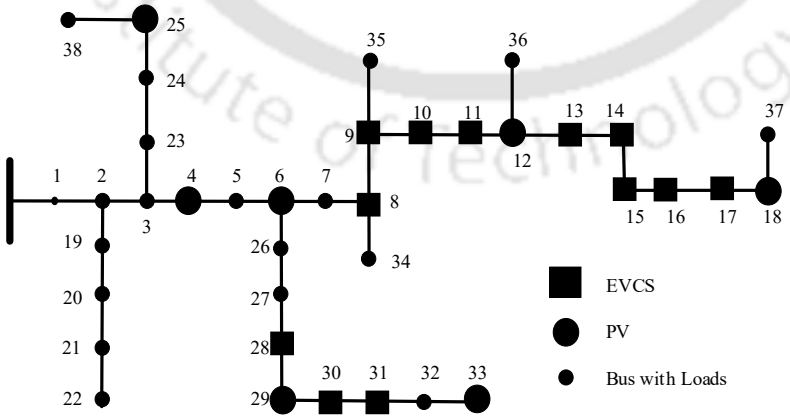

Figure 5.11: Test network: 38-bus distribution network

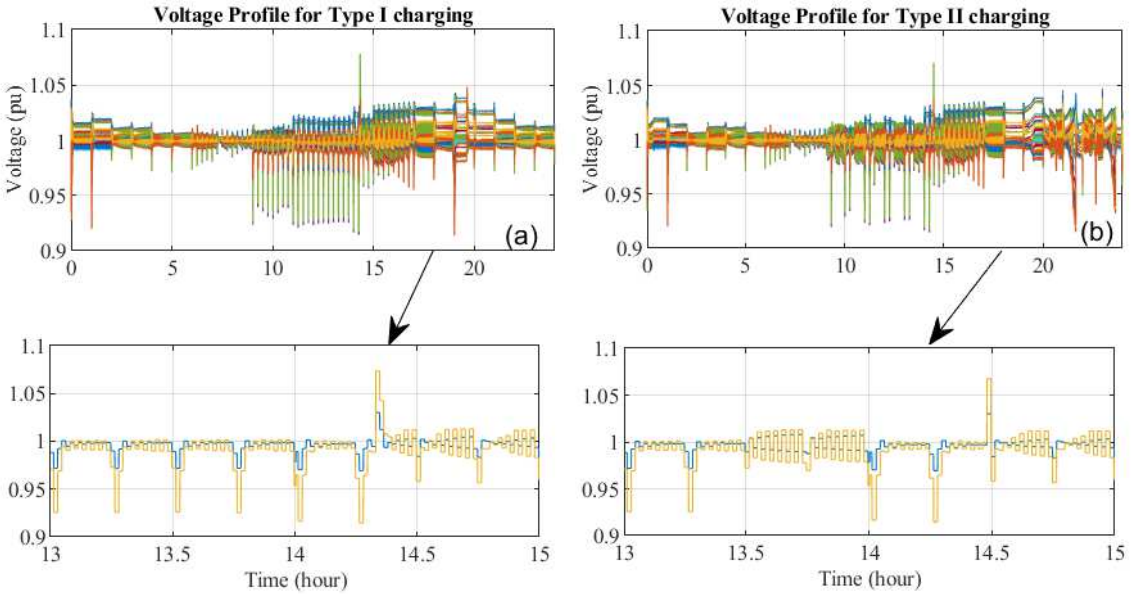

Figure 5.12: Simulation results in 38-bus distribution networks: (a) voltage profile for Type-I charging, (b) voltage profile for Type-II charging

the simulation results for Type I and Type II charging in 38-bus distribution networks. Although at certain time instants, the bus voltages are out of the desired bounds as in Fig. 5.12, the proposed control scheme brings the voltages within desired limits. The enlarged view of the voltage profile of bus-16 is shown in Fig. 5.12 (b). The energy loss calculated during the 24-hour simulation with Type II and Type I charging are 3.762 MWh and 4.149 MWh, respectively, as depicted in Table 5.6. It is to be noted that the results obtained with this test network are found to be consistent and similar to the 33-bus distribution network.

5.4.5 Comparison of execution times for 33-bus and 38-bus distribution networks

To measure the performance of the proposed approach, computation times of the proposed approach are evaluated for both the test networks with Type I charging and Type II charging. Table 5.7 depicts the execution times of the proposed approach. It is observed that computation times increase with increase in network dimensions. Moreover, due to the presence of third stage of the proposed approach, execution times of the proposed approach are more in Type II charging than in Type I charging for both the distribution networks.

Table 5.7: Comparison of execution times

	33-bus ADN (Type-I)	33-bus ADN (Type-II)	38-bus ADN (Type-I)	38-bus ADN (Type-II)
Execution time for one sampling instant	3.0214 s	3.5734 s	3.1234 s	3.6429 s
Execution time for 24-hour interval	4320 s	4500 s	5100 s	6000 s

5.5 Conclusions

In this chapter, a three-stage voltage control method has been developed for distribution networks. The proposed method aims to coordinate different volt/var devices that possess different temporal characteristics in the first and second stages, and calculates the power outputs of EVCS in the third stage. The EV charging behaviors have been taken into consideration while modeling EVCS. The reactive power support from EVCS has also been utilized to regulate the voltages. Moreover, the localized volt/var curve integrated into the DG units is adjusted according to the reactive power set-points obtained from the MPC-based centralized controller. The performance of the proposed method is validated in a 33-bus as well as 38-bus distribution networks. The findings of this Chapter can be summarized as follows:

- The bus voltage magnitudes of the distribution networks are regulated within allowable voltage ranges, and the SoCs of the EVs reach the desired values at the time of their departure for all the operating conditions. However, the energy loss and resource utilization in Type I charging are more compared to Type II charging. With coordinated charging, energy loss decreases by 20.16% as compared to uncoordinated charging method.
- It is observed that energy consumption due to EV charging during high price charging hours is 40.36% less for Type II charging compared to Type I charging.
- In Scenario II, due to heavy loading and cloudy condition, more voltage dips are observed in the voltage magnitudes. However, the proposed approach shows that the voltage could be brought back to the desirable value with active and reactive power injections of EVCS.
- With increase in the network dimension and control variables, the computation times increase proportionately.

6

Receding Horizon Control for Voltage Regulation of Active Distribution Networks with Aggregators' Profit-Based Electric Vehicle Charge Scheduling

Contents

In Chapter 5, a three-stage, two-level receding horizon control (RHC) based volt/var optimization has been developed for the optimal power dispatch of EVs and solar inverters in ADN. The approach in Chapter 5 aims at coordinating different voltage regulating devices depending on their slow (first stage) or fast (second stage) responses to maintain the bus voltages magnitudes and scheduling the charging of electric vehicles (third stage) in the first level of operation. The EV aggregators (EVA) coordinate the EVs and act as an interface between the DNO and EV users. In this chapter, the proposed control algorithm of Chapter 5 further attempts to maximize the benefit of EVA while performing ancillary services through grid-to-vehicle and vehicle-to-grid infrastructure. Demand response is also used through the EVA. The model is formulated as a mixed-integer non-linear programming problem and implemented in general algebraic modeling system (GAMS) software. Furthermore, the reactive power of the fast converters are dispatched through the local Q(V) characteristics in the second control level. Further, simulation results depict that the proposed approach results in better performance than uncoordinated charging method. Moreover, the profit gained by EVAs is more in fast charging scheme compared to slow charging scheme.

6.1 Introduction

6.1.1 Background and motivation

With increasing penetration of DG units in the distribution networks, the transformation from passive to active distribution networks has become evident. The bi-directional power flow in the network induces several challenges to the network operators, such as increment in power loss, power quality problems, voltage and line congestion, to name a few. The secure operation of ADN relies on voltage regulation, thus identified as the most severe problem due to high penetration of DG units. Several volt/var techniques are used to mitigate voltage violation problems. The traditional voltage regulation devices have been used solely or in coordination with the fast control devices in the literature [27],

6.1.2 Related works

The voltage control methods with wide variety of control elements are explored in literature. These methods are mainly classified into distributed [27,59,87] and centralized [14,21]. In [87], a distributed coordinated voltage control framework has been developed considering different temporal characteristics of volt/var devices (DSTATCOM, DG units and OLTC). Authors in [59] have included smart

buildings in the distributed coordinated control structure. However, the real time implementation of distributed control scheme requires effort in reconfiguration of the overall structure. So sticking to centralized techniques, several authors have developed a centralized control structure coordinating both traditional and smart inverter interfaced devices for voltage regulation in different timescales [14, 21]. However, the aforesaid papers have not discussed the capabilities of EV in voltage regulation.

Few works report the utilization of reactive power support from electric vehicles as another voltage control strategy in distribution networks [20, 31]. An optimal coordinated control strategy has been developed in [20] to maximize the EV demand while maintaining desired voltage levels, minimizing power curtailment from DG units and OLTC operations. In Chapter 4, an online optimization strategy based on RHC principles to coordinate EV reactive power with other control efforts to mitigate line congestion and voltage deviations. The reactive power compensation capability of EV inverters has also been used in conservation voltage reduction technique [43]. However, EV charge scheduling has not been taken into consideration in these papers.

There are several works that discuss the smart charging of EV [30, 82, 85, 88–91]. Authors in [88] allow the EVAs to provide optimal charging demand as well as to bid in electricity market. In [30], EV charge scheduling has been performed to shape the load curve in the residential areas. In [85], voltage limits constraint has been added to the charge scheduling algorithm. Several authors have further developed charge scheduling algorithms with consideration of EVA's profit and EV users' charging demands and costs [82, 89, 90]. Ref. [89] emphasizes on the benefits of the three parties: system operators, EVAs and the customers from charging/discharging events. EV charge scheduling has been done in coordination with a two-level voltage control algorithms [82]. Although these aforesaid works have obtained the voltage regulation objective through the charge scheduling schemes, it is to be noted that coordination with other volt/var devices (OLTC, DSTATCOM, PV inverters) is missing.

6.1.3 Contributions and organization of the chapter

This chapter thus proposes a three-stage MPC-based centralized coordinated voltage control for ADN with PV, EV and OLTC. The reactive power outputs of PV and EV are dispatched through the integrated local Q(V) characteristics. Compared with the existing studies, the main contributions of the work are summarized as follows:

(i) A RHC-based centralized coordinated voltage control for distribution networks is developed with PV, EV and OLTC that optimally coordinates the slow timescale devices in the first stage, fast

timescale devices in the second stage and EV scheduling in the third stage.

(ii) The EV charging/discharging considering benefits for the system operators, EV users and EVA is performed in the third stage of operation. The EVs are charged to their desired SoC before the departure time with minimum cost of electricity consumption. A profit optimization problem is formulated for EVA considering revenue generation from regulation services and provision of energy to EV users. The system operators benefit from voltage regulation objective.

(iii) Demand response is further incorporated in the third stage of the objective function for better energy management.

The rest of this chapter is organized as follows: Section 6.2 describes the system model; Section 6.3 discusses the receding horizon voltage control model. The optimization problems at the three stages are discussed in Section 6.4. The simulation results and discussions are presented in Section 6.5. Section 6.6 presents the conclusions of the chapter.

6.2 System model

Fig. 6.1 depicts the overall structure of the considered system. The distribution network consists of N number of buses with PV generators, loads and EVCS at specified buses as depicted in Fig. 6.1. The substation transformer is equipped with OLTC that controls bus-1 of the radial distribution network. The loads are modeled as constant power loads where the active power absorbed by loads varies hourly over the day depending on their types (residential, industrial, or commercial). The active power generation of the PV units varies with atmospheric factors (solar irradiation). The reactive power generation of PV generators is a function of inverter rating and active power production, as in (3.1). The PV inverter is modeled as an oversized inverter in such a manner that there is at least 44% reactive power injection, even at 100% active power production [51]. The active power profiles of loads and PV are shown in Fig 6.2. The EVCS models are developed considering the EV characteristics, such as, initial SoC, time of arrival, and time of departure as in Chapter 5. Moreover, these EV characteristics change based on their placements in the DN. The EVs are considered to be located in the industrial and residential lateral of the DN. The EV owners are managed and controlled by an EV aggregator of an area. The EV owners of residential and industrial laterals receive the data and accordingly, models of EVs are developed [31, 85] as shown in Fig. 5.1. The data for initial SoC,

plug-in and plug-out times of EVs are generated from a normal probability distribution function, as described in Section 5.2. Both parking as well as charging events take place in the EVCS. The EV owners' daily energy consumption shall be in accordance with the agreement signed between the EVA and EV users. According to the agreement, EV owners submit their data (battery capacity, initial SoC, all-electric range, SoC requirement, and their parking time, (t_{park}) to the EVA upon their arrival to EVCS. The EVA then calculates the energy required by each EV owners and further optimizes the charging schedule. The modeling of energy requirements of each EV owner is represented below:

t_{park} is evaluated by eq. (5.1). With battery capacity B_{cap} for each EV of 24 kWh, the required energy for each EV, E_{req} as calculated from eq. (5.2) by EVA depending on SoC requirement. The symbol, η represents efficiency of the EV charger and soc_{req} is given by eq. (5.3). The SoC at every time instant is updated using eq. (6.1)

$$soc(k+1) = soc(k) + \frac{P_{EV}}{B_{cap}} \Delta t \eta. \tag{6.1}$$

The EVs in the EVCS are allowed to charge and discharge to provide grid-to-vehicle (G2V) and vehicle-to-grid (V2G) services. EVs are able to inject as well as absorb reactive power in order to incorporate the reactive power service provision from the EVCS while managing G2V/V2G dispatch. However, the capacity of reactive power provision is limited by the charger rating as in eq. (5.4).

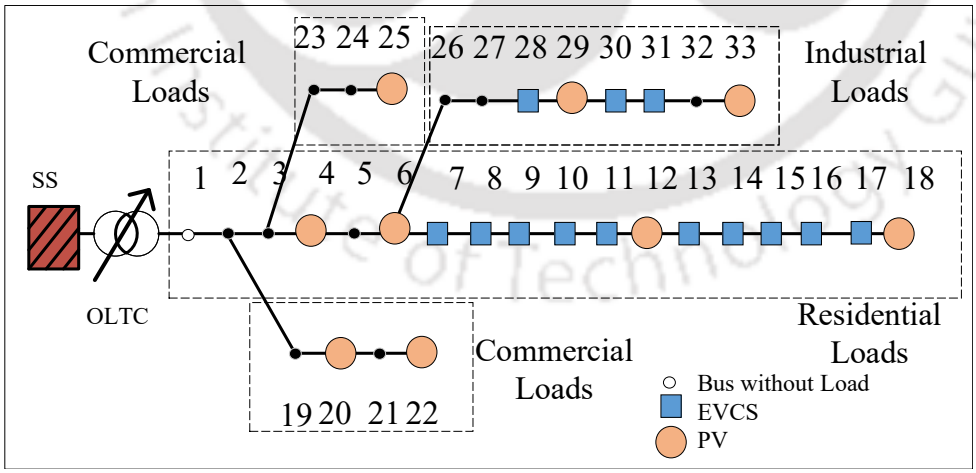

Figure 6.1: System considered: 33-bus distribution network

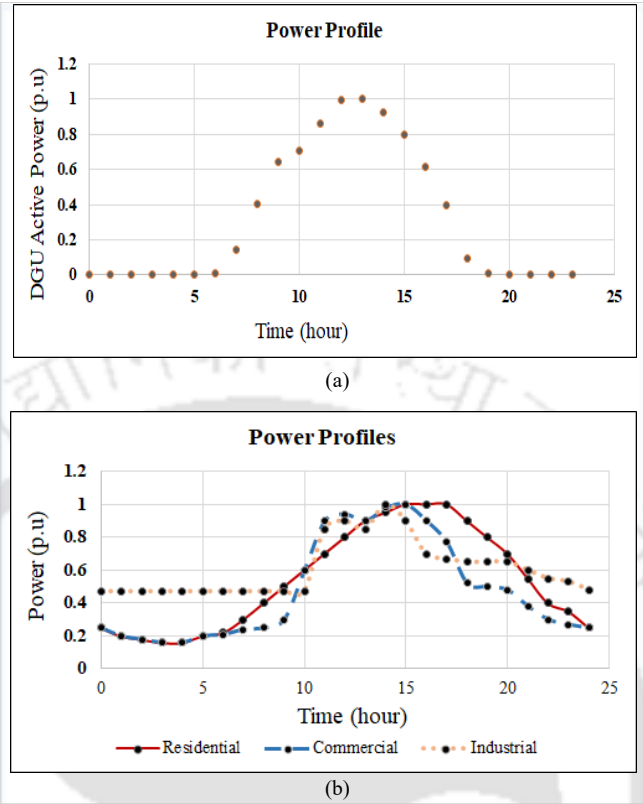

Figure 6.2: Power profiles of (a) PV generators and (b) loads

6.3 Receding horizon based voltage control framework

RHC solves an optimization problem that is developed on the basis of state-space equations as described in eq. (6.2).

$$\begin{aligned} min(y_{ref} - y)^T \boldsymbol{Q}(y_{ref} - y) + \Delta u^T \boldsymbol{R} \Delta u \\ x(k+1) = \boldsymbol{A}x(k) + \boldsymbol{B}\Delta u(k) \\ y(k+1) = \boldsymbol{C}x(k) \end{aligned} \tag{6.2}$$

The output matrix $\boldsymbol{y_p}$ is represented along the prediction horizon N_P by:

$$\boldsymbol{Y} = \boldsymbol{F}x(k) + \boldsymbol{\phi}\Delta u$$

$$where$$

$$\boldsymbol{F} = [\boldsymbol{CA} \quad \boldsymbol{CA}^2 \quad \boldsymbol{CA}^3....\boldsymbol{CA}^{N_P}]^T$$

$$\boldsymbol{\phi} = \begin{bmatrix} \boldsymbol{CB} & 0 & 0.... & 0 \\ \boldsymbol{CAB} & \boldsymbol{CB} & 0.... & 0 \\ \boldsymbol{CA}^2\boldsymbol{B} & \boldsymbol{CAB} & \boldsymbol{CB}.... & 0 \\ \boldsymbol{CA}^{N_P-1}\boldsymbol{B} & \boldsymbol{CA}^{N_p-2}\boldsymbol{B} & \boldsymbol{CA}^{N_P-3}\boldsymbol{B}.... & \boldsymbol{CA}^{N_P-N_C}\boldsymbol{B} \end{bmatrix} \tag{6.3}$$

Further, the control inputs can be written along the control horizon N_C as:

$$u = \boldsymbol{G}u(k-1) + \boldsymbol{\Lambda}\Delta u$$

$$where$$

$$\boldsymbol{G} = [\boldsymbol{I} \quad \boldsymbol{I} \quad \boldsymbol{I}....\boldsymbol{I}]^T \quad \boldsymbol{\Lambda} = \begin{bmatrix} \boldsymbol{I} & \boldsymbol{0} & \boldsymbol{0}.... & \boldsymbol{0} \\ \boldsymbol{I} & \boldsymbol{I} & \boldsymbol{0}.... & \boldsymbol{0} \\ \boldsymbol{I} & \boldsymbol{I} & \boldsymbol{I}.... & \boldsymbol{0} \\ \boldsymbol{I} & \boldsymbol{I} & \boldsymbol{I}.... & \boldsymbol{I} \end{bmatrix} \tag{6.4}$$

where $\boldsymbol{I}$ and $\boldsymbol{0}$ are identity and null matrices, respectively. In eq. (6.2), $\boldsymbol{Y}$ refers to the predicted output vector, and is the change in predicted control input vector. The optimization problem in eq. (6.2) is solved at every sampling instant for N_P time interval. The solution leads to an optimal control sequence of N_C dimension. While the first value is applied to the system in the next time instant, the other values are discarded. Thus, a new control sequence is obtained again at the next sampling instant, that characterizes the receding horizon principle.

Fig. 6.3 depicts the centralized voltage control and charge scheduling framework. All the voltage control operations are performed by DNO centrally. The DNO manages the controllable resources, such as, PV units, EV and OLTC by monitoring their set-point status and voltage magnitudes of the monitored buses. The information of EVs are conveyed through the residential and industrial EVAs. It is assumed that there exits a well established communication infrastructure for the transfer of information between the central controller and the controllable resources. As power system operation

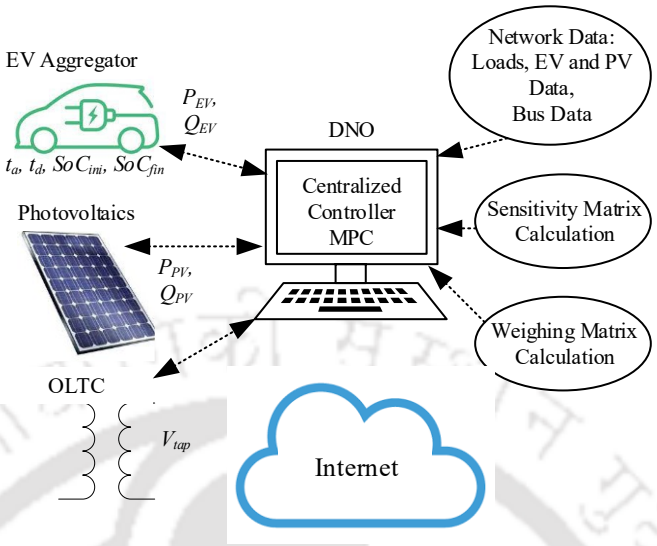

Figure 6.3: Voltage control framework

and control are executed in different time scales, the control architecture in this chapter operates on three stages. In the first stage, the RHC based controller optimizes the OLTC tap operations hourly. The fast power electronics based devices are operated every one minute in the second stage. The charge scheduling of EVs, based on RTP of electricity consumption that is updated half-hourly, is done at the third stage. The optimal control inputs are calculated accordingly and are sent to the respective actuators. The local controller embedded in the converter based devices modify the reactive power injection/absorption according to the local droop characteristics [10, 28].

6.4 Problem formulation

The control architecture consists of two levels of control as discussed in this section [Refer to Fig. 6.4]. While the upper level control is a centralized control scheme, the lower level control is a decentralized control scheme.

6.4.1 Upper level control

Three stages of operation constitute the upper level control. These stages are defined based on the operation time of volt/var devices. Let, incremental control variables over the control horizon be denoted by $[\Delta u(k), \Delta u(k+1), ..., \Delta u(k+N_C-1)]$ and control inputs be $[u(k), u(k+1), ..., u(k+N_C-1)]$. The outputs over the prediction horizon are represented as $[y(k+1), y(k+2), ..., y(k+N_P)]$.

Being discrete and slow, the OLTC reference voltage $[V_{tap}(k)]$ is input for the first stage. The

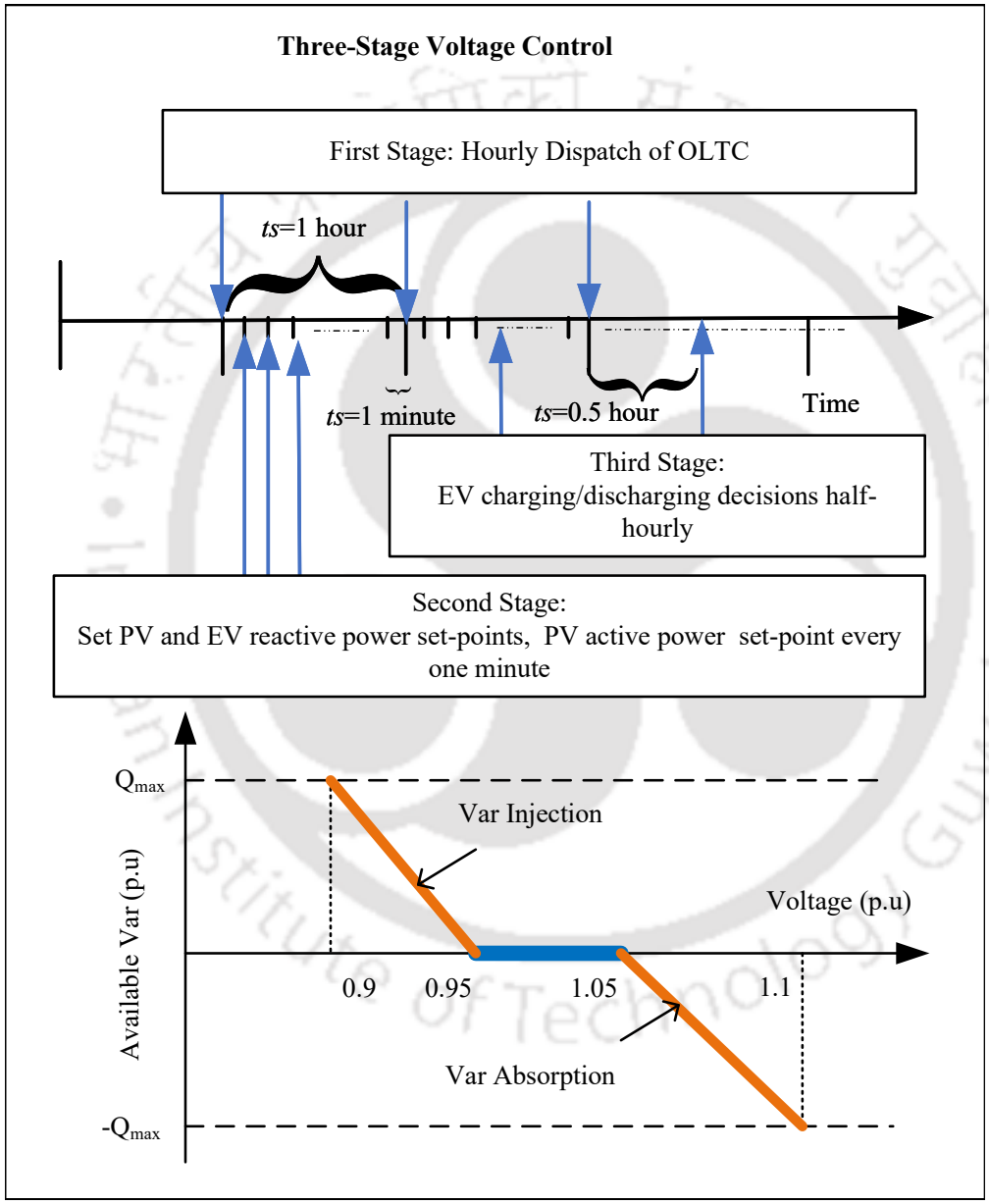

Figure 6.4: Control architecture

active power set-points of PV, and reactive power set-points of PV and EV $[P_{PV}(k), Q_{PV}(k), Q_{EV}(k)]$ are the second stage inputs. Considering the dependence of charging/discharging events on the half-hourly real time price of electricity and ancillary services, active power set-point of EV $[P_{EV}(k)]$ is the input for the third stage. The incremental input vectors $[\Delta u(k)]$ for first, second and third stage are $[\Delta V_{tap}(k)]$, $[\Delta P_{PV}(k), \Delta Q_{PV}(k), \Delta Q_{EV}(k)]$, and $[\Delta P_{EV}(k)]$, respectively. While the set of voltage magnitudes $[V(k)]$ is the output of MPC for all the stages, the set of state-of-charge of the EVs $[soc(k)]$ is the additional output of the third stage. The first and the second stages aim to minimize the voltage error (deviations from the reference voltage), the slack variables and the control variables.

$$min \sum_{i=1}^{N_P} [(V_{ref} - V)^T Q (V_{ref} - V) + \sigma^T S \sigma] + \sum_{i=0}^{N_C - 1} \Delta u^T R \Delta u \tag{6.5}$$

The above objective functions are subjected to the following constraints:

$$\Delta u^{min} \leq \Delta u(k+i) \leq \Delta u^{max} \tag{6.6}$$

$$u^{min} \leq u(k+i) \leq u^{max} \tag{6.7}$$

$$-\sigma_1 1 + V^{min}(k+i) \leq V(k+i|k) \leq V^{max}(k+i) + \sigma_2 1 \tag{6.8}$$

$$V(k+i|k) = V(k+i-1|k) + \frac{\delta V}{\delta u^T} \Delta u(k+i-1) \tag{6.9}$$

for $i = 1, 2, ..., N_P$. Here, u and Δu are changed according to the stage of operation. It is to be noted that the active power of PV is curtailed to 20% of its rated capacity.

Eq. (6.6) represents the constraint on manipulated variables or inputs of the model. The ramp movements of these inputs in both the stages are restricted through constraint eq. (6.7). By using slack variables, the output variable, voltage magnitude constraint [refer to eq. (6.8)] is softened. Further, the voltage equality constraint is represented as the state-space model of MPC.

The objective of the third stage is to consider the benefits of the three parties: EVA, EV users and the DNO.

$$\begin{cases} min \sum_{i=1}^{N_P} [(V_{ref} - V)^T Q (V_{ref} - V) + \sigma^T S \sigma] \\ + min \sum_{i=0}^{N_C - 1} \Delta u^T R \Delta u \\ + max \sum_{i=1}^{N_P} [Profit_{EVA}] \end{cases} \tag{6.10}$$

where, profit for aggregators is the difference of revenue generation and cost of charging/discharging, i.e., $Profit_{EVA} = Rev_{EVA} - Cost_{EVA}$. The eq. (6.10) is a min-max problem, and consequently,

converted to a either min or max problem. Here, it is converted to a minimization problem.

The cost for EVA is the aggregation of buying price of energy during charging and degradation of battery lifetime during discharging process [90, 92]. The buying price of energy is the real time price (RTP) offered by DNO as shown in Fig. 6.5 [31].

$$Cost_{EVA} = \begin{cases} P_{EV} RTP|_{\tau_{ch}=1} \\ (0.042 B_{cap}/5000) + \{0.15 \frac{(1-\eta^2)}{(\eta)}\} P_{EV}|_{\tau_{dis}=1}. \end{cases} \tag{6.11}$$

The revenue earned by EVA from the charging and regulation services,

$$Rev_{EVA} = \begin{cases} d_t[min(P_{EV}^{max}, P^{max}) - P_{EV}] + (SP) P_{EV}|_{\tau_{ch}=1} \\ u_t P_{EV}|_{\tau_{dis}=1}. \end{cases} \tag{6.12}$$

where, P^{max} is updated at every sampling instant and is evaluated by

$$P^{max} = \frac{soc_{fin} - soc_{ini}}{\eta}.B_{cap}. \tag{6.13}$$

In eq. (6.12), d_t and u_t are the real time regulation down and regulation up prices, respectively as depicted in Fig 6.6 [90]. Regulation capacity is referred to as the amount of charging rate that can be increased/decreased by EVA as asked by DNO. The regulation capacity of each EV is the sum of regulation up and regulation down capacities. The EVA is paid by DNO based on these regulation capacities, since these regulation capacities help in frequency regulation [90].

In eq. (6.12), selling price, SP is $SP = M + RTP1$; M is the mark up price above the buying price of electricity. $RTP1$ is the selling price of electricity by EVA to the EV users for charging by incorporating demand response (DR). DR is enabled in this third stage through price-based DR and incentive-based DR. The RTP1, being dynamic in nature, is made high during peak load and low during the off-peak load by the DNO to maintain stability of the network. Moreover, in the incentive-based DR program, EV users for charging are charged an extra penalty on top of the RTP when the load level of the system is above 80% of the system's peak load. On the contrary, if the EVs are discharged during these times, they are paid a reward on the purchasing price offered by the DNO [89]. Furthermore, to ensure that EV either charges or discharges at a given time, two binary variables τ_{ch} and τ_{dis} are defined for each EV to convert the problem to a non-linear mixed integer

programming problem. Eq. 6.10 is further subjected to the following constraints

$$\Delta P_{EV}^{min} \leq \Delta P_{EV}(k+i) \leq \Delta P_{EV}^{max} \tag{6.14}$$

$$P_{EV}^{min} \leq P_{EV}(k+i) \leq P_{EV}^{max} \tag{6.15}$$

$$soc^{min}(k+i) \leq soc(k+i|k) \leq soc^{max}(k+i) \tag{6.16}$$

$$soc(k+i|k) = soc(k+i-1|k) - \frac{P_{EV}(k+i-1)}{B_{cap}}\Delta t \tag{6.17}$$

for $i = 1, 2, ..., N_P$. Further, the optimization problem is subjected to the voltage equality and inequality constraints as in eqs. (6.8)-(6.9).

Moreover, each EVs' SoC shall reach the desired SoC by the departure time, t_d, referred to as EV user's constraint,

$$soc(t_d) \geq soc_{req} \tag{6.18}$$

To reach the desired SoC before t_d, the lower bound constraint, $soc^{min}(k)$ of eq. (6.16) needs to be updated at every sampling instant. $soc^{min}(k)$ is determined by two factors for every sampling instant. The first factor is the physical lower limit of energy as in eq. (6.16). The second one is the EV user's constraint in Eq (6.18). These two factors can be combined together as:

$$soc^{min}(k) = max[soc_{req} - max(0, (t_d - t)\frac{P_{EV}^{max}\Delta t\eta}{B_{cap}}), soc_{low}] \tag{6.19}$$

Here, soc_{low} is limited to 0.2 due to physical considerations.

6.4.2 Lower level control

The local control level in addition to upper level control is beneficial to DNO as it responds faster to voltage disturbances [10, 28]. Further, reliability of the system increases with such combined level of control. According to the recent distributed energy resources integration standard [93], every DER shall be equipped with local control characteristics, such as, $cos(\phi)$ or $Q(V)$ characteristics. The $Q(V)$ characteristic is chosen in this work. The set-points dispatched from the centralized control are further sent to the local control layer embedded in each DG unit. The var injection/absorption from the smart inverters are adjusted according to this piecewise linear autonomous Q(V) characteristics

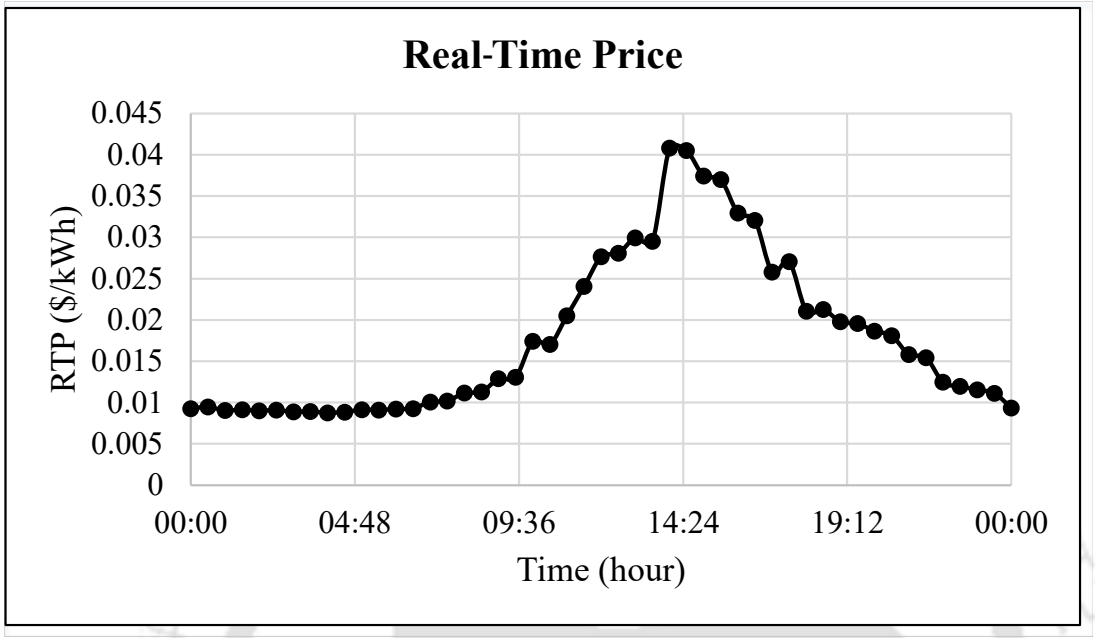

Figure 6.5: Real-time price of electricity consumption.

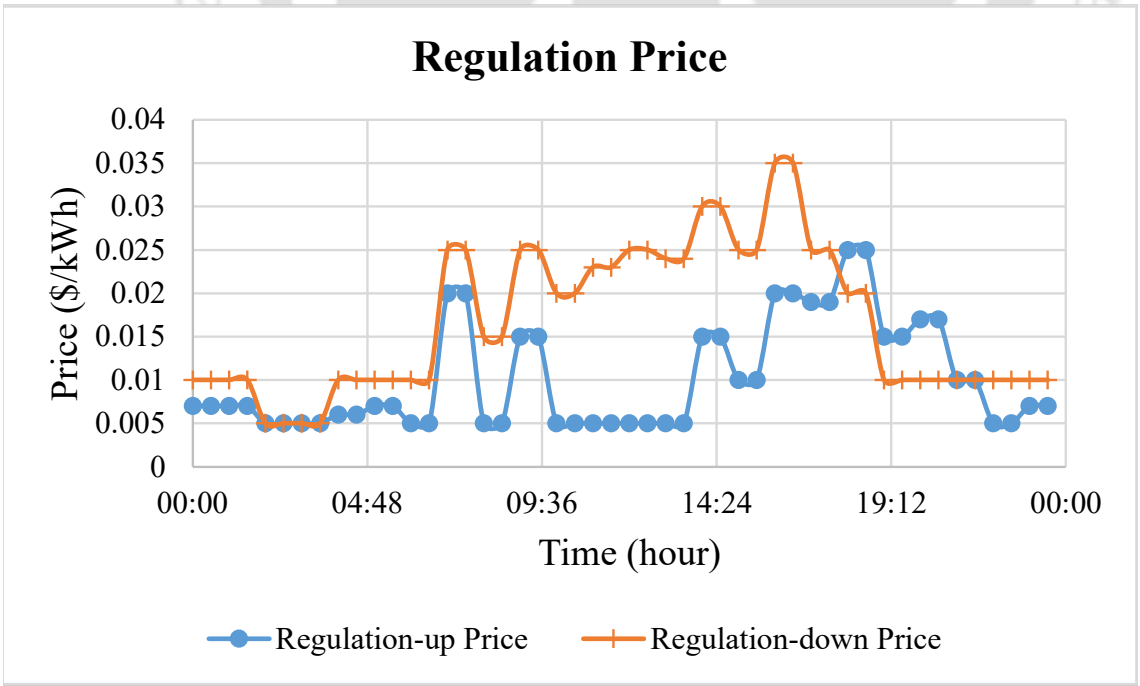

Figure 6.6: Real-time price of regulation-up and regulation-down services.

Table 6.1: EV characteristics.

Material	Battery capacity	Charger rating	Battery cost
Li-ion	24kWh	2 kW (slow) 4 kW (fast)	$ 13000

in this level of control as in (6.20).

$$Q(V) = \begin{cases} Q^{max}, V < 0.9 \\ Q_0 + \frac{Q^{max} - Q_0}{0.9 - 0.95}(0.95 - V), 0.9 < V < 0.95 \\ Q_0, 0.95 < V < 1.05 \\ Q_0 - \frac{Q^{max} + Q_0}{1.1 - 1.05}(V - 1.05), 1.05 < V < 1.1 \\ -Q^{max}, V > 1.1 \end{cases} \tag{6.20}$$

6.5 Numerical results

The simulation results and analysis of the proposed approach is presented in this section.

6.5.1 Implementation and test network

The proposed control method is implemented in a 33-bus balanced distribution network [56] with system base of 10 MVA, 12.6 kV as shown in Fig. 6.1. The simulations are carried out on a PC with Intel Core i5-6500 processor, 3.20 GHz, and 16 GB RAM. The power system analysis toolbox (PSAT) in MATLAB R2018a is chosen as the simulation platform. The optimization problem is solved by CPLEX solver in GAMS environment [55].

The DN is divided into three areas, namely residential, commercial and industrial, based on the load profiles (refer to Fig. 6.2) [31]. There are nine PV units of 0.5 MW rating and are located at the buses numbered 4, 6, 12, 18, 20, 22, 25, 29, and 33. There are two EVAs in the industrial and residential areas that control the charging/discharging of 1000 EVs and 1100 EVs, respectively. The characteristics of the EVs are assumed to be same for both the areas and is shown in Table 6.1 [90]. Fig. 6.6 depicts the prices of ancillary services brought from the system operator [90]. Table 6.2 provides the controller parameters used for numerical simulations.

Table 6.2: RHC parameters.

First-stage	Second-stage	Third-stage
N_C=N_P=3 Δu= $\Delta V_{tap'}$ t_s= 1 hour	N_C=N_P=3 Δu=[ΔQ_{PV} ΔP_{PV},ΔQ_{EV}] t_s=1 minute	N_C=N_P=3 Δu=[ΔP_{EV}] t_s=30 minutes

Table 6.3: PV/EV reactive power injection/absorption

Type of resource	Slow (uncoordinated) MVAr	Slow (Proposed) MVAr	Fast (uncoordinated) MVAr	Fast (Proposed) MVAr
PV	1.870 -1.923	1.665 -1.731	2.412 -2.279	1.926 -1.731
EV	2.252 -2.043	2.034 -1.0436	2.793 -2.363	2.501 -1.536

6.5.2 Simulation results and analysis

6.5.2.1 Technical aspects of the proposed control method

The RHC-based voltage control algorithm is implemented in the test network to keep the voltage within the range of [0.95 - 1.05] p.u. The PV active power curtailment is limited to 20% of the active power production. The box plots of voltages for slow and fast charging scheme with the proposed method has been shown in Figs. 6.7 and 6.8. It can be observed that due to high charging rate, the voltage dips are more in fast charging scheme. Fig. 6.9 presents the results of the voltage control in a critical bus (Bus no. 18), with the proposed (Type II) charging method as well as uncoordinated (Type I) charging method for the slow charging scheme. It can be seen from the plots that due to charging of EV batteries, voltage magnitudes decrease, but the RHC-based corrective controller reduces the deviations and brings the voltages within their acceptable limits. In the uncoordinated charging method, the EVs are charged at their rated power as soon as the EVs are plugged into the grid. This results into more voltage deviations and more corrective actions are required in uncoordinated charging method as shown in Table 6.3. Moreover, the EVs at all the buses reach their desired SoC before departure times in all the scenarios. The time taken by the EVs at each bus is depicted in Tables. 6.4 and 6.5 for the proposed and uncoordinated charging schemes, respectively.

Table 6.4: Technical results for the proposed method

Type of charging	Min voltage magnitude (p.u)	Max voltage magnitude (p.u)	Time taken to reach final SoC (hour)
Slow	0.916	1.0496	[28,30,31]:5.41;[7,8,9,10]:4.067; [12,13,14,15]:6.016;[16]:12.13
Fast	0.832	1.0496	[28,30,31]:2.7;[7,8,9,10]:2.016; [12,13,14,15]:3.016;[16]:6.067

Table 6.5: Technical results for uncoordinated charging

Type of charging	Min voltage magnitude (p.u)	Max voltage magnitude (p.u)	Time taken to reach final SoC (hour)
Slow	0.9	1.065	[28,30,31]:5.33;[7,8,9,10]:3.983; [12,13,14,15]:5.96;[16]:12.05
Fast	0.785	1.11	[28,30,31]:2.683;[7,8,9,10]:1.983; [12,13,14,15]:2.967;[16]:5.95

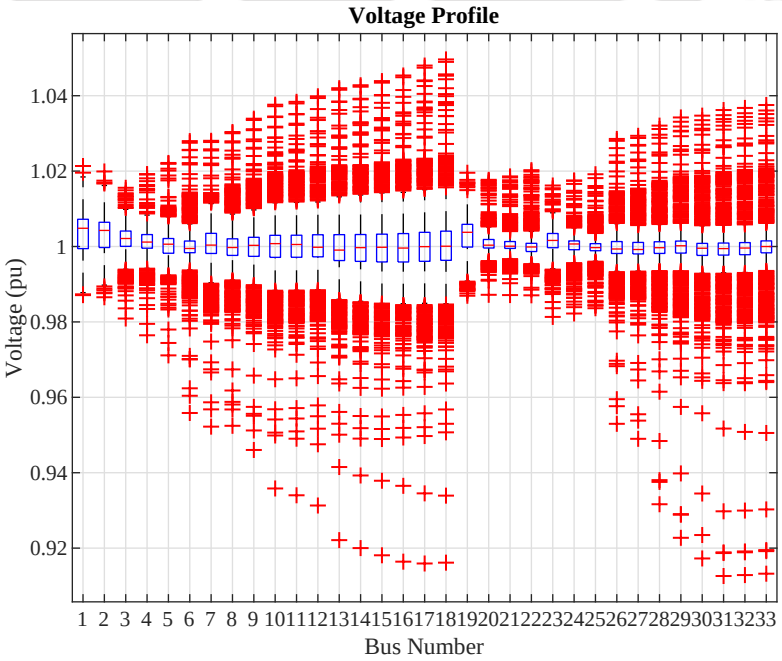

Figure 6.7: Voltage profile with slow charging (proposed method)

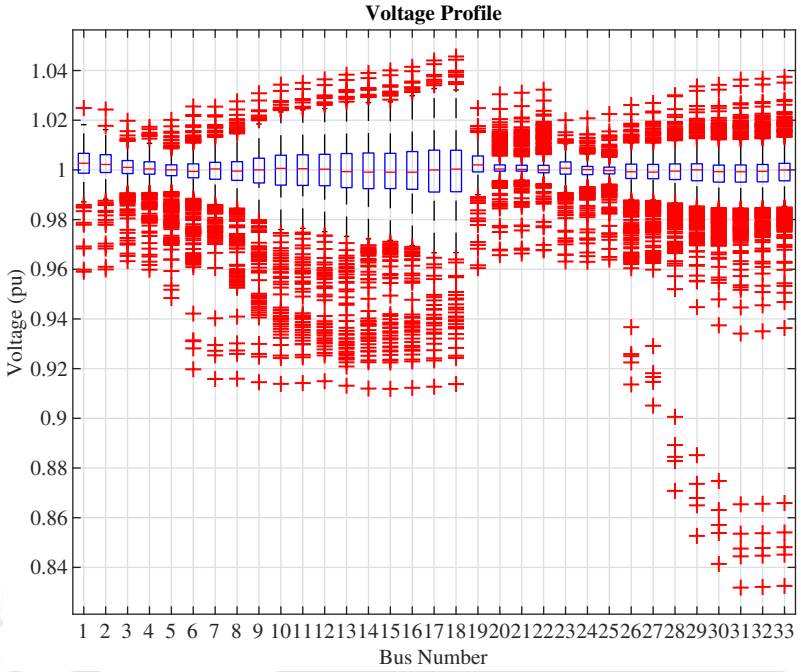

Figure 6.8: Voltage profile with fast charging (proposed method)

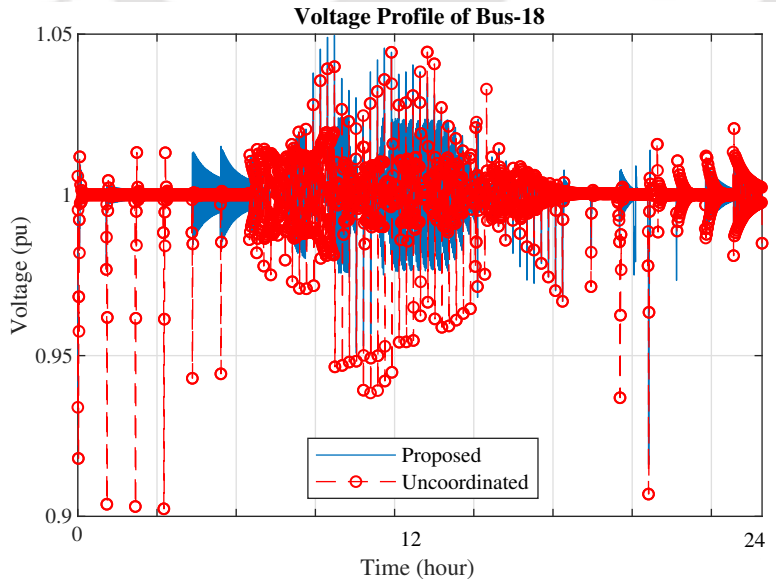

Figure 6.9: Voltage profile of bus 18

Table 6.6: Economical results

Type of charging	Revenue ($)	Cost ($)	Profit ($)
Slow charging	EVA1: 5.8726; EVA2: 13.8284	EVA1: 1.6632; EVA2: 3.0276	EVA1: 4.2093; EVA2: 10.8008
Fast charging	EVA1: 10.2113; EVA2: 27.5124	EVA1: 3.3264; EVA2: 6.3496	EVA1: 6.8848; EVA2: 20.8028

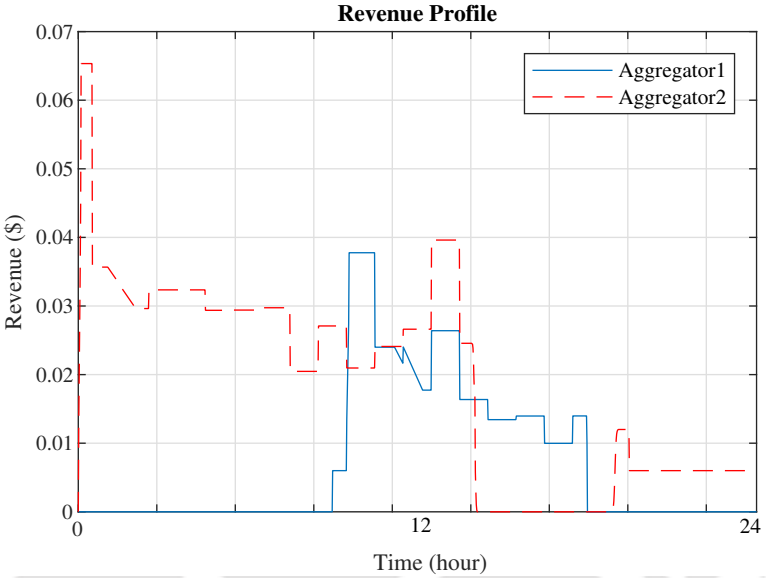

Figure 6.10: Revenue profile

6.5.2.2 Economical aspects of the proposed control method

Table 6.6 depicts the aggregated revenue, cost and profit of the EVAs for both slow and fast charging schemes. The revenue, cost and profit profiles for the slow charging scheme are depicted in Figs. 6.7, 6.8 and 6.9. It can be observed from the simulation results in Table 6.6 that the profit gained by EVA in the residential area is more than in the industrial area for both the schemes. The revenue gained by EVAs is due to both the charging as well as discharging events.

6.5.2.3 DR analysis

Table 6.7 tabulates the penalty/incentive imposed/gained by EVAs due to the incentive based DR for both slow and fast charging schemes. This implies when charging is done during high peak load, a penalty has been imposed on the EVAs. Thus, highest penalty is imposed on EVAs when peak load is highest as shown in Fig. 6.13.

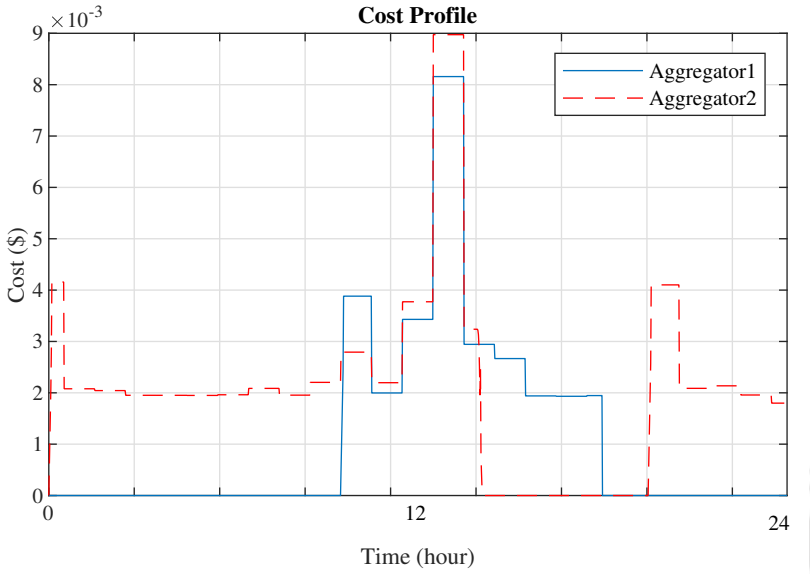

Figure 6.11: Cost profile

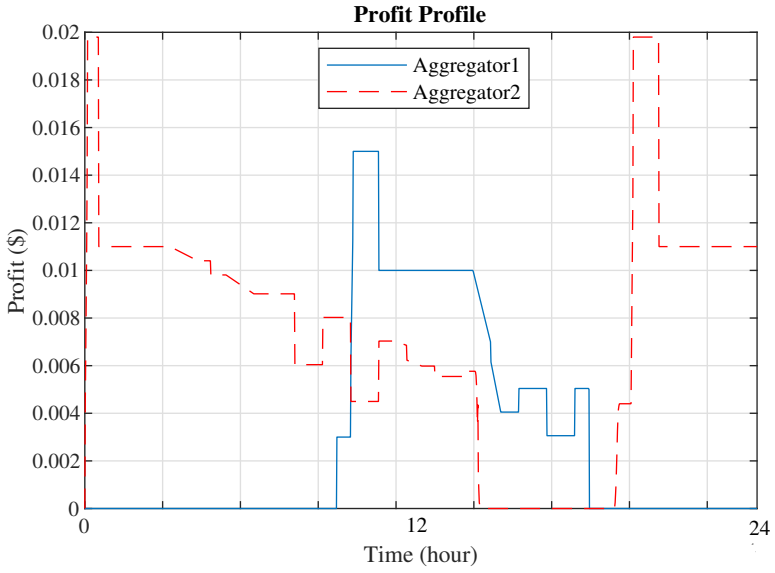

Figure 6.12: Profit profile

Table 6.7: DR results

Type of charging	Penalty ($)
Slow-charging	EVA1:0.2765; EVA2:1.872
Fast-charging	EVA1:0.5530; EVA2:0.3743

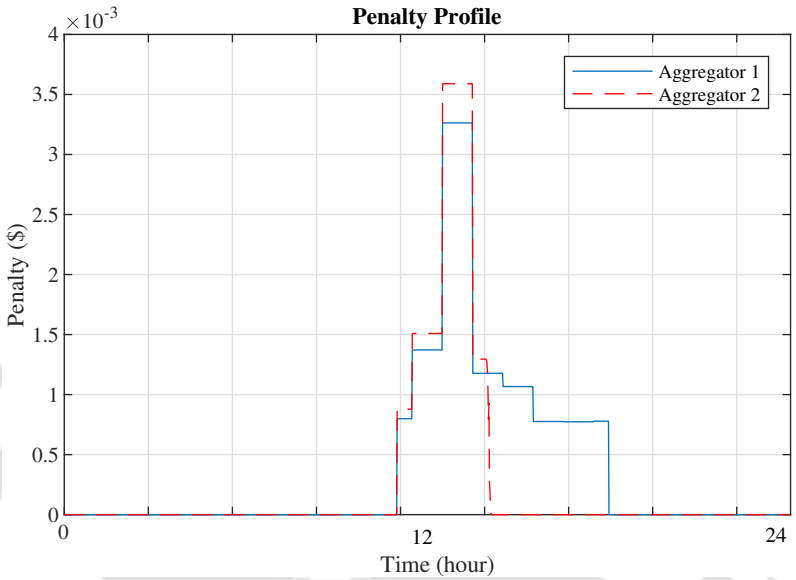

Figure 6.13: Penalty profile for fast charging scheme

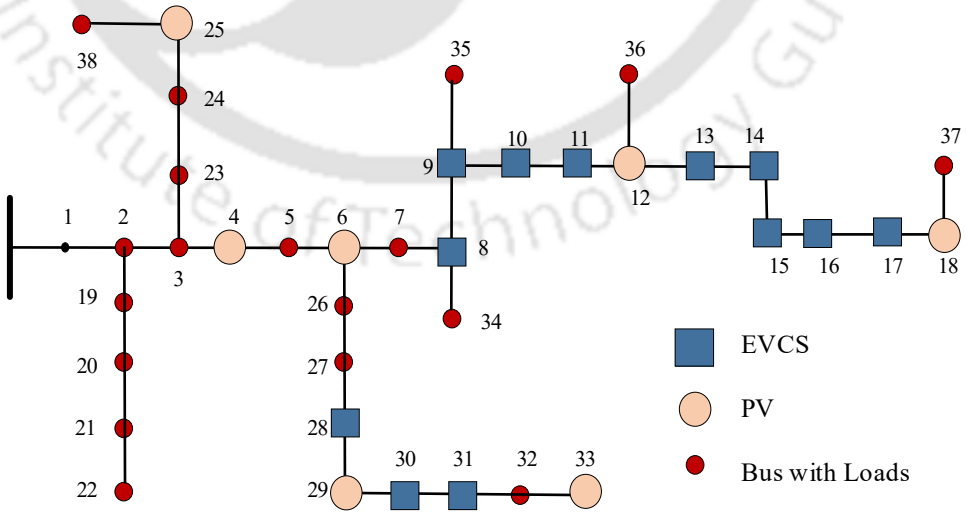

Figure 6.14: Test network: 38-bus distribution network.

6.5.2.4 Cost-economic analysis

To study the economic cost analysis of V2G when deployed to perform voltage support for the distribution network in the presence of PV systems, a case study is presented to evaluate the total profit earned by EV aggregators in only G2V and in both G2V and V2G conditions. The profit earned by EV aggregator is given by the difference between revenue earned and cost incurred during the charging/discharging process. The cost for EV aggregator (EVA) is the aggregation of buying price of energy during charging and the degradation of battery lifetime during discharging process. The buying price of energy is the real-time price (RTP) offered by the network operator. The revenue earned by EV aggregators is due to the provision of regulation and charging prices. In this coordinated scenario, it is assumed that the EVs can operate in both V2G and G2V modes. The injected/absorbed power at every time interval is the decision variable in the proposed charging methodology.

Table 6.8 presents the performance metrics such as revenue earned, cost incurred and profit earned by EVA for the G2V as well as both G2V and V2G scenario. The profit earned has the potential to recover the operational cost of V2G as shown in Table 6.8. Due to the V2G effect and the presence of PV power, the revenue earned and net profit is more in V2G operation mode. However, due to the inclusion of the battery degradation cost in the V2G scenario, the cost incurred is more (4.7306 $/kwh) than in the G2V scenario (4.5312 $/kwh).

Table 6.8: Profit analysis during G2V and V2G conditions.

Particulars	Both G2V and V2G	Only G2V
Total Cost incurred ($/kwh)	4.7306	4.5312
Total revenue earned ($/kwh)	20.1124	19.224
Net Profit for EVA ($/kwh)	15.3818	14.6928

6.5.2.5 Validation of the proposed approach in 38-bus distribution networks

To further validate the proposed control approach, a 38-bus balanced distribution system is chosen as the test network. The test network with accommodation of PV units, loads, and EVCS is shown in Fig. 6.14. The data associated with the network is taken from [57]. The sampling time is 60 minutes for the first stage; 1 minute for the second stage and 30 minutes for the third stage. Fig. 6.15 depicts the simulation results for the proposed and uncoordinated charging methods in 38-bus distribution networks. The energy loss calculated during the 24-hour simulation with proposed and uncoordinated charging are 1.017 MWh and 1.840 MWh, respectively, as depicted in Table 6.9. It is to be noted

that the results obtained with this test network are found to be consistent and similar to the 33-bus distribution network.

Table 6.9: Technical results for the proposed and uncoordinated charging methods in 38-bus distribution network.

Type of charging	Min voltage magnitude (p.u)	Max voltage magnitude (p.u)	Time taken to reach final SoC (hour)	Energy loss
Proposed (Type II)	0.9135	1.04	[28,30,31]:5.41;[7,8,9,10]:4.067; [12,13,14,15]:6.016;[16]:12.13	1.017 MWhr
Uncoordinated (Type I)	0.9004	1.0795	[28,30,31]:2.7;[7,8,9,10]:2.016; [12,13,14,15]:3.016;[16]:6.067	1.840 MWh

6.6 Conclusions

In this chapter, an RHC based three-stage, two-level voltage control and EV charge scheduling method has been developed. The first two stages focus on correction of voltage deviations based on temporal characteristics of voltage control devices. The third stage, however schedules EV charging considering benefits of EV users, EVAs as well as DNO. The proposed method ensures that the EV users' fulfillment of desired SoC at departure time is attained at all the buses. Simulations have been performed with slow and fast charging schemes. It has been observed that the maximum voltage dip in fast charging scheme is 9.17% more compared to slow charging scheme with same charging infrastructure capacity. Moreover, profit gained from charging and regulation services is almost 50% more in fast charging scheme than slow charging scheme for both the aggregators. Furthermore, it is observed that the proposed method is better than uncoordinated charging method in terms of better voltage profile, reduced energy losses, and more profit.

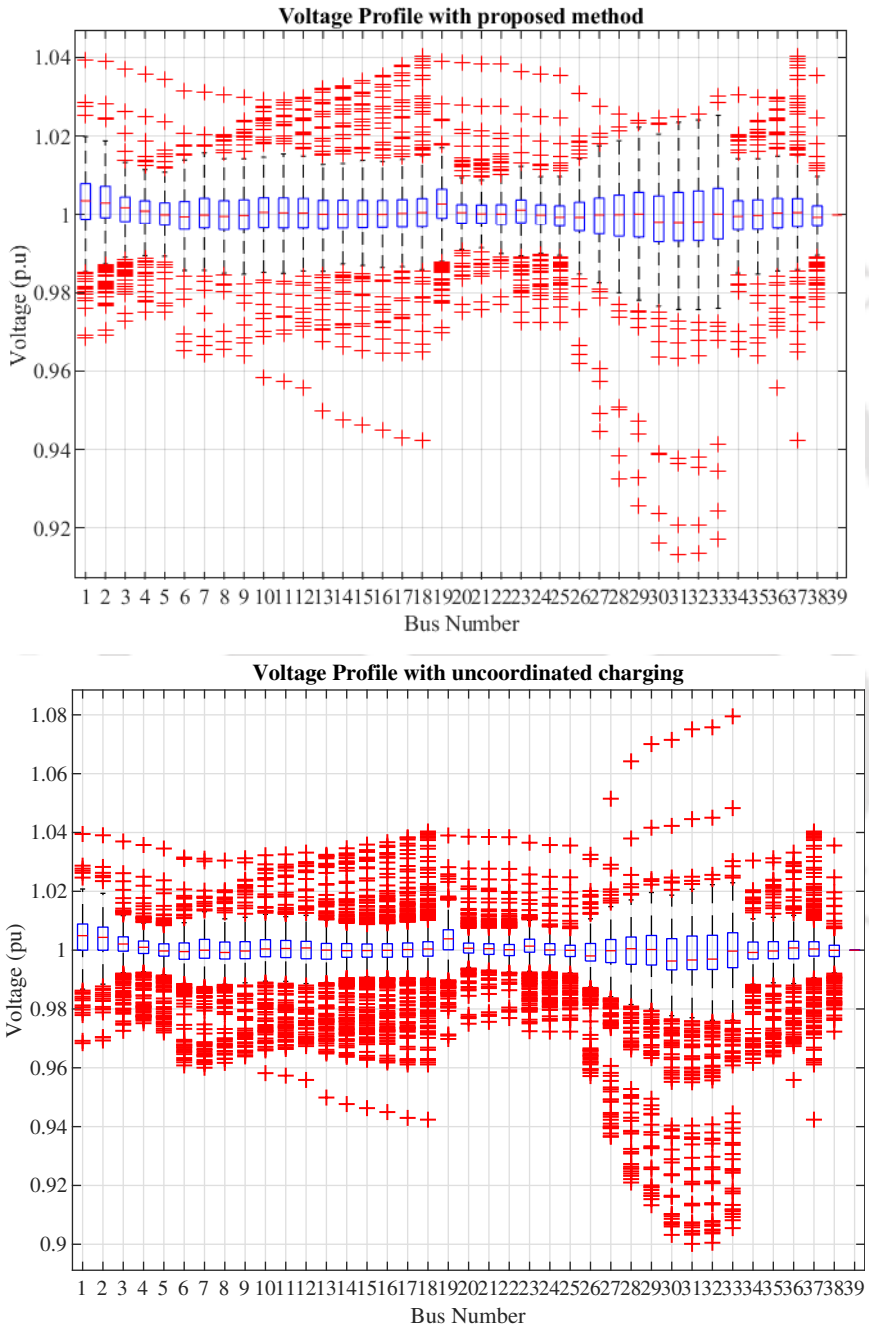

Figure 6.15: Box plots of voltages for proposed and uncoordinated charging methods.

7

Conclusions

Contents

7.1 Summary

Driven by rising energy demand and environmental concerns, proliferation of RES and EVs in the power distribution networks have increased manifold. However, high integration of these DERs into the existing distribution networks introduces significant opportunities as well as challenges to the DNO. The voltage profile management is identified as one of the major challenges due to huge integration of DERs. The bidirectional power flow due to penetration of DG units elevates the voltage magnitudes across feeders. Besides, intermittent power fluctuations of RES exacerbate voltage regulation problem. Similarly, proliferation of EVs charging adds further stress to the aging distribution network infrastructure, and thereby this causes severe voltage fluctuations and congestion in the networks. This necessitates an advanced VVC to overcome the negative effects of DG units and EVs.

The power system researchers have significantly contributed to voltage control approaches in last few years. In Chapter 1, the works on voltage control approaches are systematically presented. The voltage control approaches are classified into a three-level classification tree. It consists of three levels based on different attributes. The Level #1 classification is based on the functionality of the control approach. The way the different control schemes are implemented is the basis of Level #2 classification. The Level #3 classification is based on the different voltage control methodologies reported in literature. The special emphasis is given in the literature review to identify the optimal voltage control approaches. A wide variety of literature on optimal control of voltage is presented in Chapter 1.

The contributions of this thesis are summarized as follows:

- In Chapter 2, an MPC-based centralized control approach is presented for maintaining the voltages of the buses within permissible limits in the presence of high PV penetration. The proposed control scheme optimally coordinates the actions of OLTC and active/reactive powers set-points of PV inverters to fulfill the desired objectives. The objectives are minimization of change in control variables, slack variables, energy loss, and voltage error. These objectives are weighted to form the overall objective function. Three rules are formulated based on the severity of voltage magnitudes. The weights of the objectives are adjusted according to these predefined rules. Simulations are performed in an ADN integrated with and without microgrids, where both demands and generations vary hourly over the day. As power is injected by the microgrids during most of the time of the day, the excursions of bus voltages are slightly higher

in the microgrids integrated ADN. Moreover, the incorporation of the proposed rule-based MPC reduces the energy loss due to active power loss in distribution networks, as is evident from the simulation results obtained by comparing the proposed approach with an existing MPC-based approach. Besides, in terms of the computational burden, the computation time of the proposed controller is found to be less for one sampling period in solving optimization problem, when compared with an existing MPC approach. Furthermore, control performance is evaluated using SSVE performance index.

- In Chapter 3, a dual-stage model predictive based voltage control is proposed that optimally coordinates the reference voltage of OLTC in the first stage, and PV inverters' active and reactive power set points, and reference voltage of DSTATCOM in the second stage to maintain network voltages within the operating limits. This dual-timescale coordinated algorithm effectively reduces power loss as well as OLTC tap operations. The two functionalities of active distribution management system, i.e., demand response and conservation voltage reduction are further explored in the voltage control methodology to enhance energy efficiency of the distribution networks. Simulation results depict that the integration of these two functions in the MPC-based VVC helps in reduction of energy loss, peak demand, energy consumption and controllable resource utilization. The CVR operation with PV inverters' reactive power capability yields better results in terms of higher reduction in energy consumptions (0.7%), system losses (5.8%), and deeper voltage reduction within ANSI standard in comparison with only CVR (absence of PV inverter).

- In Chapter 4, a dual-stage coordinated control approach has been presented for voltage regulation and congestion management of ADN in the presence of PV generators and EVCS. The proposed scheme operates on RBMPC to optimally manage the settings of the regulating devices, i.e., OLTC, DSTATCOM, PV generators, and EV inverters that have different temporal characteristics. Here, the voltage and branch current magnitudes are the outputs as well as the states of MPC. Three cases are defined to study the effects of locations of EVCS in the distribution networks. In Case C, although the charging demand is more than the other two cases with two EVCS, the controller performs better than Case B. This is due to the increased availability of reactive power support from on-board chargers of EVs. The number of tap movements and line congestion in the proposed approach are considerably less than the other compared approaches due to the inclusion of timescale decomposition of volt/var devices and branch current constraint in the proposed scheme. It is evident from the sensitivity analysis that the proposed approach,

with proper coordination among the control elements, could fulfill the desired objectives. Each control element has a role to play in the voltage regulation scheme. While the DSTATCOM helps to limit the maximum voltage magnitudes, the reactive power support from PV inverters aids in minimizing voltage error and energy loss. Moreover, the computation time for a particular sampling instant is evaluated to be few milliseconds, which makes the proposed approach compatible for practical use.

- The Chapter 5 proposes a three-stage MPC-based centralized coordinated approach to schedule charging of EV and volt/var devices. The approach aims at maintaining bus voltage magnitudes and state-of-charge of EV battery within desired limits with minimal usage of control resources and cost of electricity consumption. The first stage determines the optimal operating points of traditional discrete control devices on an hourly basis. The second stage dispatches the optimal set-points of power electronics interfaced fast devices [PV and EV inverters] every one minute. The third stage schedules charging of EV half-hourly with respect to the real-time electricity price. The control approach ensures that EVs attain the desired state-of-charge (SoC) at the time of their departure from the charging station without violating the voltage limits. The EV charging behaviors have been taken into consideration while modeling EVCS. The reactive power support from EVCS has also been utilized to regulate the voltages. Moreover, the localized volt/var curve integrated into the DG units is adjusted according to the reactive power set-points obtained from the MPC-based centralized controller. From the simulation results, it can be observed that the bus voltage magnitudes of the distribution networks are regulated within allowable voltage ranges and the SoCs of the EVs reach the desired values at the time of their departure for all the operating conditions. However, the energy loss and resource utilization in Type I charging (uncoordinated charging) are more compared to Type II charging. With coordinated charging, energy loss decreases by 20.16% compared to uncoordinated charging method. It is observed that energy consumption due to EV charging during high price charging hours is 40.36% less for Type II charging compared to Type I charging. In Scenario II, due to heavy loading and cloudy condition, more voltage dips are observed in the voltage magnitudes. However, the proposed approach shows that the voltage could be brought back to the desirable value with active and reactive power injections of EVCS. Moreover, it is observed that, with increase in the network dimension and control variables, the computation times increase proportionately.

- The Chapter 6 proposes a three-stage, two-level receding horizon control-based volt/var optimization for the optimal power dispatch of EV and solar inverters in ADN. The approach aims

at coordinating different voltage regulating devices depending on their slow (first stage) or fast (second stage) responses to maintain the nodal voltages magnitudes and scheduling the charging of electric vehicles (third stage) in the first level of operation. EV aggregators, being the interface between DNO and EV users, is an independent entity that also seeks its own sustainable benefits from the coordinated optimal scheduling and regulation services. In the proposed control algorithm, attempts have been taken to maximize the benefit of EVA while performing ancillary services through grid-to-vehicle and vehicle-to-grid infrastructure. Demand response is also used in the third stage of operation. The model has been formulated as a mixed-integer nonlinear programming problem and implemented in general algebraic modeling system software. Furthermore, the reactive power of the fast converters are dispatched through the local Q(V) characteristics in the second control level. Moreover, the voltage regulation objective in all the stages benefits DNO technically. The proposed method ensures that the EV users' satisfaction of desired SoC at departure time is attained at all the buses. Simulations have been performed with slow and fast charging schemes. It has been observed that the maximum voltage dip in fast charging scheme is 9.17% more compared to slow charging scheme with same charging infrastructure capacity. Moreover, profit gained from charging and regulation services is almost 50% more in fast charging scheme than slow charging scheme for both the aggregators. Furthermore, it is observed that the proposed (Type II charging) method is better than uncoordinated (Type I charging) method in terms of technical (reduced energy loss, voltage deviations) and economical (more profit) considerations.

The simulation study is conducted for different cases in MATLAB software. The CONOPT/CPLEX solver of General Algebraic Modelling System /IBM ILOG community edition software is used as the solution tool. The validation of the proposed control approach is done in 33-bus as well as 38-bus distribution networks. The summary of this thesis are as follows:

(i) A rule-based MPC approach has been formulated for coordinating OLTC and PV inverters which can minimize energy losses and can maintain the node voltages, as well. The proposed approach acts as a corrective controller that brings the voltage magnitudes within their desired limits in ADN integrated with and without microgrids.

(ii) An MPC scheme based on dual-time scale coordinated algorithm has been developed, that coordinates OLTC, PV inverters and DSTATCOM that possess different temporal characteristics.

Moreover, integrating CVR and DR techniques in MPC framework aids in reducing energy consumption, energy loss, and peak demand by 0.5%, 4.1%, and 2.9%, respectively.

(iii) An MPC-based dual-stage voltage control algorithm has been developed to manage line congestion in addition to voltage violations of ADN due to increased penetration of EVs and PVs, with minimal actions of the OLTC tap positions and dispatch of active power from PV, reactive power from DSTATCOM, EVCS, and PV units.

(iv) To study the effects of EVCS on the dual-stage coordinated algorithm, detailed modeling has been further done. Furthermore, the local level control has been added to the centralized control in dispatching DG reactive power through the integrated local Q(V) characteristics.

(v) A third stage is added to the previously developed two-stage MPC framework to perform EV charge scheduling by taking into consideration the balance between the operating cost and customer satisfaction. The optimal EV scheduling fulfills the objectives of reaching the desired state-of-charge at desired time, reducing voltage fluctuations and charging of EVs at less price.

(vi) Furthermore, the EV aggregators' profit from charging/discharging and ancillary services has been considered in the economic MPC-based charge scheduling of EVs. Moreover, DR is also used in the third stage of the MPC-based framework to enhance economic efficiency.

7.2 Scope for future work

There are many practical aspects which can be incorporated in the real-time optimal voltage control approaches. The following aspects need to be investigated in future.

- Consideration of unbalanced distribution networks: In this thesis, the test networks considered for validation are assumed to be balanced networks. The study can be extended in future with consideration of unbalanced distribution networks.

- Consideration of load, generation and EV uncertainties in the modeling of ADN for voltage control purposes: The real-time optimal voltage control approaches proposed in this thesis have assumed the output power of PV units, loads and EVs as deterministic and neglected the uncertainty associated with these DERs. The future extensions of this work might include these uncertainties in the prediction model and a robust MPC approach can be developed to handle these uncertainties.

- Consideration of interface between transmission and distribution networks: The real-time control of the distribution networks could be further extended to support the transmission network when the later operates in stressed conditions. The real-time interface between transmission and distribution systems could be further investigated.

- Consideration of smart transformers' capabilities for voltage support: Recently, the smart transformers' capabilities for voltage support have been investigated. The future study encompasses the usage of MPC to coordinate the smart transformers with other voltage regulation devices of distribution networks.

- Consideration of a framework to enable EVs to participate in local energy markets: In this thesis, price-based electric vehicle charging/discharging scheduling has been considered to mitigate voltage issues as well as to fulfill EV users' desired SoC. However, this study can be extended to develop a flexible framework that combines the economic and control mechanisms through EV owners' active participation in real-time local energy markets. Moreover, as part of the feasibility studies of V2G, the replacement cost and degradation cost of the battery in the EV would need to be considered to provide the EV owner a good indication whether it is profitable to participate in providing voltage support to the grid via V2G.

- Validation of the proposed approach in real-time simulation platform: The proposed control methodology could be further validated in real-time co-simulation platform using a real-time digital simulator in future. Since the communication delay via the centralized scheme and the accuracy of the predicted target value of MPC for the next control cycle may affect the performance of the voltage control, they need to be carefully considered in the setup of the real-time digital simulation platform.

References

[1] D. E. Olivares, A. Mehrizi-Sani, A. H. Etemadi, C. A. Cañizares, R. Iravani, M. Kazerani, A. H. Hajimiragha, O. Gomis-Bellmunt, M. Saeedifard, R. Palma-Behnke, G. A. Jiménez-Estévez, and N. D. Hatziargyriou, "Trends in microgrid control," *IEEE Transactions on Smart Grid*, vol. 5, no. 4, pp. 1905–1919, July 2014.

[2] L. Meng, Q. Shafiee, G. F. Trecate, H. Karimi, D. Fulwani, X. Lu, and J. M. Guerrero, "Review on control of dc microgrids and multiple microgrid clusters," *IEEE Journal of Emerging and Selected Topics in Power Electronics*, vol. 5, no. 3, pp. 928–948, Sep. 2017.

[3] "Microgrid supervisory controllers and energy management systems: A literature review," *Renewable and Sustainable Energy Reviews*, vol. 60, pp. 1263 – 1273, 2016.

[4] A. Bidram and A. Davoudi, "Hierarchical structure of microgrids control system," *IEEE Transactions on Smart Grid*, vol. 3, no. 4, pp. 1963–1976, Dec 2012.

[5] Y. Han, K. Zhang, H. Li, E. A. A. Coelho, and J. M. Guerrero, "Mas-based distributed coordinated control and optimization in microgrid and microgrid clusters: A comprehensive overview," *IEEE Transactions on Power Electronics*, vol. 33, no. 8, pp. 6488–6508, Aug 2018.

[6] G. Valverde and T. V. Cutsem, "Model predictive control of voltages in active distribution networks," *IEEE Transactions on Smart Grid*, vol. 4, no. 4, pp. 2152–2161, Dec 2013.

[7] G. Lou, W. Gu, Y. Xu, M. Cheng, and W. Liu, "Distributed mpc-based secondary voltage control scheme for autonomous droop-controlled microgrids," *IEEE Transactions on Sustainable Energy*, vol. 8, no. 2, pp. 792–804, April 2017.

[8] V. Calderaro, G. Conio, V. Galdi, G. Massa, and A. Piccolo, "Optimal decentralized voltage control for distribution systems with inverter-based distributed generators," *IEEE Transactions on Power Systems*, vol. 29, no. 1, pp. 230–241, Jan 2014.

[9] N. Daratha, B. Das, and J. Sharma, "Coordination between oltc and svc for voltage regulation in unbalanced distribution system distributed generation," *IEEE Transactions on Power Systems*, vol. 29, no. 1, pp. 289–299, Jan 2014.

[10] H. S. Bidgoli and T. Van Cutsem, "Combined local and centralized voltage control in active distribution networks," *IEEE Transactions on Power Systems*, vol. 33, no. 2, pp. 1374–1384, 2018.

[11] B. A. Robbins, C. N. Hadjicostis, and A. D. Domínguez-García, "A two-stage distributed architecture for voltage control in power distribution systems," *IEEE Transactions on Power Systems*, vol. 28, no. 2, pp. 1470–1482, 2013.

[12] A. L. Bella, S. R. Cominesi, C. Sandroni, and R. Scattolini, "Hierarchical predictive control of microgrids in islanded operation," *IEEE Transactions on Automation Science and Engineering*, vol. 14, no. 2, pp. 536–546, April 2017.

[13] X. Yang, Y. Du, J. Su, L. Chang, Y. Shi, and J. Lai, "An optimal secondary voltage control strategy for an islanded multibus microgrid," *IEEE Journal of Emerging and Selected Topics in Power Electronics*, vol. 4, no. 4, pp. 1236–1246, Dec 2016.

[14] Y. Guo, Q. Wu, H. Gao, X. Chen, J. Østergaard, and H. Xin, "Mpc-based coordinated voltage regulation for distribution networks with distributed generation and energy storage system," *IEEE Transactions on Sustainable Energy*, vol. 10, no. 4, pp. 1731–1739, 2019.

[15] Y. Li, L. Li, C. Peng, and J. Zou, "An mpc based optimized control approach for ev-based voltage regulation in distribution grid," *Electric Power Systems Research*, vol. 172, pp. 152–160, 2019.

[16] X. Wang, C. Wang, T. Xu, L. Guo, P. Li, L. Yu, and H. Meng, "Optimal voltage regulation for distribution networks with multi-microgrids," *Applied Energy*, vol. 210, pp. 1027 – 1036, 2018. [Online]. Available: http://www.sciencedirect.com/science/article/pii/S0306261917311376

[17] A. A. Mohamed, A. T. Elsayed, T. A. Youssef, and O. A. Mohammed, "Hierarchical control for dc microgrid clusters with high penetration of distributed energy resources," *Electric Power Systems Research*, vol. 148, pp. 210 – 219, 2017. [Online]. Available: http://www.sciencedirect.com/science/article/pii/S0378779617301505

[18] A. Arefi and F. Shahnia, "Tertiary controller-based optimal voltage and frequency management technique for multi-microgrid systems of large remote towns," *IEEE Transactions on Smart Grid*, vol. 9, no. 6, pp. 5962–5974, Nov 2018.

[19] S. Adhikari, Q. Xu, Y. Tang, and P. Wang, "Decentralized control of dc microgrid clusters," in *2017 IEEE 3rd International Future Energy Electronics Conference and ECCE Asia (IFEEC 2017 - ECCE Asia)*, June 2017, pp. 567–572.

[20] M. A. Azzouz, M. F. Shaaban, and E. F. El-Saadany, "Real-time optimal voltage regulation for distribution networks incorporating high penetration of pevs," *IEEE Transactions on Power Systems*, vol. 30, no. 6, pp. 3234–3245, 2015.

[21] Y. Guo, Q. Wu, H. Gao, S. Huang, B. Zhou, and C. Li, "Double-time-scale coordinated voltage control in active distribution networks based on mpc," *IEEE Transactions on Sustainable Energy*, vol. 11, no. 1, pp. 294–303, 2020.

[22] K. Christakou, M. Paolone, and A. Abur, "Voltage control in active distribution networks under uncertainty in the system model: A robust optimization approach," *IEEE Transactions on Smart Grid*, vol. 9, no. 6, pp. 5631–5642, Nov 2018.

[23] M. Zeraati, M. E. Hamedani Golshan, and J. M. Guerrero, "A consensus-based cooperative control of pev battery and pv active power curtailment for voltage regulation in distribution networks," *IEEE Transactions on Smart Grid*, vol. 10, no. 1, pp. 670–680, 2019.

[24] S. N. Salih and P. Chen, "On coordinated control of oltc and reactive power compensation for voltage regulation in distribution systems with wind power," *IEEE Transactions on Power Systems*, vol. 31, no. 5, pp. 4026–4035, Sep. 2016.

[25] K. M. Muttaqi, A. D. T. Le, M. Negnevitsky, and G. Ledwich, "A coordinated voltage control approach for coordination of oltc, voltage regulator, and dg to regulate voltage in a distribution feeder," *IEEE Transactions on Industry Applications*, vol. 51, no. 2, pp. 1239–1248, 2015.

[26] P. Li, J. Ji, H. Ji, J. Jian, F. Ding, J. Wu, and C. Wang, "Mpc-based local voltage control strategy of dgs in active distribution networks," *IEEE Transactions on Sustainable Energy*, vol. 11, no. 4, pp. 2911–2921, 2020.

[27] H. Li, M. A. Azzouz, and A. A. Hamad, "Cooperative voltage control in mv distribution networks with electric vehicle charging stations and photovoltaic dgs," *IEEE Systems Journal*, vol. 15, no. 2, pp. 2989–3000, 2021.

[28] S. Maharjan, A. M. Khambadkone, and J. C.-H. Peng, "Robust constrained model predictive voltage control in active distribution networks," *IEEE Transactions on Sustainable Energy*, vol. 12, no. 1, pp. 400–411, 2021.

[29] M. S. Hossan and B. Chowdhury, "Integrated cvr and demand response framework for advanced distribution management systems," *IEEE Transactions on Sustainable Energy*, vol. 11, no. 1, pp. 534–544, 2020.

[30] C. Le Floch, S. Bansal, C. J. Tomlin, S. J. Moura, and M. N. Zeilinger, "Plug-and-play model predictive control for load shaping and voltage control in smart grids," *IEEE Transactions on Smart Grid*, vol. 10, no. 3, pp. 2334–2344, 2019.

[31] M. Mazumder and S. Debbarma, "Ev charging stations with a provision of v2g and voltage support in a distribution network," *IEEE Systems Journal*, vol. 15, no. 1, pp. 662–671, 2021.

[32] M. S. Sadabadi, Q. Shafiee, and A. Karimi, "Plug-and-play voltage stabilization in inverter-interfaced microgrids via a robust control strategy," *IEEE Transactions on Control Systems Technology*, vol. 25, no. 3, pp. 781–791, May 2017.

[33] Y. Wang, X. Wang, Z. Chen, and F. Blaabjerg, "Distributed optimal control of reactive power and voltage in islanded microgrids," *IEEE Transactions on Industry Applications*, vol. 53, no. 1, pp. 340–349, Jan 2017.

[34] G. Chen and E. Feng, "Distributed secondary control and optimal power sharing in microgrids," *IEEE/CAA Journal of Automatica Sinica*, vol. 2, no. 3, pp. 304–312, July 2015.

[35] X. Dou, P. Xu, Q. Hu, W. Sheng, X. Quan, Z. Wu, and B. Xu, "A distributed voltage control strategy for multi-microgrid active distribution networks considering economy and response speed," *IEEE Access*, vol. 6, pp. 31 259–31 268, 2018.

[36] P. Olival, A. Madureira, and M. Matos, "Advanced voltage control for smart microgrids using distributed energy resources," *Electric Power Systems Research*, vol. 146, pp. 132 – 140, 2017. [Online]. Available: http://www.sciencedirect.com/science/article/pii/S0378779617300366

[37] M. Chamana and B. H. Chowdhury, "Optimal voltage regulation of distribution networks with cascaded voltage regulators in the presence of high pv penetration," *IEEE Transactions on Sustainable Energy*, vol. 9, no. 3, pp. 1427–1436, July 2018.

[38] S. Chen, W. Hu, C. Su, X. Zhang, and Z. Chen, "Optimal reactive power and voltage control in distribution networks with distributed generators by fuzzy adaptive hybrid particle swarm optimisation method," *IET Generation, Transmission Distribution*, vol. 9, no. 11, pp. 1096–1103, 2015.

[39] V. Calderaro, V. Galdi, F. Lamberti, and A. Piccolo, "A smart strategy for voltage control ancillary service in distribution networks," *IEEE Transactions on Power Systems*, vol. 30, no. 1, pp. 494–502, Jan 2015.

[40] G. Ferro, R. Minciardi, M. Robba, and M. Rossi, "Optimal voltage control and demand response: Integration between distribution system operator and microgrids," in *2017 IEEE 14th International Conference on Networking, Sensing and Control (ICNSC)*, May 2017, pp. 435–440.

[41] C. Deckmyn, T. L. Vandoorn, J. V. de Vyver, J. Desmet, and L. Vandevelde, "A microgrid multilayer control concept for optimal power scheduling and voltage control," *IEEE Transactions on Smart Grid*, vol. 9, no. 5, pp. 4458–4467, Sep. 2018.

[42] Y. Chai, L. Guo, C. Wang, Z. Zhao, X. Du, and J. Pan, "Network partition and voltage coordination control for distribution networks with high penetration of distributed pv units," *IEEE Transactions on Power Systems*, vol. 33, no. 3, pp. 3396–3407, May 2018.

[43] S. Singh, V. B. Pamshetti, and S. P. Singh, "Time horizon-based model predictive volt/var optimization for smart grid enabled cvr in the presence of electric vehicle charging loads," *IEEE Transactions on Industry Applications*, vol. 55, no. 6, pp. 5502–5513, 2019.

[44] Y. Jiang, C. Wan, J. Wang, Y. Song, and Z. Y. Dong, "Stochastic receding horizon control of active distribution networks with distributed renewables," *IEEE Transactions on Power Systems*, vol. 34, no. 2, pp. 1325–1341, 2019.

[45] C. Tzanetopoulou, "Impacts of high penetration of pv in distribution grids and mitigation strategies," *Semester thesis, EEH-Power Systems Laboratory, ETH Zurich*, 2013.

[46] "Future of solar photovoltaic: Deployment, investment, technology, grid integration and socio-economic aspects." [Online]. Available: https://www.irena.org/-/media/Files/IRENA/Agency/Publication/2019/Nov/IRENA_Future_of_Solar_PV_2019.pdf

[47] A. M. Nour, A. Y. Hatata, A. A. Helal, and M. M. El-Saadawi, "Review on voltage-violation mitigation techniques of distribution networks with distributed rooftop pv systems," *IET Generation, Transmission & Distribution*, vol. 14, no. 3, pp. 349–361, 2020. [Online]. Available: https://ietresearch.onlinelibrary.wiley.com/doi/abs/10.1049/iet-gtd.2019.0851

[48] "Analysis of indian electricity distribution systems for the integration of high shares of rooftop pv' (federal ministry for the environment, nature conservation, building, and nuclear safety, 2017)." [Online]. Available: http://www.comsolar.in/news-events/news-events/#c954

[49] R. K. Varma, "Multivariable modulator controller for power generation facility, pct application," *U.S. Patent*, 2016.

[50] J. Ding, Q. Zhang, S. Hu, Q. Wang, and Q. Ye, "Clusters partition and zonal voltage regulation for distribution networks with high penetration of pvs," *IET Generation, Transmission & Distribution*, 2018.

[51] R. K. Varma and E. M. Siavashi, "Pv-statcom: A new smart inverter for voltage control in distribution systems," *IEEE Transactions on Sustainable Energy*, vol. 9, no. 4, pp. 1681–1691, 2018.

[52] D. M. e. a. D. Seborg, T.F. Edgar, "Process, dynamics and control," *(Wiley, Hoboken, NJ, 2011, 3rd edn.),*, p. 414–438, 2011.

[53] L. Wang, "Model predictive control system design and implementation using matlab, (advances in industrial applications)'," *(Springer, London, 2008)*, 2008.

[54] F. Milano, "Power system analysis toolbox: Documentation for psat, version 2.0.0," 2008.

[55] A. Soroudi, "Power system optimization modeling in gams," 2017.

[56] M. Baran and F. Wu, "Network reconfiguration in distribution systems for loss reduction and load balancing," *IEEE Transactions on Power Delivery*, vol. 4, no. 2, pp. 1401–1407, 1989.

[57] K. Qian, C. Zhou, M. Allan, and Y. Yuan, "Modeling of load demand due to ev battery charging in distribution systems," *IEEE Transactions on Power Systems*, vol. 26, no. 2, pp. 802–810, 2011.

[58] H. Ruan, H. Gao, Y. Liu, L. Wang, and J. Liu, "Distributed voltage control in active distribution network considering renewable energy: A novel network partitioning method," *IEEE Transactions on Power Systems*, vol. 35, no. 6, pp. 4220–4231, 2020.

[59] S. C. Dhulipala, R. V. A. Monteiro, R. F. d. Silva Teixeira, C. Ruben, A. S. Bretas, and G. C. Guimarães, "Distributed model-predictive control strategy for distribution network volt/var control: A smart-building-based approach," *IEEE Transactions on Industry Applications*, vol. 55, no. 6, pp. 7041–7051, 2019.

[60] "Reducing voltage using dstatcoms and reactive power of pv inverters in a medium voltage distribution system," *Journal of Engineering*, vol. 18, pp. 5274–5279, 2019.

[61] R. Manojkumar, C. Kumar, and S. Ganguly, "Optimal demand response in a residential pv storage system using energy pricing limits," *IEEE Transactions on Industrial Informatics*, vol. 18, no. 4, pp. 2497–2507, 2022.

[62] B. Bakhshideh Zad, J. Lobry, and F. Vallée, "Coordinated control of on-load tap changer and d-statcom for voltage regulation of radial distribution systems with dg units," in *2013 3rd International Conference on Electric Power and Energy Conversion Systems*, 2013, pp. 1–5.

[63] F. Ding and M. Baggu, "Coordinated use of smart inverters with legacy voltage regulating devices in distribution systems with high distributed pv penetration—increase cvr energy savings," in *2019 IEEE Power Energy Society General Meeting (PESGM)*, 2019, pp. 1–1.

[64] H. Gharavi, L. F. Ochoa, X. Liu, G. Paterson, B. Ingham, and S. McLoone, "Cvr and loss optimization through active voltage management: A trade-off analysis," *IEEE Transactions on Power Delivery*, vol. 36, no. 6, pp. 3466–3476, 2021.

[65] N. Karthikeyan, J. R. Pillai, B. Bak-Jensen, and J. W. Simpson-Porco, "Predictive control of flexible resources for demand response in active distribution networks," *IEEE Transactions on Power Systems*, vol. 34, no. 4, pp. 2957–2969, 2019.

[66] H. Sheng, C. Wang, B. Li, J. Liang, M. Yang, and Y. Dong, "Multi-timescale active distribution network scheduling considering demand response and user comprehensive satisfaction," *IEEE Transactions on Industry Applications*, vol. 57, no. 3, pp. 1995–2005, 2021.

[67] V. A. Freire, L. V. R. De Arruda, C. Bordons, and J. J. Márquez, "Optimal demand response management of a residential microgrid using model predictive control," *IEEE Access*, vol. 8, pp. 228 264–228 276, 2020.

[68] V. B. Pamshetti and S. P. Singh, "Coordinated allocation of bess and sop in high pv penetrated distribution network incorporating dr and cvr schemes," *IEEE Systems Journal*, pp. 1–11, 2020.

[69] C. S. Lai, Y. Jia, M. D. McCulloch, and Z. Xu, "Daily clearness index profiles cluster analysis for photovoltaic system," *IEEE Transactions on Industrial Informatics*, vol. 13, no. 5, pp. 2322–2332, 2017.

[70] M. V. Gururaj and N. P. Padhy, "A novel decentralized coordinated voltage control scheme for distribution system with dc microgrid," *IEEE Transactions on Industrial Informatics*, vol. 14, no. 5, pp. 1962–1973, 2018.

[71] T. Tewari, A. Mohapatra, and S. Anand, "Coordinated control of oltc and energy storage for voltage regulation in distribution network with high pv penetration," *IEEE Transactions on Sustainable Energy*, vol. 12, no. 1, pp. 262–272, 2021.

[72] Z. Wang, J. Wang, B. Chen, M. M. Begovic, and Y. He, "Mpc-based voltage/var optimization for distribution circuits with distributed generators and exponential load models," *IEEE Transactions on Smart Grid*, vol. 5, no. 5, pp. 2412–2420, 2014.

[73] H. Zhao, Q. Wu, Q. Guo, H. Sun, S. Huang, and Y. Xue, "Coordinated voltage control of a wind farm based on model predictive control," *IEEE Transactions on Sustainable Energy*, vol. 7, no. 4, pp. 1440–1451, 2016.

[74] Y. Xu, Z. Y. Dong, R. Zhang, and D. J. Hill, "Multi-timescale coordinated voltage/var control of high renewable-penetrated distribution systems," *IEEE Transactions on Power Systems*, vol. 32, no. 6, pp. 4398–4408, 2017.

[75] S. Xia, Z. Ding, T. Du, D. Zhang, M. Shahidehpour, and T. Ding, "Multitime scale coordinated scheduling for the combined system of wind power, photovoltaic, thermal generator, hydro pumped storage, and batteries," *IEEE Transactions on Industry Applications*, vol. 56, no. 3, pp. 2227–2237, 2020.

[76] C. Kumar and M. K. Mishra, "A voltage-controlled dstatcom for power-quality improvement," *IEEE Transactions on Power Delivery*, vol. 29, no. 3, pp. 1499–1507, 2014.

[77] J. Wang, G. R. Bharati, S. Paudyal, O. Ceylan, B. P. Bhattarai, and K. S. Myers, "Coordinated electric vehicle charging with reactive power support to distribution grids," *IEEE Transactions on Industrial Informatics*, vol. 15, no. 1, pp. 54–63, 2019.

[78] S. Shao, M. Pipattanasomporn, and S. Rahman, "Grid integration of electric vehicles and demand response with customer choice," *IEEE Transactions on Smart Grid*, vol. 3, no. 1, pp. 543–550, 2012.

[79] S. Deb, A. K. Goswami, P. Harsh, J. P. Sahoo, R. L. Chetri, R. Roy, and A. S. Shekhawat, "Charging coordination of plug-in electric vehicle for congestion management in distribution system integrated with renewable energy sources," *IEEE Transactions on Industry Applications*, vol. 56, no. 5, pp. 5452–5462, 2020.

[80] H. Bidgoli, "Real-time corrective control in active distribution networks," *PhD Dissertation, University of Liege, Belgium*, 2017.

[81] A. Fathy and A. Y. Abdelaziz, "Competition over resource optimization algorithm for optimal allocating and sizing parking lots in radial distribution network," *Journal of Cleaner Production*, vol. 264, p. 121397, 2020. [Online]. Available: https://www.sciencedirect.com/science/article/pii/S095965262031444X

[82] Y. Wang, T. John, and B. Xiong, "A two-level coordinated voltage control scheme of electric vehicle chargers in low-voltage distribution networks," *Electric Power Systems Research*, vol. 168, pp. 218–227, 2019. [Online]. Available: https://www.sciencedirect.com/science/article/pii/S0378779618304024

[83] S. Debbarma and A. Dutta, "Utilizing electric vehicles for lfc in restructured power systems using fractional order controller," *IEEE Transactions on Smart Grid*, vol. 8, no. 6, pp. 2554–2564, 2017.

[84] M. F. Shaaban, M. Ismail, E. F. El-Saadany, and W. Zhuang, "Real-time pev charging/discharging coordination in smart distribution systems," *IEEE Transactions on Smart Grid*, vol. 5, no. 4, pp. 1797–1807, 2014.

[85] R. Mehta, D. Srinivasan, A. M. Khambadkone, J. Yang, and A. Trivedi, "Smart charging strategies for optimal integration of plug-in electric vehicles within existing distribution system infrastructure," *IEEE Transactions on Smart Grid*, vol. 9, no. 1, pp. 299–312, 2018.

[86] Y. Zheng, Y. Song, D. J. Hill, and K. Meng, "Online distributed mpc-based optimal scheduling for ev charging stations in distribution systems," *IEEE Transactions on Industrial Informatics*, vol. 15, no. 2, pp. 638–649, 2019.

[87] W. Jiao, J. Chen, Q. Wu, C. Li, B. Zhou, and S. Huang, "Distributed coordinated voltage control for distribution networks with dg and oltc based on mpc and gradient projection," *IEEE Transactions on Power Systems*, vol. 37, no. 1, pp. 680–690, 2022.

[88] M. M. Hoque, M. Khorasany, R. Razzaghi, H. Wang, and M. Jalili, "Transactive coordination of electric vehicles with voltage control in distribution networks," *IEEE Transactions on Sustainable Energy*, vol. 13, no. 1, pp. 391–402, 2022.

[89] H. Ren, A. Zhang, F. Wang, X. Yan, Y. Li, N. Duić, M. Shafie-khah, and J. P. Catalão, "Optimal scheduling of an ev aggregator for demand response considering triple level benefits of three-parties," *International Journal of Electrical Power Energy Systems*, vol. 125, p. 106447, 2021. [Online]. Available: https://www.sciencedirect.com/science/article/pii/S0142061519339456

[90] C. Jin, J. Tang, and P. Ghosh, "Optimizing electric vehicle charging: A customer's perspective," *IEEE Transactions on Vehicular Technology*, vol. 62, no. 7, pp. 2919–2927, 2013.

[91] B. Hashemi, M. Shahabi, and P. Teimourzadeh-Baboli, "Stochastic-based optimal charging strategy for plug-in electric vehicles aggregator under incentive and regulatory policies of dso," *IEEE Transactions on Vehicular Technology*, vol. 68, no. 4, pp. 3234–3245, 2019.

[92] E. Sortomme and M. A. El-Sharkawi, "Optimal scheduling of vehicle-to-grid energy and ancillary services," *IEEE Transactions on Smart Grid*, vol. 3, no. 1, pp. 351–359, 2012.

[93] I. S. Association, "Standard for interconnection and interoperability of distributed energy resources with associated electric power systems interfaces," *IEEE*, 2018.

[94] "Solar radiant energy over india," *India Meteorological Department, Ministry of Earth Sciences, New Delhi*, 2009.

A

APPENDIX

This Appendix provides the simulation data for all the test networks used in the simulation which includes the bus data, line data, base MVA, base kV etc. Bus data provides the information of active and reactive power load demand of each bus of a network. However, line data of the network provides the information of connectivity of each bus to other buses and the values of resistance and reactance of each line of the network. The simulation data for the time varying load demand and PV generation are also provided in this Appendix.

A.1 Simulation data for 33-bus radial distribution network

The 33-bus radial distribution network is a single feeder network with single substation. The bus 1 of this network is the substation bus and rest all are load buses. Simulation data for the 33-bus radial distribution network are taken from [56]. The bus data and line data for the 33-bus radial distribution network are shown in Tables A.1. The base VA and base kV of the network are 100 MVA and 12.66 kV, respectively. The single line diagram of 33-bus network is shown in Fig. A.1.

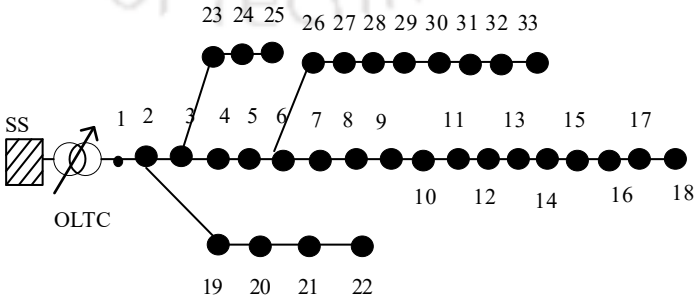

Figure A.1: Single line diagram of 33-bus distribution network.

Table A.1: Bus data of 33-bus radial distribution network

Bus No.	Load Demand		Branch No.	From bus	To bus	R (Ω)	X (Ω)	Maximum line capacity	
	Active Power (kW)	Reactive Power (kVAr)						P(kW)	Q(kVAr)
1	0	0	1	1	2	0.0922	0.047	4600	4600
2	100	60	2	2	3	0.493	0.2511	4100	4100
3	90	40	3	3	4	0.366	0.1864	2900	2900
4	120	80	4	4	5	0.3811	0.1941	2900	2900
5	60	30	5	5	6	0.819	0.707	2900	2900
6	60	20	6	6	7	0.1872	0.6188	1500	1500
7	200	100	7	7	8	0.7114	0.2351	1050	1050
8	200	100	8	8	9	1.03	0.74	1050	1050
9	60	20	9	9	10	1.044	0.74	1050	1050
10	60	20	10	10	11	0.1966	0.065	1050	1050
11	45	30	11	11	12	0.3744	0.1238	1050	1050
12	60	35	12	12	13	1.468	1.155	500	500
13	60	35	13	13	14	0.5416	0.7129	450	450
14	120	80	14	14	15	0.591	0.526	300	300
15	60	10	15	15	16	0.7463	0.545	250	250
16	60	20	16	16	17	1.289	1.721	250	250
17	60	20	17	17	18	0.732	0.574	100	100
18	90	40	18	2	19	0.164	0.1565	500	500
19	90	40	19	19	20	1.5042	1.3554	500	500
20	90	40	20	20	21	0.4095	0.4784	210	210
21	90	40	21	21	22	0.7089	0.9373	110	110
22	90	40	22	3	23	0.4512	0.3083	1050	1050
23	90	50	23	23	24	0.898	0.7091	1050	1050
24	420	200	24	24	25	0.896	0.7011	500	500
25	420	200	25	6	26	0.203	0.1034	1500	1500
26	60	25	26	26	27	0.2842	0.1447	1500	1500
27	60	25	27	27	28	1.059	0.9337	1500	1500
28	60	20	28	28	29	0.8042	0.7006	1500	1500
29	120	70	29	29	30	0.5075	0.2585	1500	1500
30	200	600	30	30	31	0.9774	0.963	500	500
31	150	70	31	31	32	0.3105	0.3619	500	500
32	210	100	32	32	33	0.341	0.5302	100	100
33	60	40							

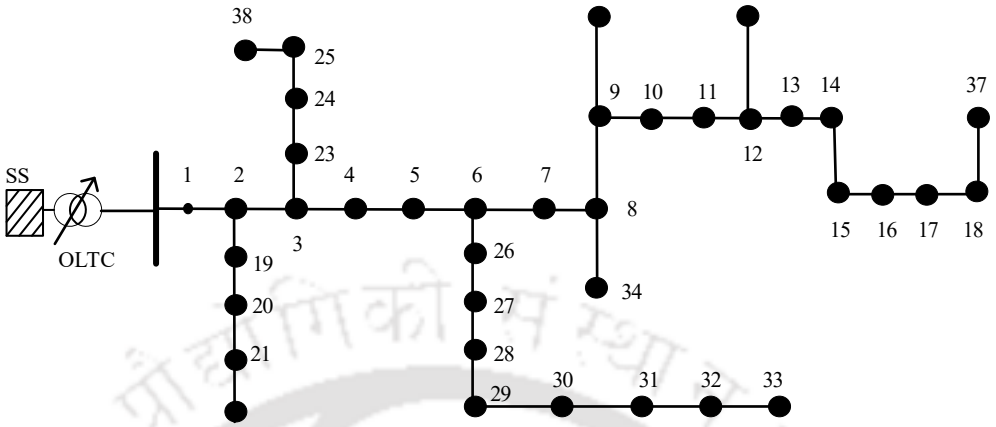

Figure A.2: Single line diagram of 38-bus distribution network.

A.2 Simulation data for 38-bus radial distribution network

The 38-bus radial distribution network is also a single feeder network with single substation. The bus-1 of this network is the substation bus and rest all are load buses. Simulation data for the 38-bus radial distribution network are taken from [57]. The bus data and line data for the 38-bus radial distribution network are shown in Tables A.2, respectively. The base VA and base kV of the network are 10 MVA and 12.66 kV, respectively. The single line diagram of 38-bus network is shown in Fig. A.2.

A.3 Simulation data for time varying load demand

The hourly average load data of three different types of loads [8] are considered in this thesis to have daily variation in load demand. The hourly average load demand data in terms of percentage of peak load demand for three different types of loads (residential, commercial or industrial) are shown in Table A.3.

A.4 Simulation data for time varying PV generation, EV demand and MG

The simulation data for time varying PV generation are taken from [94]. The PV generation data of a sunny as well as a cloudy day are considered for the simulation studies. Moreover, the EV data and the microgrid data are taken from [20, 78] and [16], respectively. The hourly average PV generation, EV and microgrids data in terms of their peak values are shown in Table A.4.

Table A.2: Bus data of 38-bus radial distribution network

Bus No.	Load Demand		Branch No.	From bus	To bus	R (pu)	X (pu)	Maximum line capacity S(pu)
	Active Power (pu)	Reactive Power (pu)						
1	0	0	1	1	2	0.000574	0.000293	4.6
2	0.1	0.06	2	2	3	0.00307	0.001564	4.1
3	0.09	0.04	3	3	4	0.002279	0.001161	2.9
4	0.12	0.08	4	4	5	0.002373	0.001209	2.9
5	0.06	0.03	5	5	6	0.0051	0.004402	2.9
6	0.06	0.02	6	6	7	0.001166	0.003853	1.5
7	0.2	0.1	7	7	8	0.00443	0.001464	1.05
8	0.2	0.1	8	8	9	0.006413	0.004608	1.05
9	0.06	0.02	9	9	10	0.006501	0.004608	1.05
10	0.06	0.02	10	10	11	0.001224	0.000405	1.05
11	0.04	0.03	11	11	12	0.002331	0.000771	1.05
12	0.06	0.035	12	12	13	0.009141	0.007192	0.5
13	0.06	0.035	13	13	14	0.003372	0.004439	0.45
14	0.12	0.08	14	14	15	0.00368	0.003275	0.3
15	0.06	0.01	15	15	16	0.004647	0.003394	0.25
16	0.06	0.02	16	16	17	0.008026	0.010716	0.25
17	0.06	0.02	17	17	18	0.04558	0.003574	0.1
18	0.09	0.04	18	2	19	0.001021	0.000974	0.5
19	0.09	0.04	19	19	20	0.009366	0.00844	0.5
20	0.09	0.04	20	20	21	0.00255	0.002979	0.21
21	0.09	0.04	21	21	22	0.004414	0.005836	0.11
22	0.09	0.04	22	3	23	0.002809	0.00192	1.05
23	0.09	0.05	23	23	24	0.005592	0.004415	1.05
24	0.42	0.2	24	24	25	0.001264	0.004366	0.5
25	0.42	0.2	25	6	26	0.00177	0.000644	1.5
26	0.06	0.025	26	26	27	0.006594	0.000901	1.5
27	0.06	0.025	27	27	28	0.005007	0.005814	1.5
28	0.06	0.02	28	28	29	0.00316	0.004362	1.5
29	0.12	0.07	29	29	30	0.006067	0.00161	1.5
30	0.2	0.6	30	30	31	0.001933	0.005996	0.5
31	0.15	0.07	31	31	32	0.002123	0.002253	0.5
32	0.21	0.1	32	32	33	0.012453	0.003301	0.1
33	0.06	0.04	33	8	34	0.012453	0.012453	0.5
34	0.0	0.0	34	9	35	0.012453	0.012453	0.5
35	0.0	0.0	35	12	36	0.012453	0.012453	0.5
36	0.0	0.0	36	18	37	0.003113	0.003113	0.5
37	0.0	0.0	37	25	38	0.003113	0.003113	0.1
38	0.0	0.0						

Table A.3: Hourly average load demand in percentage of peak load.

Hour	Residential	Commercial	Industrial
12-1 am	25	25	47
1-2	20	20	47
2-3	18	18	47
3-4	16	16	47
4-5	16	16	47
5-6	20	20	47
6-7	22	21	47
7-8	30	24	47
8-9	40	25	47
9-10	50	30	47
10-11	60	60	47
11-12 pm	70	90	85
12-1 pm	80	94	90
1-2	90	90	85
2-3	95	98	100
3-4	100	100	90
4-5	100	90	70
5-6	100	77	67
6-7	90	52	65
7-8	80	50	65
8-9	70	48	65
9-10	55	38	60
10-11	40	30	55
11-12	35	27	53

Table A.4: Hourly average PV generation, EV demand and MG in percentage of peak PV generation, EV demand and MG rating, respectively.

Hour	PV (Sunny)	PV (Cloudy)	EV (Industrial)	EV (Residential)	MG1	MG2	MG3
12-1 am	0	0	0	0	0	0	0
1-2	0	0	0	0	0	0	0
2-3	0	0	0	0	0	0	0
3-4	0	0	0	0	0	0	0
4-5	0	0	0	0	0	0	0
5-6	0	0	0	0	0	0	0
6-7	0.88	5	5	0	0	0	0
7-8	14.7	20	20	0	0	0	0
8-9	40.59	35	50	0	0	0	0
9-10	64.11	50	85	0	0	0	0
10-11	70.89	55	95	0	0	0	0
11-12 pm	85.89	50	95	0	0	0	0
12-1 pm	99.7	60	95	0	54	75	100
1-2	100	65	65	0	55	77	100
2-3	92.65	55	30	5	52	76	100
3-4	79.41	43	5	20	53	76	100
4-5	61.47	20	0	50	54	66	80
5-6	39.71	0	0	85	25	67	80
6-7	9.71	0	0	95	25	56	80
7-8	0.88	0	0	95	25	25	75
8-9	0	0	0	95	25	25	75
9-10	0	0	0	65	25	25	75
10-11	0	0	0	30	0	0	0
11-12	0	0	0	5	0	0	0

LIST OF PUBLICATIONS

Journal Publications:

1. Arunima Dutta, Sanjib Ganguly, Chandan Kumar, "Model Predictive Control-based Optimal Voltage Regulation of Active Distribution Networks with OLTC and reactive power capability of PV Inverters," *IET Generation Transmission Distribution*, vol. 14, no. 22, pp. 5183–5192, Nov. 13, 2020.

2. Arunima Dutta, Sanjib Ganguly, Chandan Kumar, "Coordinated Volt/Var Control of PV and EV Interfaced Active Distribution Networks Based on Dual-Stage Model Predictive Control," *IEEE System Journal*, (early access), doi: 10.1109/JSYST.2021.3110509, 2021.

3. Arunima Dutta, Sanjib Ganguly, Chandan Kumar, "MPC based Coordinated Voltage Control in Active Distribution Networks incorporating CVR and DR," *IEEE Transaction on Industrial Applications*, (early access), doi: 10.1109/TIA.2022.3163108, 2022.

4. Arunima Dutta, Sanjib Ganguly, Chandan Kumar, "Coordinated Control Scheme for EV Charging and Volt/Var Devices Scheduling to Regulate Voltages of Active Distribution Networks" *Sustainable Energies, Grids and Network*, (accepted on 5^{th} May, 2022), 2022.

Conference Publications:

1. Arunima Dutta, Sanjib Ganguly, Chandan Kumar, "Voltage Control in Active Distribution Networks and an Approach based on Model Predictive Control," *Proc.* 8^{th} *IEEE International Conference on Power Systems (ICPS)* Jaipur, India, pp. 1-6, 2019.

2. Arunima Dutta, Sanjib Ganguly, Chandan Kumar, "Model Predictive Control based Coordinated Voltage Control in Active Distribution Networks utilizing OLTC and DSTATCOM," *Proc.* 9^{th} *IEEE International Conference on Power Electronics, Drives and Energy Systems (PEDES)*, Jaipur, India, pp. 1-6, 2020.

3. Arunima Dutta, Sanjib Ganguly, Chandan Kumar, "Coordinated Voltage Control of Active Distribution Networks in presence of PV and Energy Storage System," *Proc.* 12^{th} *IEEE Energy Conversion Congress Exposition - Asia (ECCE-Asia)*, Singapore, pp. 2028-2033, 2021.

4. Arunima Dutta, Sanjib Ganguly, Chandan Kumar, "Model Predictive based Coordinated Voltage Control of Active Distribution Networks with Distributed Generation and Electric Vehicles," 4^{th} *IEEE International Conference on Energy and Power Engineering (ICEPE)* (accepted), to be held in Shillong, India, 2022.

Author's Biography

Arunima Dutta (Student Member, IEEE) received the B.E. degree in Electrical Engineering from Jorhat Engineering College, Assam, India, in 2012, and the M.Tech. Degree in Power and Energy systems from the National Institute of Technology Meghalaya, Meghalaya, India, in 2016.

She is currently working towards the doctoral degree with the Department of Electronics and Electrical Engineering, Indian Institute of Technology Guwahati, Guwahati, India. Her research interests include power system operation, model predictive based voltage control and energy management, modeling of electric vehicles and power electronics appliances to be utilized in modern distribution systems.